

---

# Relativistic corrections and dynamic decoupling in trapped ion optical atomic clocks

---

Von der QUEST-Leibniz-Forschungsschule  
der Gottfried Wilhelm Leibniz Universität Hannover  
zur Erlangung des Grades

**Doktor der Naturwissenschaften**  
**Dr. rer. nat.**

genehmigte Dissertation von

**M. Sc. Víctor José Martínez Lahuerta**  
geboren am 16. April 1994 in Girona, Spanien

**Referent:** Prof. Dr. Klemens Hammerer  
Institut für Theoretische Physik  
Leibniz Universität Hannover

**Korreferent:** Prof. Dr. Piet O. Schmidt  
Institut für Quantenoptik  
Leibniz Universität Hannover

**Korreferent:** Prof. Dr. Ana Maria Rey  
Department of Physics  
University of Colorado, Boulder

**Tag der Promotion:** 01.02.2023

## Abstract

This thesis describes relativistic corrections and the use of dynamical decoupling in the context of trapped ion optical atomic clocks. The shifts that contribute to trapped ion optical atomic clocks can be divided into relativistic effects and environmental perturbations, which correspond to the two parts of this thesis.

In the first part, we investigate how to properly account for relativistic corrections from an *ab initio* derivation. For that purpose, we start from a charged two-particle system in external electromagnetic and gravitational fields described by the classical Lagrangian for two particles interacting with the electromagnetic field. From this starting point, we derive a quantum Hamiltonian including leading order relativistic corrections in a systematic way. We then apply this Hamiltonian to describe the relativistic coupling of external and internal dynamics of cold ions in Paul traps, including the effects of micromotion, excess micromotion and trap imperfections. This approach provides a systematic and fully quantum mechanical treatment of relativistic frequency shifts in atomic clocks based on single trapped ions. Additionally, we reproduce well-known formulae for the second-order Doppler shift for thermal states, which were previously derived on the basis of semiclassical arguments. We complement and clarify recent discussions in the literature on the role of time dilation and mass defect in ion clocks. Furthermore, we also study the problem of an ion in a Penning trap for the case of a transition between manifolds with spin 0. Our Hamiltonian gives a basis for properly treating the *relativistic effects* of an ion that can be applied to an extensive variety of experiments after the proper implementation.

The second part considers the mechanism of continuous dynamical decoupling, focusing on gaining insensitivity to some environmental perturbations, such as magnetic field fluctuations and quadrupole shifts. This mechanism consists in the application of a radio-frequency magnetic field orthogonal to the quantization axis of a given spin manifold. We show how this is achieved for one manifold and then extend the treatment to two manifolds. In that process, we make some approximations, consisting of rotating wave approximations and neglecting the effect that the off-resonant radio-frequency magnetic field of one manifold has on the other manifold and vice versa. Nevertheless, we account for those approximations perturbatively by using the so-called Magnus expansion, showing that they can be considered as an effective shift of the Zeeman splitting of the manifolds. Afterwards, we can apply our formalism to properly describe a quadrupole transition between two manifolds, where the particular case of a transition between  $S = 1/2$  and  $D = 5/2$  of  $^{40}\text{Ca}^+$  is studied; a comparison with experimental data will be presented elsewhere. We compare our approximate treatment with the true solution of the periodic Hamiltonian presented in the introductory part of the thesis, finding that the corrected dressed basis corresponds to the time-independent part of the Floquet states. We finish this part by considering the implementation of a Mølmer-Sørensen gate within the framework of continuous dynamical decoupling.

**Keywords:** Optical atomic clocks, Paul traps, trapped ions, relativistic corrections, continuous dynamical decoupling, precision measurements



## Author contributions

Parts of this thesis have appeared elsewhere, as peer-reviewed publications or on pre-print servers. Here I summarize my personal contributions to these works. Note that contributions of other co-authors without my involvement are not explicitly listed. In order of the corresponding chapter, they are:

### Chapter 3:

**V. J. Martínez-Lahuerta**, S. Eilers, T. E. Mehlstäubler, P. O. Schmidt, K. Hammerer, *Ab initio quantum theory of mass defect and time dilation in trapped-ion optical clocks*, Physical Review A, 106(3):032803, sep 2022

**Author contribution:** **VJML** contributed considerably to the development of the general Hamiltonian without the integration of gravity, along with SE and KH. The application of the general Hamiltonian to the case of an ion in a Paul trap were performed by **VJML** with input from POS, TEM and KH. **VJML** wrote the manuscript with contributions from all authors.

### Chapter 4:

**V. J. Martínez-Lahuerta et al.**, *Quadrupole transitions with Dynamical Decoupling*, In progress

**Author contribution:** **VJML** contributed considerably to the development of the application of the continuous dynamical decoupling mechanism, as well as its interpretation, along with KH. The interpretation and derivation of the laser ion interaction with this mechanism were performed by **VJML** along with KH. **VJML** account for the Bloch-siegart and cross-field effects with input from KH. **VJML** considered the implementation of a MS-gate in combination with the continuous dynamical decoupling scheme with inputs from all authors. **VJML** wrote the theory part of the manuscript with contributions from all authors.

Patrik Mönkeberg, *Floquet Theory of Dynamical Decoupling*, Bachelor thesis, Leibniz University Hannover

**Author contribution:** **VJML** contributed to the supervision of the aforementioned Bachelor thesis.

For completeness I add that the following article, which was published during my time as a PhD student, but it is not included in this thesis as it was already presented in the PhD thesis of Marius Schulte [1]:

M. Schulte, **V. J. Martínez-Lahuerta**, M. S. Scharnagl, K. Hammerer, *Ramsey interferometry with generalized one-axis twisting echoes*, Quantum 4, 268 (2020)



## Acknowledgements

Work on my PhD has been incredibly rewarding and overall a tremendously positive experience. This is in a large part due to a lot of wonderful people who have helped to make it possible and have supported me before and during my PhD. The truth is there are too many people I owe thanks to to comprehensively list here, but what follows is a summary of those people.

First and foremost I would like to thank Klemens Hammerer, Piet Schmidt and Ana María Rey for agreeing to act as referees for my thesis.

As concerns the science of the report, the first person I would like to thank is, of course, Klemens Hammerer. You invited me to meet your group and I will never forget my first impression. I thought at first that the people here in general were quite a bit more formal when meeting new people than I was used to, but as I found that this quickly gave way to a series of deeply rewarding friendships both personally and intellectually. During my first meeting with the group, I remember that as soon as they started discussing their projects and the physics behind what they were working on, their faces lit up and the worries and formality of meeting someone new were brushed aside in favour of passion and genuine enjoyment. It was at that moment I was certain this was the environment I had wanted for my PhD. I want to thank you for always having your door open for any discussion and for mentoring me during these years. I especially appreciated how, after every large meeting, you would stay long after with me and other students who had been present to go through the key points again to make sure we understood everything and to really see things from another perspective. In particular, I would like to thank you for making me realize that not knowing an answer is completely fine, and the importance of being transparent about this rather than trying to blindly guess at answers.

As I have alluded to earlier, during my PhD I was part of the 'AG Hammerer' group. I would therefore like to thank several colleagues and friends from this group who accompanied me during this time.

I would like to start with Marius, with whom I had the pleasure of working with specially at the beginning of my PhD. We had many fruitful discussions and he was always willing to discuss for as long as it took for me to understand everything. For that I am very thankful. I would like to thank other past and present members of the group as well: Sahand, Timm and Maja with whom I had the pleasure of sharing an office and particularly Timm and Maja for being invested in the writing process throughout its various ups and downs; Michael, Kasper, Florian, Ivan, Corentin, Jannis and Julian, with whom I have had several valuable discussions among the years, on a wide range of topics from physics to fitness and even economics, particularly thanks to Michael for the several times he helped me with different projects, Kasper for our several experiments in our Barista career and Jannis for helping me in the

beginning with several small things that made my life a lot easier. I would also like to thank, the Bachelor student Patrik Mönkeberg, who I supervised, for the work he put on his project, which was closely aligned with my own interests, Simon Eilers for his work during his Bachelor and Master thesis and his meticulous proof-reading over the work we did together, and Kirill for his several visits to the group which I hope can continue in the future! We really enjoyed your visits and discussions. On top of that I would like to take some time to give special thanks to an often overlooked member of the group who has given her continuous support every day in the office these past 4 years, and that is our coffee machine. It is fair to say that without you this experience would have been really different, and not necessarily for the better! In particular, I would like to thank Jan-Niclas, with whom we shared this stressful period of writing the thesis. Having someone struggling through similar things made a huge difference. Being able to comment on the problems we encounter, as well as cheering each other on and celebrating the small victories, made this process a lot nicer, and I am deeply grateful for that.

Finally, I would also like to thank an indispensable person of the group, Birgit Gemmeke, for handling the many administrative tasks in the group. During the years you helped me with a vast number of problems, work related and not, and I want to thank you for always being there with your door open for advice and help.

I was also blessed during my PhD to have really good collaborators for my projects. It is always really interesting to see the point of view of the experimentalists when working on a project and where I ought to focus on. I want to thank Ludwig, Lennart and Kai for always being there if I needed any discussion, entertaining my barrage of questions and also for showing me around the lab. In particular, I would like to thank Lennart for many discussions about the project and the time spent to match the experiment and the theory, which I found to be a very exciting endeavour. I also want to thank Tanja Mehlstäubler for all the discussions we had together, where she was always raising interesting questions or points that maybe we overlooked. It was a pleasure to work with you. Finally, I would like to thank Piet Schmidt, not only for the very interesting discussions that we had, but also for how your face glowed with excitement and interest in every discussion.

I would like to thank Matthew Bohman, with whom I had interesting discussions during a conference. These discussions continue after the conference and evolve into expanding one of my projects. After the almost two years of confinement due to Covid, part of a project evolving from a conference was an experience I missed during my PhD, thanks for making that possible.

I was in the lucky position to have benefited from the scientific environment of the CRC 1227 (Dq-mat), which allowed me to interact with a variety of scientists and attend several talks and retreats. Even though they were online as a result of the pandemic, I found them incredibly valuable and am delighted to see them starting up again face to face.

Special thanks need to go for those who reviewed parts of the thesis: Klemens, Michael, Perancha, Timm, Kasper, Simon, Jaime, Jesus and Cole. I really appreciated your feedback.

Before entering with friends and family, I would like to give a few words about



those who helped me maintain an active life and a variety of healthy distractions from academia. Thanks to the basketball team for a great competition every year. I also enjoyed the time I spent with the people from the dancing courses I took during the years. Special thanks to Marius, Jan-Niclas, Kasper and Ivan for our almost weekly great adventures in our DnD campaigns. Particular thanks to my online DnD group which helped me through the pandemic as it was almost the only activity I could do being enforced to stay at home. We had many memorable adventures.

I know these acknowledgments have been quite long so far, but if someone is forced to read all of them are definitely friends and family, and I am sure if you have been able to endure so far can endure just a little bit more!

I would like to start with Javier Tejada Palacios, one of my professors at the University of Barcelona. Thank you very much for mentoring with such a passion, and, particularly, thank you for encouraging me to go to Germany for my PhD, where I got the opportunity to work in an amazing research environment.

I would also like to thank as well my friends Jesus and Jaime. They were great companions during the University, Jaime's extremely nice and humorous notes regarding several lectures were a blessing in particular, and they have continuously supported me after that.

A mis padres, Cayo y Joaquina, por apoyarme a que pudiera perseguir lo que me propusiera, aunque no siempre entendieran que es lo que quera hacer, su apoyo ha sido incondicional. Y tambien por aguantarme tantos años, para que engañarnos.

Of course, I also have to thank my brother, Daniel, and my *other brother* Oriol, for supporting me, in their own really special way but supporting me nevertheless. I know I will always be able to count on them for anything, but if it has a castle involved, they will be even happier.

And last, and most importantly, someone for which the words "thank you" seem not enough, my girlfriend Perancha, who has been supporting me long before my PhD (and helping me with the procedures to get in one), during it, and, (hopefully!) will keep supporting me long after. Mainly I would like to express how grateful I am to her for believing that I could do anything, even when I was not so sure myself.



# Contents

<b>1</b>	<b>Introduction</b>	<b>1</b>
<b>2</b>	<b>Mathematical methods for time-dependent Hamiltonians</b>	<b>5</b>
2.1	Motivation . . . . .	5
2.2	Rotating wave approximation . . . . .	6
2.3	Magnus expansion . . . . .	8
2.4	Introduction to Floquet theory . . . . .	11
2.4.1	Quasienergies ambiguity . . . . .	14
2.4.2	The extended Hilbert space . . . . .	15
<b>3</b>	<b><i>Ab initio</i> quantum theory of mass defect and time dilation in trapped-ion optical clocks</b>	<b>19</b>
3.1	Motivation and research problem . . . . .	19
3.2	Hamiltonian of a charged composite system in external electromagnetic and gravitational fields . . . . .	22
3.2.1	Classical Lagrangian and quantization of a composite system . . . . .	23
3.2.2	Hamiltonian for internal and external degrees of freedom (DOFs) . . . . .	24
3.3	Relativistic coupling of internal and external DOF in ion clocks . . . . .	29
3.3.1	Ramsey spectroscopy . . . . .	30
3.3.2	Quantum theory of an ion trap . . . . .	33
3.3.3	Fractional frequency shift due to mass defect: Second-order Doppler effect . . . . .	37
3.3.4	Ion trap with a linear potential . . . . .	39
3.3.5	Fractional frequency shift due to dc forces and excess micromotion . . . . .	40
3.3.6	Fractional frequency shift due to gravity . . . . .	41
3.3.7	Variance of the fractional frequency shift . . . . .	43
3.3.8	Effect of additional quadrupole fields . . . . .	45
3.4	Relativistic coupling of internal and external DOFs in Penning traps . . . . .	47
3.4.1	Introduction to Penning traps . . . . .	47
3.4.2	Mass defect in Penning traps . . . . .	48
3.5	Conclusion . . . . .	51
3.6	Outlook: Further research directions . . . . .	52

<b>4</b>	<b>Quadrupole transitions with continuous dynamical decoupling(CDD)</b>	<b>53</b>
4.1	Motivation and research problem . . . . .	53
4.2	Dynamical decoupling . . . . .	55
4.2.1	Doubly-dressed basis . . . . .	55
4.2.2	Suppression of Zeeman and quadrupole shifts . . . . .	58
4.3	Laser-ion interaction . . . . .	61
4.3.1	Quadrupole transitions in doubly-dressed basis . . . . .	62
4.3.2	Corrections to the bare frequencies . . . . .	64
4.3.3	Application to $^{40}\text{Ca}^+$ . . . . .	66
4.4	Dressed states vs Floquet states . . . . .	69
4.5	Mølmer-Sørensen gates. . . . .	73
4.6	Conclusion . . . . .	76
4.7	Outlook: Further research directions . . . . .	77
<b>5</b>	<b>Summary and closing statements</b>	<b>79</b>
<b>A</b>	<b>Hamiltonian for ion in external electromagnetic fields with first-order relativistic corrections</b>	<b>81</b>
A.1	Classical, approximately relativistic Lagrangian for charges in external radiation fields . . . . .	82
A.2	From classical Lagrangian to quantum Hamiltonian in minimal-coupling form . . . . .	85
A.3	Power-Zienau-Woolley transformation to a multipolar Hamiltonian in center of mass coordinates for charged composite particles . . . . .	86
A.4	Change to the center of mass $\mathbf{R}$ and relative $\mathbf{r}$ coordinates . . . . .	89
A.5	Separation of central and relative dynamics . . . . .	91
<b>B</b>	<b>Hamiltonian for ions in gravitational fields</b>	<b>93</b>
B.1	Classical Lagrangian . . . . .	94
B.2	Minimal-coupling Hamiltonian and multipolar Hamiltonian . . . . .	95
B.3	Hamiltonian in center of mass frame . . . . .	96
<b>C</b>	<b>Equation of motion for a trapped ion</b>	<b>99</b>
C.1	Homogeneous solution . . . . .	100
C.2	Quasienergie values for the inhomogeneous case . . . . .	102
	<b>Bibliography</b>	<b>107</b>

# Abbreviations and Acronyms

---

<b>GPS</b>	Global Positioning System
<b>TAI</b>	International Atomic Time
<b>UTC</b>	Coordinated Universal Time
<b>RF</b>	Rotating frame
<b>RWA</b>	Rotating wave approximation
<b>COM</b>	Center of mass
<b>DOFs</b>	Degrees of freedom
<b>dc</b>	direct current
<b>PPN</b>	parameterized post-Newtonian
<b>PZW</b>	Power-Zienau-Woolley
<b>ac</b>	alternating current
<b>rf</b>	radio frequency
<b>CDD</b>	Continuous dynamical decoupling
<b>LF</b>	Laboratory frame
<b>E2</b>	electric-quadrupole interaction
<b>PTB</b>	Physikalisch-Technische Bundesanstalt
<b>MS</b>	Mølmer-Sørensen
<b><i>h.c.</i></b>	Hermitian conjugate



# 1

## Introduction

Research to make clocks more precise is an ongoing task for centuries. With each improvement, the performance of existing applications can be improved and/or the development of new applications is enabled. Today we take several applications for granted such as the global positioning system (GPS), that was developed thanks to the use of atomic clocks. But the applications of atomic clocks go beyond navigation technology. About 400 highly precise atomic clocks help to define the International Atomic Time (TAI), which, in combination with the consideration of the Earth's rotation, define the Coordinated Universal Time (UTC). Furthermore, there is great interest in using optical clocks in space to perform tests of fundamental physics such as Einstein's theory of relativity. Also noteworthy are geodesy applications, where the combination of the measurement of the gravity potential and its derivative, which can be measured with a gravimeter, allows explorations of Earth, i.e., to explore the surface and interior of the Earth. Another interesting field of study is the variation of fundamental constants, whose bounds are further limited by more precise measurements and thus the improvement of atomic clocks. These applications of atomic clocks are only a selected few of many, which further emphasize the versatility of atomic clocks: from mere applications to addressing questions of fundamental physics.

After giving examples of these applications, we would like to focus on two physical effects, the gravitational redshift and the mass defect. We want to gain some insight into these effects and motivate how important it is to properly understand them for the performance of their applications.

For the gravitational redshift we will focus on the GPS and what an improvement in the precision would imply for this effect. Assuming an uncertainty of  $10^{-7}$  s in the time measurement translates to a precision of around 20 to 30 meters for the GPS. But, to achieve this precision a theoretical understanding of the gravitational redshift is required. If we do not account for general and special relativity, GPS calculated positions would accumulate errors up to 10 km during a day. This shows how important it is to properly understand the theory in order to characterize such

applications. Research on resolving the gravitational redshift has improved in the previous years, going from tens of cm to hundreds of  $\mu\text{m}$  in about a decade. Being able to resolve the gravitational redshift in the regime of a few tens of  $\mu\text{m}$  will allow to probe the connection between quantum physics and general relativity, opening up a whole new realm of physics to explore.

With respect to the mass defect, we want to motivate why it is important to properly characterize it in order to gain further insight into the limitations of trapped ion clocks. The mass defect, or second-order Doppler effect, comes into play if one takes the mass-energy equivalence seriously, i.e.,  $E = mc^2$ . Accounting for that in our Hamiltonian, gives rise to relativistic effects related to the so-called secular motion, micromotion and excess micromotion, which are known to play an important role in relativistic frequency shifts in trapped ion clocks. In particular, the uncertainty in the excess micromotion is one of the main limiting factors in trapped ion clocks nowadays, therefore, an *ab initio* derivation of relativistic corrections can lead to a better understanding of this effect. Improving the knowledge on these effects, and characterizing which other effects can play a significant role, is required to enable the improvement in precision, allowing us to improve some of the aforementioned applications.

As motivated above, the fields related to atomic clocks are constantly evolving, and new ideas are proposed regularly to overcome previous limitations. Therefore, the theoretical description and the experiments of all these applications have to be on an equal footing of understanding and precision. With this in mind, the first question we should ask ourselves is: What is limiting an atomic clock today? The answer is systematic effects, which can be divided in two categories. The first category consists of the shifts caused by *environmental perturbations*, e.g., due to electric or magnetic fields. The second category consists of the shifts generated by *relativistic effects*. The aim of this thesis is to gain deeper insight into some aspects of both categories of shifts in order to understand and treat them properly. For this purpose, we have divided the thesis into two parts:

In the first part, treated in chapter 3, we characterize the shifts generated by *relativistic effects*. For that purpose, we derive a Hamiltonian for the external and internal dynamics of an electromagnetically bound, charged two-particle system in external electromagnetic and gravitational fields, including leading-order relativistic corrections. We apply this Hamiltonian to describe the relativistic coupling of the external and internal dynamics of cold ions in Paul traps, providing a systematic and fully quantum mechanical treatment of relativistic frequency shifts in atomic clocks based on single trapped ions. We also study the case of an ion in a Penning trap for the case of a transition between manifolds with spin 0. We use our Hamiltonian to



treat *relativistic effects* in trapped ions, but it also serves as a basis for treating such effects in experiments with neutral atoms.

In the second part, treated in chapter 4, we study how to treat the shifts generated by *environmental perturbations*. In particular, we describe a mechanism that makes our clock transition insensitive to at least some of such shifts. We begin by considering the mechanism of continuous dynamical decoupling, focusing on gaining insensitivity to magnetic field fluctuations and quadrupole shifts. We show how this is achieved for a given spin manifold and then extend the treatment to two manifolds. Afterwards, we apply our formalism to properly describe a quadrupole transition between two manifolds, where the particular case of a transition between  $S = 1/2$  and  $D = 5/2$  of  $^{40}\text{Ca}^+$  is studied; a comparison with experimental data will be presented elsewhere. Additionally, we compare our approximate treatment with the true solution of the periodic Hamiltonian presented in chapter 2. We finish this part by considering the implementation of a Mølmer-Sørensen gate within the framework of continuous dynamical decoupling.

For both parts, the treatment of time-dependent potentials, particularly time-periodic potentials, is needed. These potentials are considered using the Floquet theory. This mathematical framework is summarized in chapter 2.

While this introduction is kept in more general to give a motivation considering the overall topic, the mentioned problems are motivated throughout the manuscript in more detail at the beginning of every chapter.



# 2

## Mathematical methods for time-dependent Hamiltonians

### 2.1 Motivation

Understanding the dynamics of a time-dependent problem is a topic of study in several branches of science. In general, the time-dependent nature of the physical problem is already present, but it can also be implemented as a tool to achieve some particular properties, e.g., insensitivity to a particular effect inherent of our system by applying external time-dependent fields. Therefore, the characterization of time-dependent properties goes beyond simply understanding the physical problem we are facing and additionally allows us to exploit the gained insight to obtain a desired effect.

Of particular relevance are the time-periodic contributions as they allow us to use several different properties used for time-independent problems. The theory that discusses time-periodic differential equations, i.e., time-periodic dynamics through the Schrödinger equation, is the well-known Floquet theory, that begins with the work of the French mathematician Achille Marie Gaston Floquet (1847–1920) on linear differential equations with periodic coefficients [2]. This theory has been studied in several works [3–5] and is used for different physical problems, for example in the context of trapped ions [6–9]. We will need this theory as in the problems treated in chapters 3 and 4 the system is subject to time-dependent fields. In the case that the reader is more familiarized with Bloch’s theorem, which states the shape for the eigenstates of the Hamiltonian with a periodic potential in space, we will try to motivate the use of Floquet theory in a similar way, as it has a similar insight exploiting a periodicity in time rather than in space. Therefore, it seems intuitive to consider the time  $t$  as a coordinate in an equal footing to the  $x$  coordinate in order to use its periodicity. This idea will be the foundation from which we will be able to find connections between the properties of time-independent Hamiltonians and time-periodic Hamiltonians.

Even though Floquet theory has been studied in several different works, we find it useful to give a summary at this point to remind the reader of its main characteristics. Additionally, we find it appropriate, as it is the theory that connects the different projects studied in this thesis. Also, as Holthaus highlights in his work [5]: “. . . there are some peculiarities of time-periodic quantum systems which, although they are known in principle [4, 8–15], appear to be rarely appreciated . . . .” Therefore, we aim with this chapter to provide a proper mathematical framework that will allow us to treat trapped particles in time-dependent potentials and the effect of implementing time-dependent magnetic fields into two spin manifolds for driving quadrupole transitions. Furthermore, with our treatment, we provide an alternate perspective for the aforementioned problems. To this goal, we will closely follow the introduction to Floquet theory of Martin Holthaus [5] and the work of Hideo Sambe [4]. We redirect the reader to those articles for a more detailed description of the notions presented in this chapter.

This chapter starts in Sec. 2.2 with an introduction on how to consider time-dependent problems in physics and the explanation of an approximate method to treat time-dependent potentials, the rotating wave approximation, followed by a perturbative treatment that goes beyond the rotating wave approximation treated in Sec. 2.3. After acquiring some insight on time-dependent problems, the basics of Floquet theory are treated in Sec. 2.4. Both will be relevant for chapter 4. Exploiting the periodicity allows us to find new constraints for the properties of the periodic Hamiltonians. Thanks to that, we define the so-called Floquet states with their so-called quasienergies. Afterwards, we treat in Sec. 2.4.1 the problem of the ambiguity of the quasienergies. We end by fixing this problem using the so-called extended Hilbert space 2.4.2, which is of particular interest as it will be a key notion for chapter 3.

## 2.2 Rotating wave approximation

Before entering into the details of treating periodic potentials using Floquet theory, we consider how to address time-dependent Hamiltonians and to explain an approximate method. However, this approximation is not valid for every problem and, therefore, the need of an exact solution using Floquet theory arises.

When dealing with a time-dependent Hamiltonian, the most natural question to ask is the following: is there a reference frame in which the Hamiltonian of the system is time-independent? The first step to answer this question is to study a change of reference frame in general. Let  $H(t)$  be the Hamiltonian of our system. We want to study the Hamiltonian from a reference frame which itself evolves under  $H_0$ , where  $H_0$  can be contained in  $H(t)$  or not. If so, we are studying the Hamiltonian in a frame

that is already undergoing part of the evolution of the system. Commonly, these frames are rotations around some axis, hence the name ‘rotating frame’. During this thesis, we will use the abbreviation  $RF$  to refer to the reference frame and to the rotating frame. A rotating frame is a reference frame but the opposite is not always true.

Let  $|\phi(t)\rangle$  be the set of states that, under the general Hamiltonian, will fulfill the Schrödinger equation

$$i\hbar \frac{d}{dt} |\phi(t)\rangle = H(t) |\phi(t)\rangle. \quad (2.1)$$

We are interested in the states

$$|\psi(t)\rangle = e^{itH_0/\hbar} |\phi(t)\rangle =: \mathcal{U} |\phi(t)\rangle, \quad (2.2)$$

which are the states  $|\phi(t)\rangle$  time evolved with respect to the Hamiltonian  $H_0$  and where we defined the operator  $\mathcal{U}$ . We ask ourselves what is the effective Hamiltonian ( $H^{RF}$ ) that describes the dynamics of these new states. This new Hamiltonian can be time dependent or not, but we will not write it explicitly. We will take the opportunity to define a notation that is going to prove useful in chapter 4. This consists on rewriting Eq. (2.1) as

$$\left( H(t) - i\hbar \frac{d}{dt} \right) |\phi(t)\rangle = 0, \quad (2.3)$$

and considering  $H(t) - i\hbar \frac{d}{dt}$  as the operator defining the Schrödinger equation. We will introduce the shorthand notation

$$\mathcal{R}_{\mathcal{U}}[A] := \mathcal{U} A \mathcal{U}^\dagger. \quad (2.4)$$

for the conjugation of an operator  $A$  with  $\mathcal{U}$ . Therefore, the transformed Schrödinger equation for the states  $|\psi(t)\rangle$  will be calculated by the transformation of the operator  $H(t) - i\hbar \frac{d}{dt}$

$$\begin{aligned} \mathcal{R}_{\mathcal{U}} \left[ H(t) - i\hbar \frac{d}{dt} \right] &= \mathcal{U} \left[ H(t) - i\hbar \frac{d}{dt} \right] \mathcal{U}^\dagger \\ &= \mathcal{U} H(t) \mathcal{U}^\dagger - i\hbar \mathcal{U} \dot{\mathcal{U}} - i\hbar \frac{d}{dt} \\ &= e^{itH_0/\hbar} H(t) e^{-itH_0/\hbar} - H_0 - i\hbar \frac{d}{dt}. \end{aligned} \quad (2.5)$$

As the previous expression corresponds to the transformation of the operator defining the Schrödinger equation, the Hamiltonian in the reference frame is given by

$$H^{RF} = e^{itH_0/\hbar} H(t) e^{-itH_0/\hbar} - H_0. \quad (2.6)$$

With this notation it will be easier to implement sequences of transformations of the form  $\mathcal{R}_{\mathcal{U}_1} \mathcal{R}_{\mathcal{U}_2} \cdots \mathcal{R}_{\mathcal{U}_n} [H(t) - i\hbar \frac{d}{dt}]$ , as will be relevant in chapter 4.

After understanding what a change of reference frame consists on, we would like to introduce the so-called rotating wave approximation (RWA), which is a tool that is also commonly used to deal with time-dependent Hamiltonians and that is going to prove useful for us, as we will see in chapter 4. For that purpose we will write  $U$  in the eigenstates  $|n\rangle$  of the Hamiltonian  $H_0$ , i.e.,  $H_0 = \sum_n E_n |n\rangle \langle n|$ , where for simplicity we will assume that there is no degeneracy in the eigenstates of  $H_0$ . Therefore, we can rewrite  $H^{RF}$  by expanding in the eigenbasis of  $H_0$  as

$$H^{RF} = -H_0 + \sum_{m,n} e^{i\omega_{mn}t} \langle m| H(t) |n\rangle |m\rangle \langle n|, \quad (2.7)$$

where we defined the frequencies  $\omega_{mn} = \frac{E_m - E_n}{\hbar}$ . The RWA consists on neglecting the terms that fulfill

$$|\langle m| H(t) |n\rangle| \ll |\hbar\omega_{mn}|, \quad (2.8)$$

as they will be off-resonant contributions, also known as fast-oscillating terms. In order for the condition in eq. (2.8) to be sufficient we also assumed that the time dependence of  $H(t)$  is slow on the time scale of  $\omega_{mn}$ .

In chapter 4 we will need to consider corrections beyond the RWA in order to have sufficient accuracy for describing the precision measurements we are going to treat. To this goal we will introduce now the Magnus expansion.

## 2.3 Magnus expansion

This section is meant to be a motivation on why the Magnus expansion [16] is a useful approximation for time-dependent Hamiltonians and how to use it. For a more detailed introduction of the Magnus expansion, we refer the reader to the pedagogical introduction of S. Blanes *et al.* [17] and for a rigorous proof of the theorem, as well as a detailed explanation of several applications, we refer the reader to another work from the same author [18].

In order to characterize the evolution of any possible initial state  $|\psi(t_0)\rangle$ , we need to find the unitary time-evolution operator,  $U(t, t_0)$ , associated with the Schrödinger equation, Eq. (2.1). With this operator, any initial state  $|\psi(t_0)\rangle$  can be propagated in the form

$$|\psi(t)\rangle = U(t, t_0) |\psi(t_0)\rangle. \quad (2.9)$$

If the time-evolution operator is well defined, it has to obey some properties. First, for consistency, it needs to fulfill the initial condition  $U(t_0, t_0) = \mathbf{1}$ , where  $\mathbf{1}$  denotes the identity operator in the Hilbert space  $\mathcal{H}$ . Additionally, the propagation of the initial state at time  $t_0$  to a later time  $t_2$  has to be the same as propagating the initial state to an intermediate time  $t_1$  and afterwards propagating it to the time  $t_2$ . This is known as the *composition* property,

$$U(t_2, t_0) = U(t_2, t_1)U(t_1, t_0), \quad t_2 \geq t_1 \geq t_0. \quad (2.10)$$

If we evolve a normalized state, it is to be expected that the norm of the state does not change with time, i.e.,

$$\langle \psi(t_0) | \psi(t_0) \rangle = \langle \psi(t) | \psi(t) \rangle = \langle \psi(t_0) | U^\dagger(t, t_0) U(t, t_0) | \psi(t_0) \rangle. \quad (2.11)$$

In order to obey this condition, the time-evolution operator needs to be *unitary*

$$U^\dagger(t, t_0) U(t, t_0) = \mathbf{1}. \quad (2.12)$$

Moreover, if we want the state to obey the Schrödinger equation at all times, the time-evolution operator also needs to fulfill the Schrödinger equation

$$i\hbar \frac{d}{dt} U(t, t_0) = H(t) U(t, t_0). \quad (2.13)$$

If the Hamiltonian is time independent, then this has the easy solution

$$U(t, t_0) = \exp(-i(t - t_0)H/\hbar), \quad (2.14)$$

which can be calculated by direct integration. When the Hamiltonian is time dependent, we cannot obtain such a simple form. One can use time-dependent perturbation theory to solve Eq. (2.13) by iteration giving the expansion, in powers of  $H(t)$  (or, equivalently, in powers of  $\hbar^{-1}$ )

$$U(t, t_0) = \mathbf{1} + \sum_{n=1}^{\infty} P_n(t, t_0), \quad (2.15)$$

where  $P_n(t_0, t_0) = 0$ . Then, one gets the expressions

$$P_n(t, t_0) = (-i/\hbar)^n \int_{t_0}^t dt_2 \int_{t_0}^{t_1} dt_2 \cdots \int_{t_0}^{t_{n-1}} dt_n H(t_1) H(t_2) \cdots H(t_n). \quad (2.16)$$

Truncating this sum will give an approximate result of our evolution operator. Nevertheless, the truncation of the series usually leads to a non-unitary evolution operator.

One of the main advantages of the Magnus expansion for the evolution operator is that it consists of a systematic way to build approximations to the time-dependent

Schrödinger equation in such a way that, in any order, the evolution operator is unitary.

If we accept that a true exponential solution of Eq. (2.13) does exist in the form

$$U(t, t_0) = \exp(\Omega(t, t_0)) = \mathbb{1} + \sum_{n=1}^{\infty} \frac{1}{n!} \Omega^n(t, t_0), \quad (2.17)$$

with  $\Omega(t_0, t_0) = 0$ , and if we rewrite  $\Omega(t, t_0)$  as  $\Omega(t, t_0) = \sum_{k=1}^{\infty} \Omega_k(t, t_0)$ . Then we can calculate  $\Omega_k(t, t_0)$  by equating Eq. (2.15) and Eq. (2.17)

$$\mathbb{1} + \sum_{n=1}^{\infty} P_n(t, t_0) = \mathbb{1} + \sum_{m=1}^{\infty} \frac{1}{m!} \left( \sum_{k=1}^{\infty} \Omega_k(t, t_0) \right)^m. \quad (2.18)$$

We can collect the terms with equal orders in  $\hbar^{-1}$  and equate them in both sides, remembering that both  $P_k$  and  $\Omega_k$  are of order  $\hbar^{-k}$ . With that we obtain, for the first three orders,

$$P_1(t, t_0) = \Omega_1(t, t_0) \quad (2.19)$$

$$P_2(t, t_0) = \Omega_2(t, t_0) + \frac{1}{2!} \Omega_1^2(t, t_0) \quad (2.20)$$

$$P_3(t, t_0) = \Omega_3(t, t_0) + \frac{1}{2!} (\Omega_1(t, t_0) \Omega_2(t, t_0) + \Omega_2(t, t_0) \Omega_1(t, t_0)) + \frac{1}{3!} \Omega_1^3(t, t_0). \quad (2.21)$$

Rearranging and using the definitions of  $P_i(t, t_0)$  we can show the expressions of  $\Omega_i(t, t_0)$  for the first three orders

$$\Omega_1(t, t_0) = -\frac{i}{\hbar} \int_{t_0}^t H(t) dt_1, \quad (2.22)$$

$$\Omega_2(t, t_0) = -\frac{1}{2\hbar^2} \int_{t_0}^t dt_1 \int_{t_0}^{t_1} dt_2 [H(t_1), H(t_2)], \quad (2.23)$$

and

$$\Omega_3(t, t_0) = \frac{i}{6\hbar^3} \int_{t_0}^t dt_1 \int_{t_0}^{t_1} dt_2 \int_{t_0}^{t_2} dt_3 ([H(t_1), [H(t_2), H(t_3)]] + [H(t_3), [H(t_2), H(t_1)]]). \quad (2.24)$$

The expressions for  $\Omega_i$  can be interpreted as generating effective Hamiltonians of order  $i$  fulfilling  $H_i^{\text{eff}} = i\hbar\Omega_i(t_0 + T, t_0)/T$ . Once more, we highlight that the effective Hamiltonian  $H^{\text{eff}} = \sum_{i=1}^k H_i^{\text{eff}}$  is Hermitian for truncation at any value of  $k$ , and therefore the evolution operator is unitary as well.



Lastly, we want to highlight another interesting property of the Magnus expansion. For the way it is constructed, if the commutator vanishes for a given order  $k$  then it means that the series is finite and therefore, it is not an approximation any more and we could find the exact solution of the evolution operator, and therefore, an exact effective Hamiltonian driving the system. This can be really useful for some time-dependent Hamiltonians for which the existence of this solution is not obvious. This is the case for the Mølmer-Sørensen gate that we use in Sec. 4.5.

In the case that the time-dependent Hamiltonian is periodic then we can go even further and treat the problem exactly using Floquet theory. We expect the eigenstates coming from the RWA and the eigenstates further corrected using Magnus expansion to be approximations of the quasienergy eigenstates defined by Floquet theory, which we will study in the following. This comparison is going to be treated in chapter 4.

## 2.4 Introduction to Floquet theory

We want to study physical problems that are symmetric under discrete time translations, and, therefore, will allow us to use the Floquet formalism [2]. With that purpose, we consider a quantum system defined on a Hilbert space  $\mathcal{H}$  with a periodic Hamiltonian  $H$  of periodicity  $T$ , i.e.,

$$H(t) = H(t + T). \quad (2.25)$$

We will assume a finite-dimensional Hilbert space to avoid discussions about technical subtleties that go beyond the intention of this introduction. Our goal is to study which implications this periodicity has on the level of the time-dependent Schrödinger equation

$$i\hbar \frac{d}{dt} |\psi(t)\rangle = H(t) |\psi(t)\rangle. \quad (2.26)$$

As we are treating  $T$ -periodic Hamiltonians, we should try exploiting this property to obtain stronger statements about the time-evolution operator attributes, this is possible for the *composition* property, see Eq. (2.10).

If we consider the operator  $V(t) := U(t + T, 0)U^{-1}(T, 0)$ , where we fix the initial time  $t_0 = 0$  for the rest of the chapter, it can be immediately seen that  $V(0) = \mathbb{1}$  and we can calculate the Schrödinger equation for the newly defined operator  $V(t)$

$$i\hbar \frac{d}{dt} V(t) = i\hbar \frac{d}{dt} U(t + T, 0)U^{-1}(T, 0) = H(t + T)U(t + T, 0)U^{-1}(T, 0) = H(t)V(t). \quad (2.27)$$

We have shown that  $V(t)$  obeys the same differential equation and initial condition as the time-evolution operator, and therefore, due to the existence and uniqueness theorem, they are the same  $U(t+T, 0)U^{-1}(T, 0) = V(t) = U(t, 0)$ , proving the modified *composition* property for periodic potentials

$$U(t+T, 0) = U(t, 0)U(T, 0). \quad (2.28)$$

This is a really strong statement, which is the core of Floquet theory as it implies that knowing the evolution operator within the period  $T$  allows us to know the evolution operator for all times.

As should be clear from our previous statement, the one-cycle evolution operator  $U(T, 0)$ , which is also known as monodromy operator in the mathematical literature [19], plays a prominent role in Floquet theory. Therefore, we will need to characterize it properly. To this goal, we will write the monodromy operator as an exponential in the form

$$U(T, 0) = \exp(-iGT/\hbar), \quad (2.29)$$

where the operator  $G$  is Hermitian, and therefore, has real eigenvalues. This ensures that  $\exp(-iGT/\hbar)$  is unitary. Now we can define a new unitary operator

$$P(t) := U(t, 0) \exp(+iGt/\hbar), \quad (2.30)$$

which is also periodic in  $T$ , as can be seen from

$$\begin{aligned} P(t+T) &= U(t+T, 0) \exp(+iG(t+T)/\hbar) \\ &= U(t, 0) (U(T, 0) \exp(+iG(T)/\hbar)) \exp(+iG(t)/\hbar) \\ &= P(t). \end{aligned} \quad (2.31)$$

By combining the  $T$ -periodic unitary operator  $P$  and the Hermitian operator  $G$  we can define the time evolution operator  $U(t, 0)$  as

$$U(t, 0) = P(t) \exp(-iGt/\hbar). \quad (2.32)$$

By writing the set of eigenvalues of  $U(T, 0) = \exp(-iGT/\hbar)$  as  $\{e^{-i\varepsilon_n T/\hbar}\}$ , and its eigenstates as  $\{|n\rangle\}$ , we can write the monodromy operator in its spectral representation as

$$U(T, 0) = \sum_n |n\rangle e^{-i\varepsilon_n T/\hbar} \langle n|, \quad (2.33)$$

implying

$$e^{-iGT/\hbar} |n\rangle = e^{-i\varepsilon_n T/\hbar} |n\rangle. \quad (2.34)$$

Thanks to Eq. (2.33), the evolution of any initial state becomes easily evaluated in the basis of eigenstates of  $U(T, 0)$ . We can see this by writing any initial state in the aforementioned basis

$$|\psi(0)\rangle = \sum_n |n\rangle \langle n|\psi(0)\rangle = \sum_n a_n |n\rangle, \quad (2.35)$$

where  $a_n = \langle n|\psi(0)\rangle$  are the coordinates of our initial state with respect to the basis of eigenvectors of the evolution operator. We apply  $U(t, 0)$  to study the time evolution of our initial state

$$\begin{aligned} |\psi(t)\rangle &= U(t, 0) |\psi(0)\rangle = \sum_n a_n P(t) e^{-iGt/\hbar} |n\rangle = \sum_n a_n P(t) |n\rangle e^{-i\varepsilon_n t/\hbar} \\ &= \sum_n a_n |u_n(t)\rangle e^{-i\varepsilon_n t/\hbar}, \end{aligned} \quad (2.36)$$

where we define the Floquet functions

$$|u_n(t)\rangle := P(t) |n\rangle, \quad (2.37)$$

which are periodic due to the periodicity of the operator  $P(t)$ , as can be seen in Eq. (2.31). With that, we define the so-called Floquet states as

$$|\psi_n(t)\rangle := |u_n(t)\rangle e^{-i\varepsilon_n t/\hbar}, \quad (2.38)$$

which are solutions of the time-dependent Schrödinger equation (2.26) and are also known as quasistationary eigenstates. We will explain the origin of this name shortly. The importance of these states is that, as  $|n\rangle$  form a complete set, and  $P(t)$  is unitary, the Floquet functions are a complete set for each instant of time  $t$ . Therefore, any solution of the time-dependent Schrödinger equation with a  $T$ -periodic Hamiltonian can be expanded with respect to the Floquet states

$$|\psi(t)\rangle = \sum_n a_n |u_n(t)\rangle e^{-i\varepsilon_n t/\hbar}. \quad (2.39)$$

The previous statement is commonly known as the Floquet theorem.

We can see that the occupation probability of a given Floquet state  $|\psi_n(t)\rangle$  is given by the norm squared of its coefficient  $a_n$ , i.e.,  $|a_n|^2$ , which is independent of time, and therefore, the time-periodic action preserves the occupation probabilities of the Floquet states. This implies that several techniques and concepts for time-independent problems can be applied to periodic time-dependent problems. The first comparison will be the phase factors in  $e^{-i\varepsilon_n t/\hbar}$ , which resembles the phase factors in  $e^{-iE_n t/\hbar}$  corresponding to the time-evolution of energy eigenstates with energies  $E_n$  in the case of time-independent Hamiltonians. For this reason, the quantities  $\varepsilon_n$

have been called quasienergies, and were named in 1966 almost simultaneously by the Soviet physicists Yakov Borisovich Zel'dovich [8] and Vladimir Ivanovich Ritus [9]. Additionally, we can also highlight the analogy between the quasienergies and the quasimomentum  $k$ , characterizing the Bloch eigenstates in a periodic solid.

### 2.4.1 Quasienergies ambiguity

Seeing the similarities of the Floquet states with the eigenstates of time-independent Hamiltonians we want to try to find an appropriate frame in which the dynamics of our problem are governed by a time-independent Hamiltonian. The difference here, with respect to Sec. 2.2, is that no approximation is going to be used. To this goal, we will start by performing the unitary transformation

$$|\psi(t)\rangle = P(t) |\tilde{\psi}(t)\rangle, \quad (2.40)$$

so that

$$i\hbar \frac{d}{dt} |\psi(t)\rangle = i\hbar \dot{P}(t) |\tilde{\psi}(t)\rangle + P(t) i\hbar \frac{d}{dt} |\tilde{\psi}(t)\rangle, \quad (2.41)$$

where  $\dot{P}(t)$  denotes derivation with respect to the time variable  $t$ . Using Eq. (2.30) we can calculate  $\dot{P}(t)$  and obtain

$$i\hbar \frac{d}{dt} |\psi(t)\rangle = H(t)U(t) \exp(iGt/\hbar) |\tilde{\psi}(t)\rangle - U(t)G \exp(iGt/\hbar) |\tilde{\psi}(t)\rangle + P(t) i\hbar \frac{d}{dt} |\tilde{\psi}(t)\rangle. \quad (2.42)$$

The first term on the right-hand side can be rewritten as  $H(t) |\psi(t)\rangle$  and therefore, cancels the term on the left-hand side, leading us to

$$i\hbar \frac{d}{dt} |\tilde{\psi}(t)\rangle = P^{-1}(t)U(t) \exp(iGt/\hbar)G |\tilde{\psi}(t)\rangle = G |\tilde{\psi}(t)\rangle. \quad (2.43)$$

Thanks to the transformation in Eq. (2.40), we managed to find a time-independent Schrödinger equation for which the time-independent Hamiltonian consists of the previously defined operator  $G$ , which is the generator of the monodromy operator  $U(T)$  defined in Eq. (2.29). That is the reasoning why the eigenstates of the operator  $G$  are related to the Floquet states.

Nevertheless, Eq. (2.43) can be misleading, as it does not solve the problem uniquely. The key resides in the definition of  $G$ . The Floquet multipliers  $\{e^{-i\varepsilon_n T/\hbar}\}$  are not uniquely defined. Even though they are the eigenvalues of the monodromy operator  $U(T, 0)$ , and therefore, well defined, the complex logarithm needed to extract its quasienergies is multi-valued. Since  $e^z = e^{z+m2\pi i}$ , where  $m = 0, \pm 1, \pm 2, \dots$

is an arbitrary integer, the Floquet multipliers thus fix the quasienergies up to an integer multiple of  $2\pi\hbar/T$ . Therefore, introducing the angular frequency

$$\omega = \frac{2\pi}{T}. \quad (2.44)$$

In reality, every quasienergy will be an entire class labeled by  $m$ , where

$$\varepsilon_{(n,m)} := \varepsilon_n + m\hbar\omega; \quad m = 0, \pm 1, \pm 2, \dots \quad (2.45)$$

Of course,  $\varepsilon_n = \varepsilon_{(n,0)}$  has to be selected by some convention, and any other member of the class is an equally valid representative. One option for this representative is the so-called first quasienergy Brillouin zone, which corresponds to the representative of every class that lays within the range  $-\hbar\omega/2 < \varepsilon \leq +\hbar\omega/2$ . Sometimes, it is not even desirable to single out one particular representative of a quasienergy class because it is precisely the  $\hbar\omega$ -indeterminacy that allows for a physically most transparent description of some physical problems. This is the case, e.g., for multiphoton transitions induced by a periodic potential [5]. Therefore, we saw that it will depend on the particular problem how to try to define the quasienergies properly.

### 2.4.2 The extended Hilbert space

Seeing the problems regarding the proper definition of the quasienergies, see Eq. (2.45), we will try to formulate the theory in an invariant manner, such that unnatural distinctions of individual quasienergy representatives are not made.

We will start by inserting the Floquet states (2.38) into the Schrödinger equation (2.26), obtaining

$$\left( H(t) - i\hbar \frac{d}{dt} \right) |u_n(t)\rangle = \varepsilon_n |u_n(t)\rangle. \quad (2.46)$$

The key now is to consider  $t$  not as the evolution variable, but rather as a coordinate on the same footing as  $\mathbf{x}$ . In that case, Eq. (2.46) becomes an equation in an extended Hilbert space  $\mathcal{H}_T = L_2(\mathbb{R}^3) \otimes \mathcal{T}$ , where  $\mathcal{T}$  is the space of  $T$ -periodic functions of time. This idea of extended Hilbert space was introduced in the literature by Hideo Sambe [4] and plays a major role in the mathematical analysis of periodically time-dependent quantum systems.

Now, we want to study what happens to the degeneracy of the quasideigenstates in this extended Hilbert space. We take one particular  $T$ -periodic solution  $|u_n(t)\rangle$  to Eq. (2.46) with eigenvalue  $\varepsilon_n$  and, multiplying by  $e^{im\omega t}$ , where  $m$  is an integer and

$\omega$  is the angular frequency defined in Eq. (2.44), the product  $|u_n(t)\rangle e^{im\omega t}$  is again  $T$ -periodic, obeying

$$\left(H(t) - i\hbar \frac{d}{dt}\right) |u_n(t)\rangle e^{im\omega t} = (\varepsilon_n + m\hbar\omega) |u_n(t)\rangle e^{im\omega t}. \quad (2.47)$$

Therefore, all the quasienergy representatives of a given class appear as individual solutions to this eigenvalue equation in  $\mathcal{H}_T = L_2(\mathbb{R}^3) \otimes \mathcal{T}$ . Nevertheless, all of them lead to the same Floquet state (2.38) in  $\mathcal{H}$ , since

$$(|u_n(t)\rangle e^{im\omega t}) e^{-i[\varepsilon_n + m\hbar\omega]t/\hbar} = |u_n(t)\rangle e^{-i\varepsilon_n t/\hbar}, \quad (2.48)$$

so that the  $\hbar\omega$ -indeterminacy drops out.

After showing how the indeterminacy can be dropped in the extended Hilbert space, we want to properly characterize it and show how some theorems corresponding to the Hilbert space  $\mathcal{H}$  can still be applied in the extended Hilbert space  $\mathcal{H}_T$ . First, we need to define the scalar product in the enlarged Hilbert space, which will involve a time average over one period  $T$ . This scalar product will be indicated as

$$\langle\langle \psi | \varphi \rangle\rangle = \frac{1}{T} \int_0^T dt \langle \psi(t) | \varphi(t) \rangle, \quad (2.49)$$

for  $|\psi\rangle, |\varphi\rangle \in \mathcal{H}_T$ , where  $\langle \psi(t) | \varphi(t) \rangle$  is the usual scalar product in  $L_2(\mathbb{R}^3)$ .

Accordingly, the average of an operator  $A(t)$  with respect to a state  $|\psi\rangle \in \mathcal{H}_T$  has to be understood as

$$\langle\langle A \rangle\rangle_\psi = \frac{1}{T} \int_0^T dt \langle \psi(t) | A(t) | \psi(t) \rangle, \quad (2.50)$$

where  $\langle \psi(t) | A(t) | \psi(t) \rangle$  is the average value in  $L_2(\mathbb{R}^3)$ .

One theorem that will be used during our work is the Feynman-Hellmann theorem. This theorem can be expressed in the context of the extended Hilbert space. If the Hamiltonian  $H(t, \lambda)$  of a system depends on a time-independent parameter  $\lambda$  and the periodic relation  $H(t + T, \lambda) = H(t, \lambda)$  holds for any  $\lambda$ , then the solution  $|u_n(t)\rangle$  of Eq. (2.46) satisfies the relation

$$\frac{d\varepsilon_n}{d\lambda} = \frac{\langle\langle u_n(t) | \frac{\partial H}{\partial \lambda} | u_n(t) \rangle\rangle}{\langle\langle u_n(t) | u_n(t) \rangle\rangle}. \quad (2.51)$$

The proof of this theorem is the same as for the time-independent theorem and therefore, it will not be shown here. It is worth highlighting that the solutions  $|u_n(t)\rangle$

can be chosen to be normalized. Combining the normalization with the notation introduced above (2.50), we can simplify the previous expression as

$$\frac{d\varepsilon_n}{d\lambda} = \left\langle\left\langle \frac{\partial H}{\partial \lambda} \right\rangle\right\rangle_{u_n}. \quad (2.52)$$

Working in the extended Hilbert space will be a key feature in chapter 3 as it will allow us to calculate  $T$ -periodic creation and annihilation operators for a given basis of our system, allowing us to calculate the average of any quantity we desire. With this mathematical introduction, we described some of the tools we need to treat the physical problems that will appear throughout this thesis.





# 3

## *Ab initio* quantum theory of mass defect and time dilation in trapped-ion optical clocks

### 3.1 Motivation and research problem

Optical ion clocks [20] have shown systematic uncertainties below  $10^{-18}$  [21]. This fulfills an early prediction of Dehmelt from 1982 [22]:

“Thus the current promise of an atomic line spectral resolution of about 1 part in  $10^{18}$  or  $\sim 10^8$  times better than achieved to date may be realized in the not too distant future.”

This achieves an important milestone on the way toward a possible redefinition of the SI second based on an optical transition [23]. Clocks at this level of uncertainty open the way to many applications, such as relativistic geodesy [24–30], tests of general relativity [31–33], and explorations of physics beyond the standard model [34]. At the same time, systematic relativistic frequency shifts and their uncertainty play a significant and even dominant role [35–41]. These concern in particular the special-relativistic second-order Doppler shift  $-\mathbf{v}^2/2c^2$ , which accounts for moving clocks ticking slower than stationary clocks, and the general-relativistic gravitational redshift [20]. Both shifts can be seen as an effect of time dilation, which occurs when the proper time measured by the clock atom along its world line is Lorentz transformed into the reference frame of the laboratory or that of another distant clock. This reasoning is entirely correct and rigorous, but implicitly assumes a semiclassical approach in which the center of mass motion of the atom is ascribed to a classical world line and only its internal (electronic) degree of freedom is treated quantum mechanically.

An alternative perspective can be gained by placing not time dilation but the mass defect, i.e., the equivalence of internal (binding) energy and external (kinematic as well as gravitational) mass, at the center of reasoning [42]. The mass defect concept

has been in the literature since 1960. Already from treatments of the Mössbauer effect [43, 44], it is known that the mass defect gives rise to a frequency shift of internal transitions that is equivalent to the second-order Doppler effect. In the context of ion clocks, this equivalence was highlighted recently in [45]. The advantage of this perspective is that the mass defect can be represented by a simple Hamiltonian coupling between electronic and center of mass (COM) degrees of freedom (DOFs), which is treated as a relativistic perturbation to the standard Hamiltonian of nonrelativistic quantum optics. The basic formulae of the known relativistic corrections can then be reproduced on the grounds of this perturbed Hamiltonian, as shown in [46, 47], which enforces the notion that the mass defect is an alternative to time dilation. Treatments based on the mass defect, however, also led to considerations of possible new types of systematic shifts [46], and alleged fundamental limits on the accuracy of atomic clocks [48], beyond what is known from time dilation. Apart from the disparities between mass defect and time dilation, approaches relying on the mass defect have not yet obtained a rigorous treatment of the micromotion and excess micromotion, which play an important role in relativistic frequency shifts in trapped ion clocks [35, 39]. These effects are intrinsic to the trapping mechanism in a Paul trap and will be defined during this chapter. Therefore, it is natural to raise the following questions:

- Are time dilation and mass defect equivalent perspectives of the same effect?
- How can we be sure that these corrections provide a complete picture and we are not missing other effects of the same magnitude?

Moreover, while these approaches have the potential to provide a fully quantum-theoretical picture of relativistic shifts, there does not appear to be a self-contained derivation of the perturbed Hamiltonian that covers the case of a trapped ion to date. Here, we set out to give a systematic derivation of the Hamiltonian for an ion in external electromagnetic and gravitational fields, including relativistic corrections involving external and internal DOFs.

Sonnleitner & Barnett [49] derived a Hamiltonian starting from the classical Lagrangian for two particles with charges  $e_1$  and  $e_2$  interacting with the electromagnetic potentials with vanishing total charge, i.e.,  $Q = e_1 + e_2 = 0$ , we extended this work to consider a total charge  $Q \neq 0$ . In another work, Schwartz & Giulini [50] expanded the work from Sonnleitner & Barnett to account for a weak gravitational field. Based on this work, we derive a Hamiltonian for a composite two particle system with a total net charge  $Q \neq 0$  interacting with electromagnetic fields in the presence of a weak gravitational field. We apply this Hamiltonian to the context of an ion clock and give a rigorous quantum mechanical derivation of the relativistic frequency shifts, including the effects of micromotion and excess micromotion in the framework of Floquet

theory [4, 6–9]; we calculate the shifts associated with these relativistic corrections and reproduce, for the special case of thermal states of motion, the shifts known in the literature, e.g., from [35, 39]. Further frequency shifts or fundamental limitations do not arise from this proper treatment.

The derivation of the Hamiltonian closely follows that in [49, 50], and merely extends this work to composite systems with nonvanishing total charge. Starting from the classical Lagrangian of an electromagnetically bound two-particle system, this derivation establishes the mass defect as the only relevant relativistic correction to the standard quantum-optical Hamiltonian, which couples COM and internal degrees of freedom. The thus corrected Hamiltonian strictly refers to the laboratory frame and completely covers all relativistic frequency shifts. A further correction of time dilation is unnecessary. The quantum-mechanical description developed in the present study also covers the effects of zero-point fluctuation as well as other arbitrary quantum states of motion. We hope that the logic developed here will also prove useful in other, more complex systems, such as multi-ion clocks or optical lattice clocks, to obtain a stringent analysis of special and general relativistic effects.

This chapter will be mainly focused on Paul traps, nevertheless, there are other relevant trapping mechanisms, such as Penning traps. The question is how this formalism could be applied to Penning traps. The problem is that the presence of a magnetic field to realize the confinement of the ion makes the description of the spin indispensable, which is not included in our formalism. Nevertheless, there are some recent proposals to have a clock transition with both clock states having  $I = J = F = 0$ , where  $I$ ,  $J$ , and  $F$  are the conventional quantum numbers specifying nuclear, electronic, and total angular momentum, respectively, see e.g. [51], making our description relevant for that case too.

The confinement in a Penning trap is characterized by three different motions defined by the axial, the modified cyclotron and the magnetron frequencies. The associated energy of the magnetron motion has a different sign than the rest, therefore, this opens the question: Could one null the second-order Doppler effect by increasing the magnetron motion? The fact that the fractional frequency shift could be nulled by adding motion to the system seems at first sight unintuitive. Thanks to the treatment developed here, one can treat the relativistic corrections for this case properly and address the previous question. Unfortunately, the answer is negative.

We start this chapter by summarizing the derivation of the relativistic Hamiltonian of a charged composite system in external electromagnetic and gravitational fields in Sec. 3.2. Once the relativistic corrections have been properly understood we continue by explaining the role of the coupling between internal and external DOF in ion clocks in Sec. 3.3, we do so by studying the interrogation scheme, in this case

Ramsey spectroscopy 3.3.1, and by properly describing the quantum theory of a Paul trap 3.3.2. With this description, we are able to calculate the fractional frequency shift due to the mass defect, applied direct current (dc) forces and gravity, recovering the second-order Doppler effect with micromotion 3.3.3, the excess micromotion 3.3.5 and the gravitational redshift 3.3.6, respectively. With our treatment, we can also calculate the variance of the fractional frequency shift and consider fundamental limits in ion clocks 3.3.7. We will finish our discussion of Paul traps by talking about possible imperfections in the trap 3.3.8, and proceed by arguing how the mass defect can be applied in the case of Penning traps in Sec. 3.4. Finally, we will present our conclusions in 3.5 and examine further ideas and possible continuations of this work in 3.6.

## 3.2 Hamiltonian of a charged composite system in external electromagnetic and gravitational fields

To properly clarify the effects of relativistic corrections, we need to develop a systematic and fully quantum mechanical treatment of relativistic frequency shifts in atomic clocks based on single trapped ions. The first step in this direction will be to derive the Hamiltonian for an ion coupled to external electromagnetic and gravitational fields including first order relativistic corrections, i.e., corrections of  $\mathcal{O}(c^{-2})$ . Summarizing the derivation of this Hamiltonian will be the goal of this section, the full details will be shown in Appendix A and B. The relativistic coupling of internal (relative) and external (COM) degrees of freedom will be responsible for generating a fractional frequency shift when measuring the energy difference between a ground and an excited state of an ion, therefore, special focus will be placed on this coupling.

As motivated in the introduction, we adopt the model of Sonnleitner & Barnett [49] for a hydrogenlike atomic ion as an electromagnetically bound two-body system composed of a core (charge  $e_1$ , coordinates  $\mathbf{r}_1$ ) and an electron ( $e_2$ ,  $\mathbf{r}_2$ ), see Fig. 3.1. Bold symbols denote three-vectors. In contrast to Sonnleitner & Barnett we will allow for a non-vanishing net charge  $Q = e_1 + e_2 \neq 0$ , and consider a non-zero gravitational field. For the latter, we follow the treatment of Schwartz & Giulini [50], who extended the calculation from Sonnleitner & Barnett by a weak gravitational background field described by the Eddington-Robertson parameterized post-Newtonian (PPN) metric, thus covering first order relativistic corrections to the Minkowski metric. The notation used in this section will correspond to the one of [50].

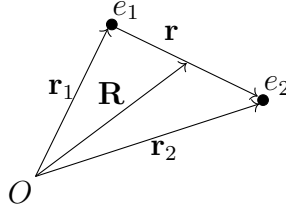


Figure 3.1: In this figure we show the coordinates and positions that we will use in the following derivation.  $O$  stands for the center of coordinates,  $\mathbf{r}_1$  and  $\mathbf{r}_2$  are the positions of the two particles of charges  $e_1$  and  $e_2$ , respectively, and  $(\mathbf{R}, \mathbf{r})$  is the center of mass coordinate system.

We note that the mass defect Hamiltonian can be derived also on other grounds, based, e.g., on effective field theory for composite systems [42, 52], or on approaches to formalize time dilation within quantum theory [53, 54]. The account of [49, 50] that we follow here proceeds in the spirit of conventional atomic structure calculations and has the benefit of systematically providing all relevant relativistic corrections, not just the mass defect. Relativistic corrections due to spin are not covered here, however, and would require suitable extensions of treatments of composite particles based on the Dirac equation along the lines of [55, 56].

### 3.2.1 Classical Lagrangian and quantization of a composite system

Our starting point is the classical Lagrangian for two particles interacting with the electromagnetic field

$$L = - \sum_{i=1,2} m_i c \sqrt{-g_{\mu\nu}(\mathbf{r}_i) \dot{r}_i^\mu \dot{r}_i^\nu} + \int d^3\mathbf{r} \sqrt{-g(\mathbf{r})} \left( J^\mu(\mathbf{r}) A_\mu(\mathbf{r}) - \frac{1}{4\mu_0} F_{\mu\nu}(\mathbf{r}) F^{\mu\nu}(\mathbf{r}) \right). \quad (3.1)$$

We use four-vector notation, with  $g_{\mu\nu}(\mathbf{r})$  being the metric tensor,  $g(\mathbf{r})$  its determinant,  $J^\mu(\mathbf{r})$  the electric four-current,  $A_\mu(\mathbf{r})$  the electromagnetic four-potential, and  $F_{\mu\nu}(\mathbf{r})$  the field strength tensor. Here, the first term gives the Lagrangian for the point particles, which describes the motional dynamics of the two particles with masses  $m_i$  and positions  $r_i^\mu = (ct, \mathbf{r}_i)$  in spacetime with corresponding velocities  $\dot{r}_i^\mu$ , where the derivative is taken with respect to the time coordinate  $t$ . The terms in the integral represent the dynamics governed by the electromagnetic field. The first contribution is the interaction of the electromagnetic field and the particles and the second contribution is the Lagrangian of the electromagnetic field, which is obtained by minimally coupling the special-relativistic action for electromagnetism to a general

spacetime metric [50]. The Eddington-Robertson metric is defined with respect to the Minkowski metric as the background structure, and has the form

$$\begin{aligned} g_{00}(\mathbf{r}) &= -1 - 2\frac{\phi(\mathbf{r})}{c^2} - 2\beta\frac{\phi^2(\mathbf{r})}{c^4} + \mathcal{O}(c^{-6}), \\ g_{jj}(\mathbf{r}) &= 1 - 2\gamma\frac{\phi(\mathbf{r})}{c^2} + \mathcal{O}(c^{-4}) \quad (j = 1, 2, 3). \end{aligned} \quad (3.2)$$

All off-diagonal components vanish for a flat background metric up to  $\mathcal{O}(c^{-5})$ . The scalar Newtonian potential is denoted by  $\phi(\mathbf{r})$ . We include here also the Eddington-Robertson parameters  $\beta$  and  $\gamma$ , which account for possible deviations from general relativity, and fulfill  $\beta = \gamma = 1$  in general relativity.

Following [50], the Lagrangian (3.1) is written in the Coulomb gauge and expanded in inverse powers of  $c$ , maintaining terms up to second order. The corresponding classical Hamiltonian function is quantized canonically, which yields the approximately relativistic Hamiltonian operator for two charged particles minimally coupled to the electromagnetic field

$$\begin{aligned} \hat{H} &= \sum_{i=1,2} \left( \frac{\hat{\mathbf{p}}_i^2}{2m_i} + m_i\phi(\hat{\mathbf{r}}_i) + e_i\Phi(\hat{\mathbf{r}}_i) \right) + \frac{e_1e_2}{4\pi\epsilon_0} \frac{1}{\hat{r}} \\ &\quad - \frac{e_1e_2}{16\pi\epsilon_0c^2m_1m_2} \left( \hat{\mathbf{p}}_1 \cdot \frac{1}{\hat{r}} \hat{\mathbf{p}}_2 (\hat{\mathbf{p}}_1 \cdot \hat{\mathbf{r}}) \frac{1}{\hat{r}^3} (\hat{\mathbf{r}} \cdot \hat{\mathbf{p}}_2) + (1 \leftrightarrow 2) \right) + \sum_{i=1,2} \left( -\frac{\hat{\mathbf{p}}_i^4}{8m_i^3c^2} \right. \\ &\quad \left. + \frac{2\gamma+1}{2m_i c^2} \hat{\mathbf{p}}_i \cdot \phi(\hat{\mathbf{r}}_i) \hat{\mathbf{p}}_i + (2\beta-1) \frac{m_i\phi^2(\hat{\mathbf{r}}_i)}{2c^2} + (\gamma+1)\phi(\hat{\mathbf{r}}_i) \frac{e_1e_2}{8\pi\epsilon_0c^2\hat{r}} \right). \end{aligned} \quad (3.3)$$

We define  $\hat{\mathbf{p}}_i = \hat{\mathbf{p}}_i - e_i\hat{\mathbf{A}}^\perp(\hat{\mathbf{r}}_i)$  and the relative distance between the particles  $\hat{\mathbf{r}} = \hat{\mathbf{r}}_1 - \hat{\mathbf{r}}_2$ , with norm  $\hat{r} = |\hat{\mathbf{r}}|$ . The electromagnetic three-potential  $\hat{\mathbf{A}}^\perp(\hat{\mathbf{r}})$  (transverse in the Coulomb gauge) and the electric potential  $\Phi(\hat{\mathbf{r}})$  are taken as classical variables describing externally applied fields<sup>1</sup>. We refer the reader to Appendix A and B for a comprehensive derivation of this result. The first line in Eq. (3.3) is the nonrelativistic two-body Hamiltonian, the second line gives the dominant relativistic corrections without a gravitational field and the last line shows the relativistic corrections due to the interplay with gravity.

### 3.2.2 Hamiltonian for internal and external degrees of freedom (DOFs)

We need to express the Hamiltonian (3.3) in the multipolar representation of the light-particle interaction, this can be achieved via a Power-Zienau-Woolley (PZW)

<sup>1</sup>This has to be understood in the sense of a mean-field treatment with respect to an externally applied electromagnetic field. The effects of the radiation reaction such as spontaneous emission or Lamb shifts are lost in this approximation.

transformation. The advantage of this representation is that, without relativistic corrections, the resulting Hamiltonian can be separated into terms referring to internal and external DOFs corresponding to COM and relative coordinates. However, with relativistic corrections, these coordinates no longer separate the two DOFs fully, so, after this change, *relativistic* variants of these coordinates have to be introduced. Since a system's energy content is part of its inertia, the proper way to discuss this problem should be to express the Hamiltonian in the center of energy frame, but this is not a canonical transformation, as is explained in [49]. Nevertheless, there exists a choice of coordinates via a canonical transformation that allows the separation of COM and relative dynamics up to our order of approximation, as shown by Close and Osborn [57] for the case of neutral systems  $Q = 0$ . We show that this transformation can be generalized to the case  $Q \neq 0$  in Appendix A.

In terms of these relativistic corrected coordinates, the Hamiltonian can be written as

$$\hat{H} = \hat{H}_{\text{com}} + \hat{H}_{\text{int}} + \hat{H}_{\text{at-emf}} + \hat{H}_{\text{metric}} + \hat{H}_{\text{mass defect}}, \quad (3.4)$$

where we separated the Hamiltonian terms as follows:  $\hat{H}_{\text{com}}$  and  $\hat{H}_{\text{int}}$  refer to the terms that depend only on the COM and only on the internal DOF, respectively. The interaction of the atom with the external electromagnetic field is described by  $\hat{H}_{\text{at-emf}}$ . The relativistic coupling of internal and COM dynamics, which will be responsible for the fractional frequency shift, is covered by the two terms  $\hat{H}_{\text{metric}}$  and  $\hat{H}_{\text{mass defect}}$ . In the following, we will give the explicit form of all these terms in the relevant limit  $m_1 \gg m_2$ .

The first contribution in (3.4) is the COM Hamiltonian

$$\hat{H}_{\text{com}}(M) = \hat{H}_{\text{com}}^{(0)} + \hat{H}_{\text{com}}^{(1)}, \quad (3.5)$$

given by the nonrelativistic COM Hamiltonian

$$\hat{H}_{\text{com}}^{(0)} = \frac{\hat{\mathbf{P}}^2}{2M} + M\phi(\hat{\mathbf{R}}), \quad (3.6)$$

and the leading relativistic corrections

$$\hat{H}_{\text{com}}^{(1)} = -\frac{1}{2Mc^2} \left( \frac{\hat{\mathbf{P}}^2}{2M} \right)^2 + (2\beta - 1) \frac{M(\phi(\hat{\mathbf{R}}))^2}{2c^2} + \frac{2\gamma + 1}{2Mc^2} \hat{\mathbf{P}} \cdot \phi(\hat{\mathbf{R}}) \hat{\mathbf{P}}, \quad (3.7)$$

where we defined the total rest mass  $M = m_1 + m_2$  and

$$\hat{\hat{\mathbf{P}}} = \hat{\mathbf{P}} - Q\hat{\mathbf{A}}^\perp(\hat{\mathbf{R}}). \quad (3.8)$$

The first two terms in (3.7) correspond to the first order relativistic corrections to the kinetic energy and the gravitational potential energy and the last term corresponds

to the cross talk between them. The explicit definition of the relativistically corrected COM variables  $\hat{\mathbf{R}}$  and  $\hat{\mathbf{P}}$  is given in Eq. (A.50). The COM Hamiltonian in Eq. (3.5) simply corresponds to the approximately relativistic Hamiltonian for a charged point particle of mass  $M$  in a gravitational field, minimally coupled to the electromagnetic field. For later use when discussing the so-called *mass defect*, the COM Hamiltonian in Eq. (3.5) is written in the form  $\hat{H}_{\text{com}}(M)$  with the total mass  $M$  as an argument.

The second contribution in Eq. (3.4) is the Hamiltonian for the internal DOF

$$\hat{H}_{\text{int}} = \hat{H}_{\text{int}}^{(0)} + \hat{H}_{\text{int}}^{(1)}, \quad (3.9)$$

where again we make the distinction between the nonrelativistic internal Hamiltonian

$$\hat{H}_{\text{int}}^{(0)} = \frac{\hat{\mathbf{p}}^2}{2\mu} + \frac{e_1 e_2}{4\pi\epsilon_0} \frac{1}{\hat{r}}, \quad (3.10)$$

consisting on the kinetic and Coulomb energies, respectively, and their first order relativistic corrections given by

$$\hat{H}_{\text{int}}^{(1)} = -\frac{1}{2\mu c^2} \left( \frac{\hat{\mathbf{p}}^2}{2\mu} \right)^2 + \frac{e_1 e_2}{4\pi\epsilon_0} \frac{1}{2\mu M c^2} \left( \hat{\mathbf{p}} \cdot \frac{1}{\hat{r}} \hat{\mathbf{p}} + (\hat{\mathbf{p}} \cdot \hat{\mathbf{r}}) \frac{1}{\hat{r}^3} (\hat{\mathbf{r}} \cdot \hat{\mathbf{p}}) \right), \quad (3.11)$$

where  $\hat{\mathbf{p}}$  is the canonical momentum associated with  $\hat{\mathbf{r}}$  and  $\mu$  is the reduced mass. We can determine the electronic energy levels of the atom by diagonalizing this Hamiltonian. One should highlight here that in a complete description, other well-known relativistic corrections (e.g. concerning spin) will contribute to this Hamiltonian too. In the following, we assume that these corrections are accounted for in the diagonalization of  $\hat{H}_{\text{int}}$ , and therefore, will be included when writing this Hamiltonian in terms of its eigenbasis.

The interaction of the atom with the electromagnetic field in the dipole approximation is given by

$$\hat{H}_{\text{at-emf}} = Q \Phi(\hat{\mathbf{R}}) - \hat{\mathbf{d}} \cdot \mathbf{E}(\hat{\mathbf{R}}) + \frac{1}{2M} \left[ \hat{\mathbf{P}} \cdot (\hat{\mathbf{d}} \times \mathbf{B}(\hat{\mathbf{R}})) + \text{H.c.} \right] + \hat{H}_{\text{other}}, \quad (3.12)$$

where  $\hat{\mathbf{d}} = \sum_{i=1,2} e_i (\hat{\mathbf{r}}_i - \hat{\mathbf{R}})$  is the electric dipole moment. The first two terms correspond to the electric potential and dipole energy, respectively, the third term represents the minimally coupled Röntgen term [58]. We suppress here further contributions involving the electromagnetic fields in  $\hat{H}_{\text{other}}$ , which are given explicitly and discussed in Appendix A and are not effective in the configuration of a Paul trap.

Finally, the last two terms of Eq. (3.4),  $\hat{H}_{\text{metric}}$  and  $\hat{H}_{\text{mass defect}}$ , describe the relativistic coupling of COM and internal DOF and thus are the pivotal points of the following discussion. The first of these two terms is

$$\hat{H}_{\text{metric}} = \gamma \frac{\phi(\hat{\mathbf{R}})}{c^2} \left( 2 \frac{\hat{\mathbf{p}}^2}{2\mu} + \frac{e_1 e_2}{4\pi\epsilon_0} \frac{1}{\hat{r}} \right). \quad (3.13)$$



It is of metric origin and a consequence of spacetime curvature, as is already evident from its proportionality to the PPN parameter  $\gamma$  in the Eddington-Robertson metric in Eq. (3.2). We remind the reader that  $\gamma = 1$  in general relativity. More formally, the term follows when the Hamiltonian for the internal DOF is written in terms of distances measured with respect to the metric given in Eq. (3.2), and expanded up to  $\mathcal{O}(c^{-4})$ ,

$$\frac{g_{ij}^{-1}(\hat{\mathbf{R}})\hat{p}_i\hat{p}_j}{2\mu} + \frac{e_1e_2}{4\pi\epsilon_0} \frac{1}{\sqrt{g_{ij}(\hat{\mathbf{R}})\hat{r}_i\hat{r}_j}} \simeq \hat{H}_{\text{int}}^{(0)} + \hat{H}_{\text{metric}}. \quad (3.14)$$

Here, summations run only over the spatial indices  $i, j = 1, 2, 3$ . We refer the reader to the work of Zych *et al.* [59] for a more detailed discussion and reference to previous literature discussing the metric correction  $\hat{H}_{\text{metric}}$ .

As a consequence of the virial theorem, the metric correction (3.13) turns out to be purely off-diagonal in the basis of stationary states with respect to the internal Hamiltonian  $\hat{H}_{\text{int}}$  in Eq. (3.9). This can be inferred from the identity

$$\frac{i}{\hbar} [\hat{\mathbf{r}} \cdot \hat{\mathbf{p}}, H_{\text{int}}] = 2 \frac{\hat{\mathbf{p}}^2}{2\mu} + \frac{e_1e_2}{4\pi\epsilon_0} \frac{1}{\hat{r}} + \mathcal{O}(c^{-2}). \quad (3.15)$$

Since the average of the left-hand side with respect to eigenstates of  $\hat{H}_{\text{int}}$  vanishes, the same holds for the right-hand side and thus also for Eq. (3.13). Further constraints on the off-diagonal matrix elements can be concluded from noting that  $\hat{H}_{\text{metric}}$  is rotationally invariant. We do not go into further detail on this since the off-diagonal form of the metric term makes it ineffective as far as energy-nondegenerate states are concerned. For this case it can be neglected in a rotating wave approximation with corrections scaling as  $c^{-4}$ .

The second term describing the relativistic coupling of COM and internal DOF is

$$\hat{H}_{\text{mass defect}} = \left( M\phi(\hat{\mathbf{R}}) - \frac{\hat{\mathbf{P}}^2}{2M} \right) \otimes \frac{\hat{H}_{\text{int}}^{(0)}}{Mc^2}. \quad (3.16)$$

This can be interpreted as a result of the mass defect of the COM DOF due to the binding energy of the internal DOF. This interpretation is supported formally by the observation that, up to corrections of  $\mathcal{O}(c^{-4})$ , the term  $\hat{H}_{\text{mass defect}}$  can be absorbed in the COM Hamiltonian

$$\hat{H}_{\text{com}}(M) + \hat{H}_{\text{mass defect}} \simeq \hat{H}_{\text{com}}\left(M + \frac{\hat{H}_{\text{int}}}{c^2}\right). \quad (3.17)$$

We remind the reader that  $\hat{H}_{\text{com}}(M)$  is defined as a *function* of  $M$  in Eq. (3.5). Thus, the COM mass  $M$  is effectively replaced with  $M + \frac{\hat{H}_{\text{int}}}{c^2}$ , which is the so-called mass

defect correction, motivated in the literature through the equivalence between mass and energy. We note that the expression on the right-hand side of Eq. (3.17) is often used as a justification of the mass-defect term on the left-hand side, i.e., one usually states equivalence between mass and energy and substitutes the mass accordingly, as e.g., in the context of ion clocks [45–47]. We would like to stress that it is the left-hand side of Eq. (3.17) that justifies the right-hand side *to order*  $c^{-2}$ , which is derived *ab initio* from Eq. (3.1) following [50].

When  $\hat{\mathbf{A}}^\perp(\hat{\mathbf{R}}) = 0$ , an alternative and no less justified interpretation of  $\hat{H}_{\text{mass defect}}$  is that of a shift of the internal energies due to the gravitational redshift and due to the second-order Doppler effect, as is evident from

$$\hat{H}_{\text{int}} + \hat{H}_{\text{mass defect}} \simeq \hat{H}_{\text{int}} \otimes \left( 1 - \frac{\hat{\mathbf{V}}^2}{2c^2} + \frac{\phi(\hat{\mathbf{R}})}{c^2} \right), \quad (3.18)$$

up to  $\mathcal{O}(c^{-4})$ , where  $\hat{\mathbf{V}}$  corresponds to the velocity of the COM. These corrections are often added on a semiclassical basis as a result of time dilation when transforming from the COM rest frame to the laboratory frame [20]. We emphasize that the relativistic correction (3.16) thus accounts equally and fully for the time dilation due to the gravitational redshift and the second-order Doppler effect. This addresses one of the questions that we made ourselves at the beginning of the chapter, showing that the mass defect and time dilation are the same effect and one should not take it into account twice. Of course, we still need to answer the question if with previous approaches we were missing some other effects; we have not found new unexpected or relevant terms in the Hamiltonian so far, but to study the role of these corrections, one will need to properly describe the interrogation scheme and how the particle is trapped in a fully quantum manner. This will be the goal of the next section.

Before that, let us rewrite the interplay between the mass defect and the internal Hamiltonian in what will be a more useful form

$$\hat{H}_{\text{int}} + \hat{H}_{\text{mass defect}} \simeq \hat{H}_{\text{int}} \otimes \left( 1 + \frac{1}{c^2} \frac{\partial \hat{H}_{\text{com}}(M)}{\partial M} \right) = \frac{\hbar\omega_0}{2} \hat{\sigma}_z \otimes \left( 1 + \frac{\delta\hat{\nu}}{\nu_0} \right), \quad (3.19)$$

which is also valid in the presence of a magnetic vector potential. This equation clearly shows the effect of the coupling between internal and external degrees of freedom and it will be a useful form to work with. In the last step, we performed a two-level approximation by restricting the description to two stationary bound states  $|g\rangle$  and  $|e\rangle$  with (negative binding) energies  $h\nu_g$  and  $h\nu_e$ , respectively, and a transition frequency  $\omega_0 = 2\pi\nu_0 = 2\pi(\nu_e - \nu_g)$ . In these eigenstates and energies, we consider the relativistic

corrections from Eq. (3.11), and further relativistic corrections including spin, already included. We define the operator corresponding to the fractional frequency shift

$$\frac{\delta\hat{\nu}}{\nu_0} = \frac{1}{c^2} \frac{\partial \hat{H}_{\text{com}}(M)}{\partial M}, \quad (3.20)$$

and implicitly absorb a constant energy offset in the internal Hamiltonian. In the next section, we will show that relativistic corrections due to coupling of internal and external DOFs in precision spectroscopy and frequency metrology can be discussed entirely on the basis of the fractional frequency shift operator in Eq. (3.20).

### 3.3 Relativistic coupling of internal and external DOF in ion clocks

In this section, we consider an optical clock based on a single ion in a Paul trap. Treating this particular case, we should study the previous general Hamiltonian in a slightly different manner. We are dealing with a physical system, and therefore, it will have some physical constraints, which will make some terms irrelevant, either because they are null for that system or because they can be neglected. That means we have to apply the relativistically corrected Hamiltonian in Eq. (3.4) to the specific case of a charged composite particle subject to several external fields: first, an external time-dependent electric potential realizing the confinement  $\Phi(\hat{\mathbf{R}}, t)$ , second, a weak gravitational field  $\phi(\hat{\mathbf{R}})$ , and third, pulsed laser fields  $\mathbf{E}(\hat{\mathbf{R}}, t)$  driving the internal transition. In a Paul trap, there is no vector potential, so that we can replace  $\hat{\mathbf{P}}$  by  $\hat{\mathbf{P}}$  in Eq. (3.4) and, therefore, the point of view of Eq. (3.18), which supports the mass defect as that of a shift of the internal energies due to the gravitational redshift and the second-order Doppler effect, is valid. The resulting Hamiltonian for a Paul trap, including the relevant relativistic corrections is given by

$$\hat{H} = \hat{H}_{\text{com}}(M, t) + \frac{\hbar\omega_0}{2} \hat{\sigma}_z \left( 1 + \frac{\delta\hat{\nu}}{\nu_0} \right) - \hat{\mathbf{d}} \cdot \mathbf{E}(\hat{\mathbf{R}}, t), \quad (3.21)$$

where the fractional frequency shift is given in Eq. (3.20), and we collect all terms referring to the COM degree of freedom in

$$\hat{H}_{\text{com}}(M, t) = \frac{\hat{\mathbf{P}}^2}{2M} + M\phi(\hat{\mathbf{R}}) + Q\Phi(\hat{\mathbf{R}}, t). \quad (3.22)$$

Here, we neglect or suppress the following relativistic corrections: (i) Terms in Eq. (3.7) affecting the COM DOF only are negligible for the small COM velocities of a cold ion and will affect the internal DOF in  $\mathcal{O}(c^{-4})$  only. (ii) In contrast, the corresponding terms of the internal DOF in Eq. (3.11) are significant and contribute to its fine

structure. We consider these terms to be absorbed in the internal states and energies. (iii) The metric term in Eq. (3.13) is dropped in a rotating-wave approximation, as explained earlier. (iv) The Röntgen term in the atom-field interaction, Eq. (3.12), scales as  $\mathbf{P}/Mc$  and is negligible for a cold ion. Furthermore, it merely rescales the Rabi frequency of the pulses in a Ramsey interrogation (to be discussed in the next section) and will be compensated by their proper calibration.

### 3.3.1 Ramsey spectroscopy

Before treating fully quantum mechanically the trap configuration, we need to treat and understand the interrogation scheme in order to show that Eq. (3.20) is sufficient and complete to characterize the relativistic corrections in an ion clock. For frequency spectroscopy, we treat a Ramsey interrogation scheme [60], which amounts to a sequence of unitary evolutions  $|\psi_{\text{out}}\rangle = \hat{U}_R(\omega_L T_R) \hat{U}(T_R) \hat{U}_R(0) |\psi_{\text{in}}\rangle$ , where  $|\psi_{\text{out(in)}}\rangle$  is the final (initial) state of internal and external DOF. For now, we consider pure states without loss of generality. Here,  $\hat{U}_R(\varphi)$  denotes the unitary during a Ramsey laser pulse, where  $\varphi$  is the laser phase with respect to the atomic reference. Since such a pulse can be considered instantaneous compared to the duration  $T_R$  of the Ramsey interrogation time, relativistic corrections can be neglected during a Ramsey pulse. Therefore,  $\hat{U}_R(\varphi) = \exp(-i\frac{\pi}{2}(-\cos\varphi\hat{\sigma}_y + \sin\varphi\hat{\sigma}_x))$ , and the laser phase in the second Ramsey pulse is  $\varphi = \omega_L T_R$ , where  $\omega_L$  is the laser frequency. During Ramsey interrogation, the ion evolves in the dark according to  $\hat{U}(T_R) = \exp(-\frac{i}{\hbar}\hat{H}T_R)$  with the Hamiltonian in Eq. (3.21), where  $\mathbf{E}(\hat{\mathbf{R}}, t) = 0$  as there are no lasers during the interrogation time. This sequence is depicted on the Bloch sphere in Fig. 3.2.

At this point, one needs to be careful with how this sequence is evaluated and which assumptions can be made. In a Ramsey interrogation scheme, we will be interested in the variance of the inferred frequency deviation of the clock laser from the atomic reference  $(\Delta\omega)^2$ . After the second Ramsey pulse, the ion's internal state population  $\hat{\sigma}_z$  is measured with average  $\langle\sigma_z^{\text{out}}\rangle = \langle\psi_{\text{out}}|\hat{\sigma}_z|\psi_{\text{out}}\rangle$  and deviation  $\Delta\sigma_z^{\text{out}}$ . With these quantities we can evaluate

$$(\Delta\omega)^2 = \frac{(\Delta\sigma_z^{\text{out}})^2}{\left|\frac{\partial\langle\sigma_z^{\text{out}}\rangle}{\partial\omega}\right|^2}. \quad (3.23)$$

Therefore, we need to study the time evolution of the internal operators according to the Hamiltonian in Eq. (3.21), taking into account that during the free evolution time we have  $\mathbf{E}(\hat{\mathbf{R}}, t) = 0$ .

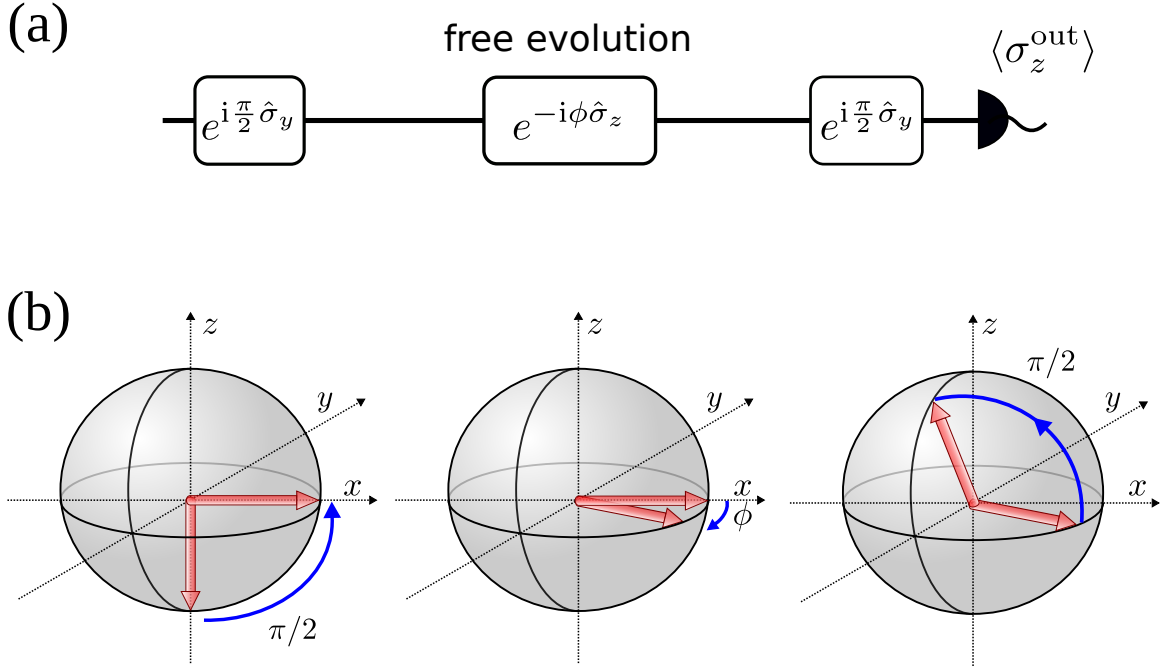


Figure 3.2: **Simple Ramsey interrogation scheme:** For clarity, we show in this figure the Ramsey interrogation scheme in a frame rotating around  $z$  with the laser frequency  $\omega_L$ . In a) we can see the series of transformations introduced in the main text, the two  $\pi/2$  rotations  $\hat{U}_R(0)$  and  $\hat{U}_R(\omega_L T_R)$  and the free evolution  $\hat{U}(T_R)$ , but now in the rotating frame and where we assumed the simplified case in which the free evolution corresponds to the Hamiltonian  $\hat{H} = \frac{\hbar\omega_0}{2}\hat{\sigma}_z$ , here  $\phi = (\omega_0 - \omega_L)T_R$ . At the end of the Ramsey sequence  $\langle\sigma_z\rangle$  is measured. In b) we see the representation of the Ramsey interrogation scheme on the Bloch sphere.

In the Heisenberg picture, the vector of Pauli operators  $\hat{\vec{\sigma}}$  evolves as

$$\frac{d}{dt}\hat{\vec{\sigma}}(t) = (\omega_0 + \delta\hat{\omega}(t)) \begin{pmatrix} 0 & 1 & 0 \\ -1 & 0 & 0 \\ 0 & 0 & 1 \end{pmatrix} \hat{\vec{\sigma}}(t), \quad (3.24)$$

where we define the mass-defect (time-dilation) shift operator in angular frequency

$$\delta\hat{\omega} = 2\pi\delta\hat{\nu}, \quad (3.25)$$

where  $\delta\hat{\nu}$  is defined in Eq. (3.20). The angular frequency fulfills

$$\frac{d}{dt}\delta\hat{\omega}(t) = -\frac{i}{\hbar}[\hat{H}_{\text{com}}, \delta\hat{\omega}(t)], \quad (3.26)$$

where  $\hat{H}_{\text{com}}$  is given in Eq. (3.22). The solution of this equation is denoted by  $\delta\hat{\omega}(t)$  and is independent of the internal DOFs.

We define a time-averaged frequency shift due to the mass-defect

$$\overline{\delta\hat{\omega}} = \frac{1}{T_R} \int_0^{T_R} dt \delta\hat{\omega}(t), \quad (3.27)$$

by which the Pauli vector at the end of the Ramsey sequence can be expressed in first order of the mass defect as

$$\hat{\sigma}(T_R) = R_z(\omega_0 T_R) \left[ 1 + T_R \overline{\delta\hat{\omega}} \begin{pmatrix} 0 & 1 & 0 \\ -1 & 0 & 0 \\ 0 & 0 & 1 \end{pmatrix} \right] \hat{\sigma}(0) \simeq R_z((\omega_0 + \overline{\delta\hat{\omega}}) T_R) \hat{\sigma}(0). \quad (3.28)$$

Here,  $R_z(\theta)$  is the matrix corresponding to a rotation around the  $z$  axis by an angle  $\theta$ . The last equivalence holds to first order in the mass defect and should be understood as short-hand notation for the previous equation.

The complete Ramsey sequence is given by

$$\begin{aligned} \hat{\sigma}_{\text{out}} &= \hat{U}_R^\dagger(0) \hat{U}^\dagger(T_R) \hat{U}_R^\dagger(\omega_L T_R) \hat{\sigma}_{\text{in}} \hat{U}_R(\omega_L T_R) \hat{U}(T_R) \hat{U}_R(0) \\ &= R_{\vec{n}}(\pi/2) R_z((\omega_0 + \overline{\delta\hat{\omega}}) T_R) R_{-y}(\pi/2) \hat{\sigma}_{\text{in}} \\ &= R_z(\omega_L T_R) R_{-y}(\pi/2) R_z((\omega_0 - \omega_L + \overline{\delta\hat{\omega}}) T_R) R_{-y}(\pi/2) \hat{\sigma}_{\text{in}}, \end{aligned} \quad (3.29)$$

where  $\vec{n} = -\cos(\omega_L T_R) \hat{\sigma}_y + \sin(\omega_L T_R) \hat{\sigma}_x$ . From here, we can now calculate Eq. (3.23). When taking averages, we assume an initial product state of internal and COM DOFs. Moreover, for the stationary COM states considered here, the time average of the mass defect Hamiltonian is irrelevant and can be dropped.

For repeated measurements at a particular value of the detuning  $\Delta_L = \omega_0 - \omega_L$ , the variance of the inferred frequency deviation of the clock laser from the atomic reference follows to be

$$(\Delta\omega)^2 = \frac{\cos^2 [(\Delta_L + \langle \delta\hat{\omega} \rangle) T_R] \Delta\sigma_z^2 + \sin^2 [(\Delta_L + \langle \delta\hat{\omega} \rangle) T_R] \Delta\sigma_y^2 + T_R^2 u^2 \sin^2 (\Delta_L T_R)}{\langle \sigma_z \rangle^2 T_R^2 \sin^2 [(\Delta_L + \langle \delta\hat{\omega} \rangle) T_R]}. \quad (3.30)$$

This formula generalizes Eq. (20) from Ref. [60] for the mass defect. We define the variance associated with the mass-defect operator  $u^2 = \langle \delta\hat{\omega}^2 \rangle - \langle \delta\hat{\omega} \rangle^2$ . Averages in Eq. (3.30) concerning the internal DOF are taken with respect to the initial state  $|\psi_{\text{in}}\rangle$ . We will first discuss the general scenario to not lose any insight and afterwards we will consider the case of standard Ramsey spectroscopy,  $\langle \sigma_z \rangle = -1$  and therefore  $\Delta\sigma_z^2 = 0$  and  $\Delta\sigma_y^2 = 1$ . Furthermore, the expression for the inferred frequency deviation holds in leading (quadratic) order of the mass-defect shift in both the numerator and denominator of Eq. (3.30). Averages of  $\hat{\omega}$  have to be understood with respect to the COM state, averaged over the interrogation time in the interaction picture with respect to the COM Hamiltonian, that is Eq. (3.22).

Equation (3.30) implies that the Ramsey resonance curve is shifted by  $\langle \delta\hat{\omega} \rangle$  and exhibits a projection noise slightly increased by

$$\frac{u \sin (\Delta_L T_R)}{\langle \sigma_z \rangle \sin [(\Delta_L + \langle \delta\hat{\omega} \rangle) T_R]} \simeq \frac{u}{\langle \sigma_z \rangle}, \quad (3.31)$$

where the last approximation is valid in first order of  $\langle \delta\hat{\omega} \rangle$ . Thus, to evaluate the magnitude and relevance of these effects, it is sufficient to consider the statistics of the operator corresponding to the fractional frequency shift in Eq. (3.20) with respect to a given COM state. This closes our discussion on how to properly treat the relativistic corrections and which terms one should take into account from the Hamiltonian. The next step will be to have a proper description of the trap. Additionally, to evaluate the average systematic frequency shift with respect to an eigenstate  $|\psi\rangle$  of the COM Hamiltonian with eigenenergy  $E_\psi(M)$ , we can use the Feynman-Hellmann theorem, which states

$$\left\langle \frac{\delta\hat{\nu}}{\nu_0} \right\rangle_\psi = \frac{1}{c^2} \frac{\partial E_\psi(M)}{\partial M}. \quad (3.32)$$

Of course, in the context of quasieigenstates we will have to adapt the previous theorem for the extended Hilbert space as shown in Eq. (2.52). Nevertheless, after treating in the next subsection the ion trap quantum mechanically, we will show that Eq. (3.32) is not needed, although it will be useful to use as a reference to compare with.

### 3.3.2 Quantum theory of an ion trap

In order to rigorously discuss the statistics of the fractional frequency shift, we are going to make an introduction to the quantum theory of an ideal Paul trap. For this purpose, we will closely follow the notation of Leibfried *et al.* [7] and we will adapt the quantum mechanical treatment by Glauber [6]. Further below, we will consider also corrections to the potentials in an ideal Paul trap (such as spurious dc electric fields and gravitational sag).

Before starting with the actual expression of the trap potentials, it is relevant to introduce the important concepts of micromotion and excess micromotion. Due to the Laplace equation, we cannot have a static confinement in three orthogonal directions, therefore, in a Paul trap the confinement is achieved by having a static confinement in one direction and a time-dependent confinement in the other two that will, on average, confine the particle, as will be shown below. The effect of this time-dependent confinement moving the particle is what we simply refer to as micromotion. If one considers some spurious dc field present in the trap, or equivalently that the confinement is not quadratic but also has a linear contribution, the so-called excess micromotion will be generated.

The potentials of a Paul trap contain direct current and alternating current (ac) components  $\Phi(\hat{\mathbf{R}}, t) = \Phi_{\text{dc}}(\hat{\mathbf{R}}) + \Phi_{\text{ac}}(\hat{\mathbf{R}}, t)$ , which at the trap center have the form of

quadrupole fields

$$\Phi_{\text{dc}}(\hat{\mathbf{R}}) + \Phi_{\text{ac}}(\hat{\mathbf{R}}, t) = \frac{1}{2}\hat{\mathbf{R}}^T U \hat{\mathbf{R}} + \frac{1}{2}\cos(\Omega t)\hat{\mathbf{R}}^T \tilde{U} \hat{\mathbf{R}}. \quad (3.33)$$

Here,  $\Omega$  corresponds to the trap frequency.  $U$  and  $\tilde{U}$  are in general symmetric traceless matrices representing the dc and ac components of the quadrupole field tensors, respectively. For an ideal trap geometry they are diagonal,  $U = U_0 \text{diag}(\alpha_1, \alpha_2, \alpha_3)$  and  $\tilde{U} = \tilde{U}_0 \text{diag}(\alpha'_1, \alpha'_2, \alpha'_3)$ , with dimensionless coefficients  $\alpha_i$  and  $\alpha'_i$ . The resulting COM Hamiltonian (neglecting gravity for the moment)

$$\hat{H}_{\text{com}}(M, t) = \frac{\hat{\mathbf{P}}^2}{2M} + Q\Phi(\hat{\mathbf{R}}, t) \quad (3.34)$$

is explicitly time dependent and periodic with period  $T = 2\pi/\Omega$ . We assume a stable trap configuration, which supports quasistationary eigenenergy states  $|\mathbf{n}, t\rangle$  satisfying the generalized eigenvalue problem discussed in Sec. 2.4.2, i.e.,

$$\left(\hat{H}_{\text{com}}(M, t) - i\hbar\partial_t\right)|\mathbf{n}, t\rangle = E_{\mathbf{n}}(M)|\mathbf{n}, t\rangle. \quad (3.35)$$

The states  $|\mathbf{n}, t\rangle$ , labeled by  $\mathbf{n} = (n_1, n_2, n_3)$ , are  $T$ -periodic Fock states whose time dependence accounts for the micromotion.

Let us remind the reader a few notions discussed in chapter 2. In the following, it will be important to note that the generalized Hamiltonian on the left-hand side of Eq. (3.35) has to be considered as acting on an enlarged Hilbert space  $\mathcal{H}_T = L_2(\mathbb{R}^3) \otimes \mathcal{T}$ , where  $\mathcal{T}$  is the space of  $T$ -periodic functions of time. We take care to construct the quasienergy eigenstates  $|\mathbf{n}, t\rangle$  within this space.

In an ideal case, the potentials in the Paul trap are separable, therefore it is sufficient to discuss the one-dimensional problem. We will follow the treatment of Glauber [6], which is summarized in [7]. The main deviation from these treatments is that we strive to identify  $T$ -periodic creation and annihilation operators in order to ensure that all states are elements of the enlarged Hilbert space  $\mathcal{H}_T$ .

We consider the (zeroth-order) Hamiltonian

$$\hat{H}^{(0)}(t) = \frac{\hat{P}^2}{2m} + \frac{m}{2}W(t)\hat{X}^2, \quad (3.36)$$

with a real periodic function  $W(t+T) = W(t)$ . Specifically, we have  $W(t) = \frac{\Omega^2}{4}(\mathbf{a} - 2\mathbf{q}\cos(\Omega t))$ , where  $\mathbf{a}_i(M) = \frac{4QU_0\alpha_i}{M\Omega^2}$  and  $\mathbf{q}_i(M) = \frac{2Q\tilde{U}_0\alpha'_i}{M\Omega^2}$  denote the so-called Mathieu parameters, but we only wrote them in the one-dimensional case so we can drop the index  $i$ . Here, we generalized the trapping potential contribution to the COM Hamiltonian in Eq. (3.34) in a way that is easier to work with. If we combine



the equations of motion of the operators  $\hat{X}$  and  $\hat{P}$  in the Heisenberg picture, we obtain

$$\ddot{\hat{X}}(t) = -W(t)\hat{X}(t). \quad (3.37)$$

We will solve this equation by replacing the operator with a time-dependent function  $u(t)$ , i.e.,  $\ddot{u}(t) = -W(t)u(t)$ , this will allow us to find a solution for the operator  $\hat{X}$ . By the Floquet theorem, solutions can be constructed of the form

$$u(t) = e^{i\omega t}v(t), \quad (3.38)$$

where  $0 \leq \omega < \Omega$  and  $v(t+T) = v(t)$ . Following [7], we write this as  $\omega = \frac{\beta\Omega}{2}$  and  $v(t) = \sum_{n=-\infty}^{\infty} C_{2n}e^{in\Omega t}$ . Inserting Eq. (3.38) into Eq. (3.37) allows us to calculate the real-valued coefficients  $\beta$  and  $C_{2n}$  with the following recursion relations

$$C_{2n+2} + C_{2n-2} - \frac{1}{\mathbf{q}}(\mathbf{a} - (2n + \beta)^2)C_{2n} = 0. \quad (3.39)$$

We also adopted the normalization condition

$$u(0) = \sum_n C_{2n} = 1, \quad (3.40)$$

which implies for the time derivative

$$\dot{u}(0) = i\nu \quad \text{and} \quad \nu = \Omega \sum_n C_{2n}(\beta/2 + n). \quad (3.41)$$

With  $u(t)$ , also  $u^*(t)$  is a linearly independent solution, which is likewise assumed to be normalized  $u^*(0) = 1$ , so that  $\dot{u}^*(0) = -i\nu$ . The Wronskian  $w = u(t)\dot{u}^*(t) - u^*(t)\dot{u}(t)$  is time independent, since  $\dot{w} = u(t)\ddot{u}^*(t) - u^*(t)\ddot{u}(t) = -W(t)u(t)u^*(t) + W(t)u^*(t)u(t) = 0$ . Thus,  $w = u(0)\dot{u}^*(0) - u^*(0)\dot{u}(0)$  is fixed by the initial conditions for the linearly independent solutions in  $u(t)$  and  $u^*(t)$ . For the specific choice made above, we thus have for all times

$$u(t)\dot{u}^*(t) - u^*(t)\dot{u}(t) = -2i\nu. \quad (3.42)$$

Thanks to these relations, and assuming  $C_{\pm 4} \approx 0$ , we can find in lowest order of the Mathieu parameters, i.e.,  $|\mathbf{a}|, \mathbf{q}^2 \ll 1$ ,

$$\beta \simeq \sqrt{\mathbf{a} + \frac{\mathbf{q}^2}{2}}, \quad v(t) \simeq \frac{1 + \frac{\mathbf{q}}{2} \cos(\Omega t)}{1 + \frac{\mathbf{q}}{2}}, \quad \nu \simeq \omega.$$

Based on this solution, we define the explicitly time-dependent operator (in the Schrödinger picture)

$$\hat{a}(t) = \frac{ie^{-i\omega t}}{\sqrt{2\hbar m\nu}} \left( u(t)\hat{P} - m\dot{u}(t)\hat{X} \right), \quad (3.43)$$

which effectively depends on the functions  $v(t)$  and  $\dot{v}(t)$  only, and therefore, is by construction periodic in time with period  $T$ . Note that for  $t = 0$  this corresponds to the expression for the annihilation operator for a harmonic oscillator with frequency  $\nu$ , that is,  $\hat{a}(0) = \sqrt{\frac{m\nu}{2\hbar}}\hat{X} + i\frac{1}{\sqrt{2\hbar m\nu}}\hat{P}$ . Now we need to show that this  $T$ -periodic operator in Eq. (3.43) plays an equivalent role to the annihilation operator in a harmonic oscillator for our  $T$ -periodic Hamiltonian. This will allow us to write any function of the position and momentum operators in terms of  $a$  and  $a^\dagger$ , and therefore, calculate their expectation values and variances. We will see that this will be crucial for discussing the effect of the mass defect on the performance of the clock.

Due to the constant value of the Wronskian (3.42),  $\hat{a}(t)$  and its adjoint operator  $\hat{a}^\dagger(t)$  satisfy bosonic commutation relations at equal times  $[\hat{a}(t), \hat{a}^\dagger(t)] = 1$ . The operator  $\hat{a}(t)$  has a unique (up to a global phase) eigenstate  $|0, t\rangle$  of eigenvalue 0,  $\hat{a}(t)|0, t\rangle = 0$ , which can be constructed by projecting this equation into the position representation

$$(i\hbar u(t)\partial_x + m\dot{u}(t)x) \langle x|0, t\rangle = 0, \quad (3.44)$$

giving the normalized solution

$$\langle x|0, t\rangle = \left(\frac{m\nu}{\pi\hbar}\right)^{1/4} \frac{e^{i\omega t/2}}{u(t)^{1/2}} \exp\left[\frac{im}{2\hbar} \frac{\dot{u}(t)}{u(t)} x^2\right] \quad (3.45)$$

$$= \left(\frac{m\nu}{\pi\hbar}\right)^{1/4} \frac{1}{v(t)^{1/2}} \exp\left[-\frac{\omega m}{2\hbar} \left(1 - \frac{i}{\omega} \frac{\dot{v}(t)}{v(t)}\right) x^2\right]. \quad (3.46)$$

The global phase in (3.45) is chosen to make the state  $|0, t\rangle$  periodic with period  $T$  and have  $|0, t\rangle \in \mathcal{T} \otimes \mathcal{H}$ . This is made to assure that all states are elements of the enlarged Hilbert space  $\mathcal{H}_T$ . The periodicity is evident in the second line. Using Eq. (3.45), it can be shown by direct calculation that

$$\left(\hat{H}^{(0)}(t) - i\hbar\partial_t\right) |0, t\rangle = E_0 |0, t\rangle, \quad E_0 = \frac{\hbar\omega}{2}. \quad (3.47)$$

We easily verify that the creation and annihilation operators satisfy eigenoperator equations with respect to the generalized Hamiltonian, i.e.,

$$\left[\hat{H}^{(0)}(t) - i\hbar\partial_t, \hat{a}(t)\right] = -\hbar\omega\hat{a}(t), \quad (3.48a)$$

$$\left[\hat{H}^{(0)}(t) - i\hbar\partial_t, \hat{a}^\dagger(t)\right] = \hbar\omega\hat{a}^\dagger(t). \quad (3.48b)$$

The bosonic commutation relation and the commutators in (3.48) are identical to those of a time-independent harmonic oscillator. Thus, the same algebra used there can be applied here to show that

$$\left(\hat{H}^{(0)}(t) - i\hbar\partial_t\right) |n, t\rangle = E_n |n, t\rangle, \quad (3.49)$$

$$E_n = \hbar\omega\left(n + \frac{1}{2}\right), \quad |n, t\rangle = \frac{1}{\sqrt{n!}} (a^\dagger(t))^n |0, t\rangle. \quad (3.50)$$

As mentioned before, it is crucial to construct the annihilation operators to be  $T$  periodic, as otherwise, the Fock states would not be proper elements of  $\mathcal{H}_T$ . Note that the quasienergy eigenvalues should respect  $E_n < \hbar\Omega$ , which will be violated for some  $n$ . However, for the physically relevant case where  $\omega \ll \Omega$ , that is,  $\beta \ll 1$ , this is of no concern practically.

Therefore, considering the three space directions, each variable and parameter gets an index  $i$  and the corresponding eigenenergies of Eq.(3.35) are

$$E_{\mathbf{n}}(M) = \sum_{i=1}^3 \hbar\omega_i(M) \left(n_i + \frac{1}{2}\right), \quad (3.51)$$

where now we highlighted the mass dependence of the motional eigenfrequencies, or trapping frequencies  $\omega_i(M) = \frac{\Omega\beta_i(M)}{2}$ , as remember  $\beta_i^2(M) \simeq \mathbf{a}_i(M) + \frac{\mathbf{q}_i^2(M)}{2}$  and the dimensionless Mathieu parameters are  $\mathbf{a}_i(M) = \frac{4QU_0\alpha_i}{M\Omega^2}$  and  $\mathbf{q}_i(M) = \frac{2Q\tilde{U}_0\alpha'_i}{M\Omega^2}$  in lowest order  $|\mathbf{a}_i|, \mathbf{q}_i^2 \ll 1$ .

When evaluating the effects of relativistic corrections, it will be necessary to calculate matrix elements of  $T$ -periodic operators with respect to  $T$ -periodic states. The corresponding scalar products have to be understood within the enlarged Hilbert space  $\mathcal{H}_T$ , and therefore involve a time average over one period  $T$  as explained in chapter 2. As a reminder, the average of an operator  $A(t)$  with respect to a state  $|\psi\rangle \in \mathcal{H}_T$  has to be understood as

$$\langle\langle A \rangle\rangle_\psi = \frac{1}{T} \int_0^T dt \langle\psi(t)|A(t)|\psi(t)\rangle, \quad (3.52)$$

where  $\langle\psi(t)|A(t)|\psi(t)\rangle$  is the average value in  $L_2(\mathbb{R}^3)$ .

### 3.3.3 Fractional frequency shift due to mass defect: Second-order Doppler effect

We are now ready to evaluate the fractional frequency shift (3.20) due to the mass defect for a given COM state. Here, we will consider in particular Fock states  $|\mathbf{n}, t\rangle$

and thermal mixtures of Fock states at (pseudo)temperatures  $T_i$  for motion along axis  $i$ . However, as we were able to find the creation and annihilation operators, the treatment is general and can be applied just as well to any other quantum state. In view of Eqs. (3.34) and (3.20), the fractional frequency shift of a trapped ion is entirely due to its kinetic COM energy since

$$\frac{\delta\hat{\nu}}{\nu_0} = -\frac{\hat{K}}{Mc^2}, \quad \hat{K} = \frac{\hat{\mathbf{P}}^2}{2M}. \quad (3.53)$$

Remember at this stage that we are treating first the case with no gravitational sag and a perfect quadratic potential for the trap. The operator for the kinetic energy can be expressed in terms of creation and annihilation operators by inversion of Eq. (3.43). In this way, mean values and uncertainties can be easily evaluated, and the only integrals that remain to be calculated are those over the period  $T$  of micromotion.

For the average fractional shift due to a COM Fock state  $|\mathbf{n}, t\rangle$ , the Feynman-Hellmann theorem can be applied. With Eqs. (3.32) and (3.51) we find

$$\left\langle\left\langle \frac{\delta\hat{\nu}}{\nu_0} \right\rangle\right\rangle_{\mathbf{n}} = \frac{1}{c^2} \frac{\partial E_{\mathbf{n}}(M)}{\partial M} = -\sum_{i=1}^3 \frac{\hbar\omega_i(n_i + \frac{1}{2})}{2Mc^2} \left(1 + \frac{\mathbf{q}_i^2}{2\mathbf{a}_i + \mathbf{q}_i^2}\right), \quad (3.54)$$

in leading order of  $\mathbf{a}_i$  and  $\mathbf{q}_i^2$ . In evaluating this and similar expressions, it is necessary to deal with fractions of polynomials in  $\mathbf{a}_i$  and  $\mathbf{q}_i$ . To simplify these expressions, we associated a small parameter  $\epsilon$  via the substitutions  $\mathbf{a}_i \rightarrow \epsilon^2\mathbf{a}_i$  and  $\mathbf{q}_i \rightarrow \epsilon\mathbf{q}_i$ , assuming  $\mathbf{q}_i^2, |\mathbf{a}_i| \ll 1$ . Finally, we performed a Taylor expansion of the rational function in terms of  $\epsilon$  and maintained the relevant contributions.

In Eq.(3.54), the first term corresponds to the secular motion and the last one to the micromotion. The fractional frequency shift for a thermal state with average occupation numbers  $\bar{\mathbf{n}} = (\bar{n}_1, \bar{n}_2, \bar{n}_3)$  will have the same form as Eq. (3.54), where the Fock state number  $n_i$  is replaced by  $\bar{n}_i = 1/(\exp(\frac{\hbar\omega_i}{k_B T_i}) - 1)$ . In the high-temperature limit, we can approximate  $\bar{n}_i \approx \frac{k_B T_i}{\hbar\omega_i}$ , so that we arrive at

$$\left\langle\left\langle \frac{\delta\hat{\nu}}{\nu_0} \right\rangle\right\rangle_{\bar{\mathbf{n}}} = -\sum_{i=1}^3 \frac{k_B T_i}{Mc^2} \frac{\mathbf{a}_i + \mathbf{q}_i^2}{2\mathbf{a}_i + \mathbf{q}_i^2}. \quad (3.55)$$

This recovers the result of Berkeland *et al.* [35] (cf. the first term on the right-hand side of Eq.(30)) on the second-order Doppler (time-dilation) shift for a thermal state. In the opposite limit  $k_B T_i \ll \hbar\omega_i$ , zero-point fluctuations in both secular and micromotion in the quantum ground state still cause a fractional shift, as follows from Eq. (3.54) for  $n_i = 0$ . Calculating the average of Eq. (3.53) directly, that is

$\langle\langle \delta\hat{\nu}/\nu_0 \rangle\rangle = -\langle\langle \hat{K} \rangle\rangle/Mc^2$ , using the algebra of creation and annihilation operators defined in Eq. (3.43) yields the same result in leading order of  $\mathbf{a}_i$  and  $\mathbf{q}_i^2$ .

So far, we have considered an ideal quadrupole potential for the trap in the form of Eq. (3.33). In reality, various deviations from this ideal geometry will occur and impact the second-order Doppler shift. In the following sections we will consider additional linear potentials due to uncompensated dc electric fields (Sec. 3.3.5) and gravity (Sec. 3.3.6) as well as their variances (Sec. 3.3.7). Afterwards we will also consider spurious electric quadrupole fields or trap imperfections (Sec. 3.3.8).

### 3.3.4 Ion trap with a linear potential

Linear potentials can be included in several ways. In this section, we examine how the annihilation and creation operators change under such a potential. Afterwards, the averages of these operators will be used to calculate the fractional frequency shift. A linear potential can also be included by solving the appropriate Mathieu equation. This approach will be more useful if one wishes to use the Feynman-Hellmann theorem and is discussed over the next sections and solved in Appendix C.

In order to study both the cases of dc forces and gravity, we will now consider a trap with a general linear potential  $-F\hat{X}$  such that the generalized Hamiltonian is

$$\hat{H}(t) = \hat{H}^{(0)} - F\hat{X} - i\hbar\partial_t, \quad (3.56)$$

where  $\hat{H}^{(0)}$  corresponds to the Hamiltonian in Eq. (3.36). By studying this general case, we will be able to treat the effect of gravity and the spurious dc field.

We seek operators of the form

$$\hat{b}(t) = \hat{a}(t) + \alpha(t), \quad (3.57)$$

which fulfill the eigenoperator equation  $[\hat{H}(t), \hat{b}(t)] = -\hbar\bar{\omega}\hat{b}(t)$ , with a  $T$ -periodic function  $\alpha(t)$  and a new eigenfrequency  $\bar{\omega}$ , which is to be determined. In order for  $\alpha(t)$  not to be an operator, one finds that  $\bar{\omega} = \omega$ . Therefore,  $\alpha(t)$  needs to obey the differential equation

$$\dot{\alpha}(t) + i\omega\alpha(t) = -\frac{iFe^{-i\omega t}u(t)}{\sqrt{2\hbar m\nu}} = -\frac{iFv(t)}{\sqrt{2\hbar m\nu}}. \quad (3.58)$$

Imposing  $T$  periodicity on  $\alpha(t)$ , we find in lowest order of the Mathieu parameters

$$\alpha(t) = -\frac{F}{\sqrt{2\hbar m\omega}} \left[ \frac{\omega}{\omega^2 - \Omega^2} e^{-i\omega t} u(t) - \frac{1}{1 + \frac{q}{2}} \frac{1}{\omega(\omega^2 - \Omega^2)} \left( \Omega^2 + i\frac{q}{2}\omega\Omega \sin(\Omega t) \right) \right], \quad (3.59)$$

where we used that in lowest-order approximation of the Mathieu parameters  $\nu \sim \omega$ . With this solution, we have determined the eigenoperator of the trap potential including a linear force. Again, this formalism needs to be applied for each Cartesian direction  $i$ , where we need to use the replacement  $F \rightarrow F_i$  and  $\omega \rightarrow \omega_i = \beta_i \Omega/2$ .

### 3.3.5 Fractional frequency shift due to dc forces and excess micromotion

Here, we consider an additional linear dc electric potential due to uncompensated stray fields [35], causing the so-called excess micromotion. We include such a spurious potential by adding to the COM Hamiltonian a perturbation

$$\hat{H}_{\text{dc}} = -QE_{\text{dc}} \cdot \hat{\mathbf{R}}, \quad (3.60)$$

where  $\mathbf{E}_{\text{dc}} = (E_{\text{dc},1}, E_{\text{dc},2}, E_{\text{dc},3})$  is the dc electric field at the trap center.

From a theoretical point of view this is equivalent to considering a non-perfect quadrupole potential for the trap and the so-called spurious dc field will just be the linear part of the real potential of the trap. We will comment more on this equivalence when we consider additional quadrupole fields or, equivalently, imperfections of the trap.

This problem can still be solved exactly. Just as in the previous sections, we assume a stable trap configuration that supports quasistationary eigenenergy states  $|\mathbf{n}, t\rangle_{\text{dc}}$  satisfying the generalized eigenvalue problem

$$\left( \hat{H}_{\text{com}}(M, t) - i\hbar\partial_t + \hat{H}_{\text{dc}} \right) |\mathbf{n}, t\rangle_{\text{dc}} = E_{\mathbf{n}}^{\text{dc}}(M) |\mathbf{n}, t\rangle_{\text{dc}}. \quad (3.61)$$

By adding Eq. (3.59) to the annihilation operators in Eq. (3.43) and considering the substitution  $F_i \rightarrow QE_{\text{dc},i}$ , we derive the modified annihilation operators generating the Fock states  $|\mathbf{n}, t\rangle_{\text{dc}}$ . The modified eigenenergies are  $E_{\mathbf{n}}^{\text{dc}}(M) = E_{\mathbf{n}}(M) + E_{\text{dc}}(M)$ , where the energy correction due to the dc field does not depend on the Fock number  $\mathbf{n}$ , and is given by

$$E_{\text{dc}}(M) = - \sum_{i=1}^3 \frac{4E_{\text{dc},i}^2 Q^2}{M(2\mathbf{a}_i(M) + \mathbf{q}_i^2(M))\Omega^2}. \quad (3.62)$$

We note that this result can also be found in different ways, the first one is to solve the new equation of motion generated in terms of a modified Mathieu equation, we will show this way in Appendix C for the joint case of a spurious dc field and a gravity contribution as well as considering imperfections of the trap. Another method consists of accounting for the perturbation in Eq. (3.60) in second-order perturbation theory. This is because the perturbation (3.60) is time independent and linear in position and

the unperturbed Hamiltonian is quadratic in position and momentum. Therefore, the exact energy eigenstates are suitably displaced Fock states and the quasienergies will be shifted by a constant quadratic term in the perturbation. Of course, another way of treating this would rely on using our generalized creation and annihilation operators.

Thus, the dc electric field causes a fractional frequency shift due to the excess micromotion that can be evaluated as before using the Feynman-Hellmann theorem. On top of the thermal shift in Eq. (3.54), the dc field adds a shift

$$\left\langle\left\langle \frac{\delta\hat{\nu}}{\nu_0} \right\rangle\right\rangle_{\text{dc}} = \frac{1}{c^2} \frac{\partial E_{\text{dc}}(M)}{\partial M} = - \sum_{i=1}^3 \left( \frac{2\mathbf{q}_i E_{\text{dc},i} Q}{Mc(2\mathbf{a}_i + \mathbf{q}_i^2)\Omega} \right)^2, \quad (3.63)$$

and again reproduces the result of Berkeland *et al.* [35]. Here, we have used the notation  $\left\langle\left\langle \right\rangle\right\rangle_{\text{dc}}$ , which emphasizes that the contribution is the same for all Fock states, independent of the index  $\mathbf{n}$ . The fractional frequency shift of a trapped ion in this case is still entirely due to its kinetic COM energy, as shown in Eq. (3.53). With the modified creation and annihilation operators one can easily verify Eq. (3.63) via  $\left\langle\left\langle \delta\hat{\nu}/\nu_0 \right\rangle\right\rangle = -\left\langle\left\langle \hat{K} \right\rangle\right\rangle/Mc^2$  in leading order of  $\mathbf{a}_i$  and  $\mathbf{q}_i^2$ .

### 3.3.6 Fractional frequency shift due to gravity

In this section, we consider a contribution to the fractional frequency shift due to an interplay between position fluctuations and gravitational redshift, as discussed in [47]. The coupling to the gravitational field is described by adding to the COM Hamiltonian

$$\hat{H}_g = M\phi(\hat{\mathbf{R}}), \quad (3.64)$$

where we approximate the gravitational potential in linear order  $\phi(\hat{\mathbf{R}}) = \phi_0 + \mathbf{g} \cdot \hat{\mathbf{R}}$ . Here,  $\phi_0$  is the gravitational potential at the trap center, and  $\mathbf{g} = (g_1, g_2, g_3)$ . In this linear approximation, the effect of gravity can again be considered with the accordingly modified creation operators, cf. Eq. (3.59) with the substitution  $F_i \rightarrow -g_i M$ .

Including gravity, the fractional frequency shift of a trapped ion is due to both, its kinetic COM energy and the contribution due to gravity. Therefore, gravity adds a shift

$$\frac{\delta\hat{\nu}}{\nu_0} = -\frac{\hat{K}}{Mc^2} + \frac{\phi_0 + \mathbf{g} \cdot \hat{\mathbf{R}}}{c^2}. \quad (3.65)$$

This follows from Eqs. (3.20), (3.34), and (3.64). In this case, we can write the fractional frequency shift as  $\left\langle\left\langle \frac{\delta\hat{\nu}}{\nu_0} \right\rangle\right\rangle = \left\langle\left\langle \frac{\delta\hat{\nu}}{\nu_0} \right\rangle\right\rangle_{\mathbf{n}} + \left\langle\left\langle \frac{\delta\hat{\nu}}{\nu_0} \right\rangle\right\rangle_{\mathbf{g}}$ , where the first contribution is

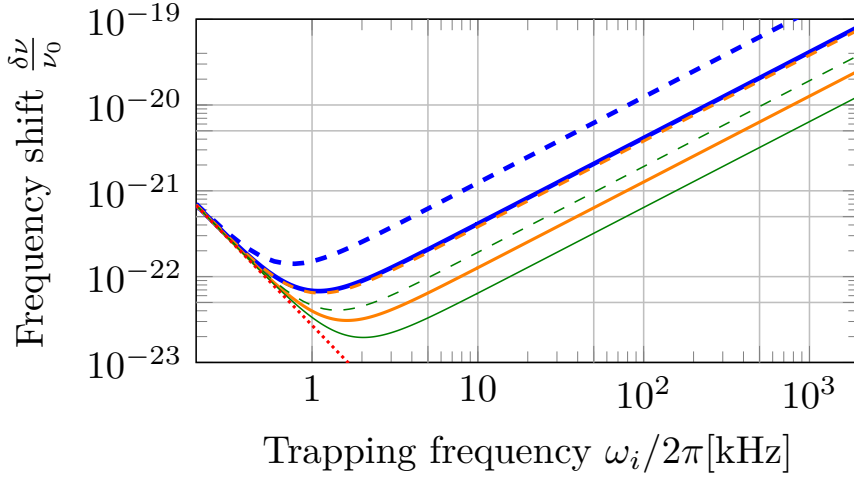


Figure 3.3: Redshift  $\frac{g^2}{\omega_i^2 c^2}$  (red dotted line) and total fractional frequency shift, i.e., redshift plus second-order Doppler shift  $\frac{\hbar\omega_i(\bar{n}+1/2)}{2Mc^2}$ , for  $\bar{n} = 0$  (solid lines) and  $\bar{n} = 1$  (dashed lines) for  $\text{Al}^+$  (thick blue lines),  $\text{Yb}^+$  (thin green lines), and neutral Sr (thick orange lines) versus trapping frequency  $\omega_i$ . Here, we considered for simplicity a static confinement  $\mathbf{q}_i = 0$ .

given in Eq. (3.54) and

$$\left\langle\left\langle \frac{\delta\hat{\nu}}{\nu_0} \right\rangle\right\rangle_{\mathbf{g}} = -\sum_{i=1}^3 \frac{4\mathbf{a}_i + 3\mathbf{q}_i^2}{4\mathbf{a}_i + 2\mathbf{q}_i^2} \frac{g_i^2}{\omega_i^2 c^2} + \frac{\phi_0}{c^2}. \quad (3.66)$$

Here, we have used the notation  $\langle\langle \rangle\rangle_{\mathbf{g}}$ , which emphasizes that the contribution is the same for all Fock states, independent of the index  $\mathbf{n}$  and dependent on gravity. Due to the linearity in  $\hat{\mathbf{R}}$  of the second term in Eq. (3.65), this shift affects all Fock states in the same way and is therefore independent of temperature for thermal states. In the case of a dc harmonic confinement,  $\mathbf{q}_i \rightarrow 0$ , and neglecting the background redshift,  $\phi_0 = 0$ , we recover the result of Haustein *et al.* [47].

It is noteworthy that the fractional frequency shift due to the kinetic energy (3.54) grows linearly with the trapping frequency (corresponding to an increased kinetic energy for tighter trapping), while the trap-dependent contribution due to gravity (3.66) decreases quadratically with the trap frequency due to a decreased fluctuation in position and therefore also in potential energy. The trade-off with respect to the trap frequency has been discussed and optimized by Haustein *et al.* [47] in order to minimize the fractional frequency shift for the case of a harmonic dc potential. For the parameter regime of a conventional ion trap, the redshift term (3.66) will be smaller than the second-order Doppler shift (3.54), see Fig. (3.3).

With the present formulae, it is straightforward to extend this discussion to account for micromotion. For that we will first write together the contribution from the



redshift and the second-order Doppler shift, convening Eqs. (3.54) and (3.66), and neglecting the background redshift,

$$\left\langle\left\langle\frac{\delta\hat{\nu}}{\nu_0}\right\rangle\right\rangle_{\mathbf{n}} = -\sum_{i=1}^3 \left( \frac{\hbar\omega_i(n_i + \frac{1}{2})}{2Mc^2} \left( 1 + \frac{\mathbf{q}_i^2}{2\mathbf{a}_i + \mathbf{q}_i^2} \right) + \frac{4\mathbf{a}_i + 3\mathbf{q}_i^2}{4\mathbf{a}_i + 2\mathbf{q}_i^2} \frac{g_i^2}{\omega_i^2 c^2} \right). \quad (3.67)$$

This expression can be minimized in the direction  $i$  obtaining a minimum value for a trapping frequency

$$\omega_i = \left( \frac{g_i^2 M (4\mathbf{a}_i + 3\mathbf{q}_i^2)}{\hbar(n + \frac{1}{2})(\mathbf{a}_i + \mathbf{q}_i^2)} \right)^{1/3}, \quad (3.68)$$

where again, if we study the case of a dc harmonic confinement,  $\mathbf{q}_i \rightarrow 0$ , we recover the result from Haustein *et al.* [47]. Unfortunately, as mentioned before, for the parameter regime of a conventional ion trap, the second-order Doppler effect is the relevant contribution.

The results from the two previous sections can be easily combined to take into account both the dc forces and gravity, which will lead to some cross terms between the two effects

$$\left\langle\left\langle\frac{\delta\hat{\nu}}{\nu_0}\right\rangle\right\rangle = \left\langle\left\langle\frac{\delta\hat{\nu}}{\nu_0}\right\rangle\right\rangle_{\mathbf{n}} + \sum_{i=1}^3 \frac{8g_i(QE_{\text{dc},i} - Mg_i)}{M\Omega^2 c^2 (2\mathbf{a}_i + \mathbf{q}_i^2)} - \left( \frac{2(QE_{\text{dc},i} - Mg_i)\mathbf{q}_i}{Mc(2\mathbf{a}_i + \mathbf{q}_i^2)\Omega} \right)^2. \quad (3.69)$$

With this final expression, we characterize the fractional frequency shift with every relativistic correction.

### 3.3.7 Variance of the fractional frequency shift

In the preceding section, we considered the *average* fractional frequency shift that enters the inferred frequency deviation in Eq. (3.30) as a systematic shift of the Ramsey resonance curves. Now we will address the role of the *uncertainty* in the frequency shift  $u^2 = \langle\delta\hat{\omega}^2\rangle - \langle\delta\hat{\omega}\rangle^2$ , which has been suggested [48] to pose a fundamental limitation to the precision of an optical clock. The fractional frequency shift, if characterized properly, can be accounted for as a shift for the clock signal, but the variance of that fractional frequency shift describes the quantum fluctuations of that shift, and therefore, it can bring a fundamental limitation. For the case of standard Ramsey interrogation (where  $\langle\sigma_z\rangle = -1$ , and therefore,  $\Delta\sigma_z^2 = 0$  and  $\Delta\sigma_y^2 = 1$ ) and taking into account  $N$  independent interrogations, Eq. (3.30) can be rewritten for the inferred relative frequency deviation

$$\left( \frac{\Delta\omega}{\omega_0} \right)^2 = \frac{1}{N} \left( \frac{1}{\omega_0^2 T_R^2} + \frac{u^2}{\omega_0^2} \right), \quad (3.70)$$

which holds to leading order in  $u^2$ . The first term on the right-hand side is the projection noise and the second term accounts for the variance of the fractional frequency shift due to the mass defect.

By means of the ladder operators (3.43), it is straightforward to evaluate the latter, and we find for a thermal COM state

$$\frac{u^2}{\omega_0^2} = \frac{\langle\langle \hat{K}^2 \rangle\rangle_{\mathbf{n}} - \langle\langle \hat{K} \rangle\rangle_{\mathbf{n}}^2}{M_0^2 c^4} = \sum_{i=1}^3 2 \left( \frac{\hbar \omega_i (\bar{n}_i + \frac{1}{2})}{2Mc^2} \right)^2 \left[ \left( 1 + \frac{q_i^2}{2a_i + q_i^2} \right)^2 + \frac{3}{4} \frac{q_i^4}{(2a_i + q_i^2)^2} \right]. \quad (3.71)$$

This expression is given in leading order of Mathieu parameters, taking into account one order more than in other cases as we are showing a variance and not the standard deviation. The standard deviation associated with this variance can be interpreted as the quantum fluctuations of the kinetic energy,  $\Delta \hat{K}/Mc^2$ . To evaluate the second moment of the kinetic energy, it is convenient to use  $\langle \hat{\mathbf{P}}^4 \rangle_{\mathbf{n}} = 3 \langle \hat{\mathbf{P}}^2 \rangle_{\mathbf{n}}^2$  for Gaussian statistics. Note that this identity only holds for the average in  $L_2(\mathbb{R}^3)$ , as the statistics with respect to time are non-Gaussian. We caution that the fractional frequency uncertainty for a COM Fock state (which is non-Gaussian) looks slightly different but can still be easily evaluated by using creation and annihilation operators.

It is interesting to consider in Eq. (3.71) the contributions along different directions  $i$  in the limit of a pure dc or ac potential. For a dc potential,  $q_i = 0$ , one finds for a thermal COM state that the standard deviation in the direction  $i$  corresponds to  $\sqrt{2}$  times the fractional frequency shift in the same direction. This agrees with the expectation that without micromotion, the Gaussian statistics entail a variance  $\text{Var}(\hat{K})_i = 2 \langle\langle \hat{K}_i \rangle\rangle^2$  for the kinetic energy along this direction. For a pure ac potential,  $a_i = 0$ , one finds instead a standard deviation in the direction  $i$  of the fractional frequency shift of  $\sqrt{19/8}$  times the fractional frequency shift in the same direction. The slight increase compared to a dc potential is due to micromotion. In the same way, the uncertainty in the fractional frequency shift can be evaluated for the contribution to the excess micromotion (3.63).

The standard deviation of the fractional frequency shift  $u/\omega_0$  implied by Eq. (3.71) has the same order of magnitude as the *average* second-order Doppler fractional frequency shift. However, in order to resolve the latter, a large number of measurements  $N$  is required to average down the projection noise (first term in Eq. (3.70)) to the level of the systematic second-order Doppler shift. It is important to note that in the same course the uncertainty of the second-order Doppler shift is suppressed by  $N$ . Thus, its contribution to Eq. (3.70) should not be misinterpreted to imply a fundamental limit to the stability of an ion clock. Rather, the standard deviation

of the fractional frequency shift should be considered as a - relatively small - correction to the quantum projection noise of a single measurement on a two-level system. However, it does imply a limit to the short-term stability.

In the previous subsection we studied the interplay between the fractional frequency shift due to gravity and the mass defect. But as we motivated before, a more relevant quantity will be its variance or standard deviation. The regime in which a minimum could be found for the fractional frequency shift is not relevant for usual ion trap parameters. Nevertheless, one can also try to study and minimize this interplay for the variance, although we expect it to be also in a non-exploitable regime, and as we just show, it will only be relevant for the short-term stability. If we make the same calculations in order to include also the effect of gravity, and we focus on the case for  $\mathbf{q}_i \rightarrow 0$ , as including the trap parameters complicates a lot the expressions and does not give a better insight or changes the discussion because the micromotion will give only a small correction, the variance becomes

$$\frac{u^2}{\omega_0^2} = \frac{\hbar}{Mc^2} \left( \bar{n}_i + \frac{1}{2} \right) \left( \frac{\hbar\omega_i^2}{2Mc^2} \left( \bar{n}_i + \frac{1}{2} \right) + \frac{g_i^2}{c^2\omega_i} \right). \quad (3.72)$$

If we minimize the variance considering the different scaling with the trapping frequency  $\omega_i$  we obtain that the minimum is fulfilled for

$$\omega_i = \left( \frac{g^2 M}{\hbar(n + \frac{1}{2})} \right)^{1/3}. \quad (3.73)$$

Comparing this with the minimization of the fractional frequency shift in Eq. (3.68), we see that this frequency is smaller by a factor of  $4^{1/3}$ , which makes it even less relevant for the parameter regime of a conventional ion trap.

### 3.3.8 Effect of additional quadrupole fields

Finally, we address the effect of a spurious electric quadrupole field. Yudin & Taichenachev [46] suggested that an additional quadrupole field beyond the ideal dc and ac potentials in Eq. (3.33), in interplay with the mass defect, could lead to systematic shifts that have not been considered before. Compared to Eq. (3.33), an additional quadrupole electric field can manifest itself in a shift of the minima between the ac and dc potentials, a change in their curvature and/or a shift in their axes.

To take this into account, we choose, without loss of generality, the origin of our coordinates to coincide with the zero point of the ac contribution and the coordinate basis to be aligned with its axes (i.e. with the eigenvectors of  $\tilde{U}$  in Eq. (3.33)). This

leaves the ac contribution unchanged from the previous sections. The *total* (intended and accidental) dc potential is now expressed in an expansion around the origin,

$$\Phi_{\text{dc}}(\hat{\mathbf{R}}) = \Phi_{\text{dc}}(\hat{\mathbf{0}}) + \mathbf{E}_{\text{dc}} \cdot \hat{\mathbf{R}} + \frac{1}{2} \hat{\mathbf{R}}^T U \hat{\mathbf{R}}, \quad (3.74)$$

where  $U_{ij} = \frac{\partial^2 \Phi_{\text{dc}}(\hat{\mathbf{0}})}{\partial R_i \partial R_j}$  and  $\hat{\mathbf{0}}$  stands for the center of the ac potential. The  $\Phi_{\text{dc}}(\hat{\mathbf{0}})$  will be a constant shift in the Hamiltonian and therefore will have no effect. The linear component can be interpreted as a contribution to the spurious  $\mathbf{E}_{\text{dc}}$  field studied before in Sec. 3.3.5. Finally, without loss of generality, we write  $U = U_0 \text{diag}(\alpha_1, \alpha_2, \alpha_3) + W$ , with dimensionless coefficients  $\alpha_i$  and a purely off-diagonal perturbation  $W$ . The diagonal terms determine the potential curvatures and hence the effective trap frequencies, as in the previous sections. A calibration of the second-order Doppler effect, based on trap spectroscopy and thermometry of the COM motion, will thus properly account for potential deviations of the  $\alpha_i$  from their nominal values. It is these changes that were discussed in [46] in a perturbative account. We thus agree with Yudin & Taichenachev that a change in potential curvature can enter the systematics in relevant magnitude, but notice that these effects are already accounted for in the operational calibration of an ion clock in the context of the second-order Doppler effect.

It remains to discuss the effect of axis misalignments. For this, we treat the nondiagonal correction as a perturbation to the Hamiltonian (3.34),

$$\hat{H}_{\text{off-diag}} = Q \hat{\mathbf{R}}^T W \hat{\mathbf{R}}. \quad (3.75)$$

Assuming for simplicity a nondegenerate spectrum of motional eigenfrequencies  $\omega_i$ , we can employ nondegenerate perturbation theory [4] in order to evaluate the corrections to the energy levels of quasistationary states  $|\mathbf{n}, t\rangle$  in Eq. (3.51). Expressing the position operator  $\hat{\mathbf{R}}$  in terms of creation and annihilation operators, it follows immediately (due to the off-diagonal nature of  $W$ ) that the first-order correction vanishes, i.e.,  $\langle\langle \hat{H}_{\text{off-diag}} \rangle\rangle_{\mathbf{n}} = 0$ . Of course, the eigenstates will change. In the case of nominal degeneracies in the trap frequencies the off diagonal terms can be treated as a perturbation on the level of the Mathieu equation, following the treatment shown by Landa *et al.* [61]. This will lead to a lifting of the degeneracies, which will again be accounted for in the trap calibration. Both cases are shown in Appendix C by solving the Mathieu equation.

## 3.4 Relativistic coupling of internal and external DOFs in Penning traps

After applying our formalism to a Paul trap, an interesting question will be how to consider other trapping schemes. Starting with this project, we did not consider Penning traps because our derivation does not cover relativistic corrections due to spin, which will be relevant in the presence of a magnetic field. Nevertheless, we became aware of some recent work that proposes to have a clock transition with both clock states having  $I = J = F = 0$ , where  $I$ ,  $J$ , and  $F$  are the conventional quantum numbers specifying nuclear, electronic, and total angular momentum, respectively, see e.g. [51]. This makes our description relevant to that particular case.

### 3.4.1 Introduction to Penning traps

We will start by recapitulating how the confinement is generated in a Penning trap [62, 63]. A dc potential confines the particle along the  $z$  direction in a similar way as in a Paul trap. We have a potential  $V(\hat{\mathbf{R}})$  and an electric field  $\mathbf{E}(\hat{\mathbf{R}})$  of the form

$$V(\hat{\mathbf{R}}) = V_R C_2 \left( \hat{z}^2 - \frac{\hat{x}^2}{2} - \frac{\hat{y}^2}{2} \right), \quad \mathbf{E}(\hat{\mathbf{R}}) = V_R C_2 \begin{pmatrix} \hat{x} \\ \hat{y} \\ -2\hat{z} \end{pmatrix}. \quad (3.76)$$

Where in general, the field is produced by applying a voltage  $V_R$  to a set of typically cylindrical electrodes with their axes also aligned along the  $z$  direction. For axial confinement, the sign of the voltage needs to agree with the charge of the trapped particle  $Q$ .  $C_2$  characterizes the geometry of the trap and defines a specific length for the trap  $\sqrt{\frac{1}{C_2}}$ .

To realize confinement in the orthogonal plane, we apply a constant magnetic field, with strength  $B_0$ , along the  $z$ -axis with

$$\mathbf{A}(\hat{\mathbf{R}}) = \frac{B_0}{2} \begin{pmatrix} -\hat{y} \\ \hat{x} \\ 0 \end{pmatrix}, \quad \mathbf{B}(\hat{\mathbf{R}}) = B_0 \begin{pmatrix} 0 \\ 0 \\ 1 \end{pmatrix}, \quad (3.77)$$

the vector potential and magnetic field, respectively.

The motional Hamiltonian for the Penning trap will look like

$$H_{\text{mot}} = \frac{\left( \hat{\mathbf{P}} - Q\hat{\mathbf{A}}^\perp(\hat{\mathbf{R}}) \right)^2}{2M} + QV, \quad (3.78)$$

where we wrote  $\hat{\mathbf{P}}$  instead of  $\hat{\mathbf{P}} = \hat{\mathbf{P}} - Q\hat{\mathbf{A}}^\perp(\hat{\mathbf{R}})$  because we want to maintain the explicit dependence of the vector potential. First, we will study this part of the Hamiltonian and afterwards discuss what happens to the relativistic corrections calculated in Sec. 3.2.

The Hamiltonian in Eq. (3.78) can be diagonalized, see e.g. [62], and decomposed into three terms corresponding to independent harmonic oscillators, one for the motion along  $z$  and two for the transverse motion

$$H_{\text{mot}} = \hbar\omega_z \left( \hat{a}_z^\dagger \hat{a}_z + \frac{1}{2} \right) + \hbar\omega_+ \left( \hat{a}_c^\dagger \hat{a}_c + \frac{1}{2} \right) - \hbar\omega_- \left( \hat{a}_m^\dagger \hat{a}_m + \frac{1}{2} \right), \quad (3.79)$$

where we define the axial, modified cyclotron and magnetron frequency, respectively,

$$\omega_z = \sqrt{2V_R C_2 \frac{Q}{M}}, \quad \omega_+ = \frac{\omega_c}{2} + \Omega_c, \quad \omega_- = \frac{\omega_c}{2} - \Omega_c, \quad (3.80)$$

where  $\omega_c = \frac{QB_0}{M}$  is the cyclotron frequency and  $\Omega_c > 0$  is defined by  $\Omega_c^2 = \frac{\omega_c^2}{4} - \frac{\omega_z^2}{2}$ . For common trap parameters, we have the hierarchy  $\omega_+ \gg \omega_z \gg \omega_-$ . The annihilation operators for the  $i = x, y, z$  directions are

$$\hat{a}_i = \frac{1}{\sqrt{2\hbar M \omega_i}} \left( M \omega_i \hat{R}_i + i \hat{P}_i \right), \quad (3.81)$$

with  $\omega_x = \omega_y = \Omega_c$ . The modified cyclotron and magnetron frequency ladder operators can be written in terms of the  $x$  and  $y$  ladder operators in the form

$$\hat{a}_c = \frac{\hat{a}_x + i\hat{a}_y}{\sqrt{2}}, \quad \hat{a}_m = \frac{\hat{a}_x - i\hat{a}_y}{\sqrt{2}}. \quad (3.82)$$

It is worth noting the negative contribution in Eq. (3.79), this may lead to the idea that one can erase the second-order Doppler effect that will come from this Hamiltonian as the contribution from the different motions will have a different sign. This is somehow physically unintuitive as it implies that one can get rid of the second-order Doppler effect by increasing the motion in one of the directions. We will return to this point at the end of the chapter.

### 3.4.2 Mass defect in Penning traps

Assuming a Ramsey interrogation scheme, our relativistic Hamiltonian in Eq. (3.4) will be the perfect starting point to treat the fractional frequency shift in a Penning trap, with the difference that we do not have a time dependent potential and therefore

no micromotion or excess micromotion will appear. We will start by studying the contributions of all terms in Eq. (3.4) in the case of a Penning trap.

The first contribution is provided by the nonrelativistic COM Hamiltonian

$$\hat{H}_{\text{com}}^{(0)} = \frac{\hat{\mathbf{P}}^2}{2M} + M\phi(\hat{\mathbf{R}}), \quad (3.83)$$

where we neglected the relativistic corrections affecting the COM DOF only, this corresponds to the terms in Eq. (3.7) that will lead only to a common shift for the ground and excited states. The main difference from the previous section is that now we have a non-zero vector potential, and therefore, it needs to be accounted for in the redefined momentum

$$\hat{\tilde{\mathbf{P}}} = \hat{\mathbf{P}} - Q\hat{\mathbf{A}}^\perp(\hat{\mathbf{R}}), \quad (3.84)$$

as shown in Eq. (3.8).

In the same spirit as in the previous section, we will assume relativistic corrections of the internal DOF, Eq. (3.11), to be absorbed in the internal states and energies under the two-level approximation.

The interaction of the atom with the electromagnetic field in the dipole approximation requires more discussion than in the previous section, remember that it is given by

$$\hat{H}_{\text{at-emf}} = Q\Phi(\hat{\mathbf{R}}) - \hat{\mathbf{d}} \cdot \mathbf{E}(\hat{\mathbf{R}}) + \frac{1}{2M} \left[ \hat{\tilde{\mathbf{P}}} \cdot (\hat{\mathbf{d}} \times \mathbf{B}(\hat{\mathbf{R}})) + \text{H.c.} \right] + \hat{H}_{\text{other}}. \quad (3.85)$$

The potential will create the trapping in a Penning trap, as explained in Sec. 3.4.1. The Röntgen term scales as  $\mathbf{P}/Mc$  and is negligible for a cold ion and will merely rescale the Rabi frequency of the pulses in a Ramsey interrogation, as discussed in the previous section. The contributions in  $\hat{H}_{\text{other}}$  will be shown in Appendix A. These terms involve the magnetic field and internal DOF, therefore, they are not effective in the case of a Paul trap. In the case of a Penning trap, even though we have a magnetic field, this field will be constant, and therefore independent of the external DOF, which will make these contributions relativistic corrections to the internal Hamiltonian that will be accounted for in the two-level approximation.

The metric term in Eq. (3.13) can be dropped in a rotating wave approximation, as in the case of a Paul trap. The mass-defect term will have the same contribution as in Eq. (3.16), with the difference that we have to account for the vector potential in  $\hat{\tilde{P}}$ . Therefore, the effect of the mass defect will be, in the two-level approximation,

$$\hat{H}_{\text{int}} + \hat{H}_{\text{mass defect}} \simeq \hat{H}_{\text{int}} \otimes \left( 1 + \frac{1}{c^2} \frac{\partial \hat{H}_{\text{com}}(M)}{\partial M} \right) = \frac{\hbar\omega_0}{2} \hat{\sigma}_z \otimes \left( 1 + \frac{\delta\hat{\nu}}{\nu_0} \right), \quad (3.86)$$

leading to a fractional frequency shift

$$\frac{\delta\hat{\nu}}{\nu_0} = \frac{1}{c^2} \frac{\partial \hat{H}_{\text{com}}(M)}{\partial M}, \quad (3.87)$$

where again one need to consider that the expression of  $\hat{H}_{\text{com}}(M)$  is different from the previous section as we will have a vector potential.

Taking this into account, the Hamiltonian for the Ramsey interrogation scheme in the Penning trap will be

$$\hat{H} = \hat{H}_{\text{com}}(M) + \frac{\hbar\omega_0}{2} \hat{\sigma}_z \left( 1 + \frac{\delta\hat{\nu}}{\nu_0} \right) - \hat{\mathbf{d}} \cdot \mathbf{E}(\hat{\mathbf{R}}, t), \quad (3.88)$$

with

$$\hat{H}_{\text{com}}(M, t) = \frac{\hat{\mathbf{P}}^2}{2M} + M\phi(\hat{\mathbf{R}}) + QV(\hat{\mathbf{R}}). \quad (3.89)$$

From now on we will drop the contribution from gravity as it will give the same insight as in the case of a Paul trap, doing so this Hamiltonian corresponds to the motional Hamiltonian in Eq. (3.78).

Now that we have properly treated the relativistic corrections, we are in a position to study the fractional frequency shift for a Penning trap, i.e.,

$$\frac{\delta\hat{\nu}}{\nu_0} = \frac{1}{c^2} \frac{\partial \hat{H}_{\text{mot}}(M_0)}{\partial M} = -\frac{1}{Mc^2} \frac{(\hat{\mathbf{P}} - Q\hat{\mathbf{A}}^\perp(\hat{\mathbf{R}}))^2}{2M} = -\frac{1}{Mc^2} (\hat{H}_{\text{mot}} - QV(\hat{\mathbf{R}})). \quad (3.90)$$

Using the diagonal form of the motional Hamiltonian in Eq. (3.79) and combining the definition of the ladder operators in the  $x$  and  $y$  directions (3.81) with the relations of the modified cyclotron and magnetron ladder operators (3.82) in order to rewrite the potential of the trap in terms of the latter, we can rewrite Eq. (3.90) as

$$\begin{aligned} \frac{\delta\hat{\nu}}{\nu_0} = & -\frac{1}{Mc^2} \left[ \frac{\hbar\omega_z}{2} \left( a_z^\dagger a_z + \frac{1}{2} \right) + \hbar \left( \omega_+ + \frac{\omega_z^2}{4\Omega_c} \right) \left( a_c^\dagger a_c + \frac{1}{2} \right) \right. \\ & \left. - \hbar \left( \omega_- - \frac{\omega_z^2}{4\Omega_c} \right) \left( a_m^\dagger a_m + \frac{1}{2} \right) - \frac{\hbar\omega_z}{4} \left[ \left( a_z^2 + a_z^{\dagger 2} \right) - \frac{\omega_z}{\Omega_c} \left( a_c a_m + a_c^\dagger a_m^\dagger \right) \right] \right]. \end{aligned} \quad (3.91)$$

We can see that the effect of the mass defect is halving the fractional frequency shift contribution from the motion in the  $z$  direction and shifting the contribution for the cyclotron and magnetron motions. Apart from that, it also adds some terms that involve  $a_z^2$  and  $a_z^{\dagger 2}$ , which in the case of a combination of Fock states will lead to mixing the effects of different Fock states.



Assuming that  $\omega_c > \omega_z$ , which is fulfilled for usual Penning trap parameters, we obtain

$$\left(\omega_- - \frac{\omega_z^2}{4\Omega_c}\right) < 0. \quad (3.92)$$

Let us now return to the question that we raised after Eq. (3.79), which was that the second-order Doppler effect maybe could be erased by adding magnetron motion. Now we see that if one considers the mass defect properly, the sign in the fractional frequency shift of the contributions of the different motions are the same, which will make it impossible to compensate one contribution with another, which, at the same time, makes more physical sense in our opinion.

Of course, one still has a negative contribution coming from the term involving  $a_z^2$  and  $a_z^{\dagger 2}$ , but the size of this contribution will be bounded by the value of  $a_z a_z^\dagger$  and therefore, the first term will always make the combined contribution positive.

## 3.5 Conclusion

In conclusion, we have presented a systematic and fully quantum mechanical treatment of relativistic frequency shifts in atomic clocks based on trapped ions. We started by deriving an approximate relativistic Hamiltonian for the center of mass and internal dynamics of an electromagnetically bound, charged two-particle system in external electromagnetic and gravitational fields. We applied this Hamiltonian to an ion in a Paul trap, including the effects of micromotion, excess micromotion and trap imperfections.

We recovered results known from semiclassical treatments based on time-dilation arguments. The Hamiltonian *ab initio* treatment given here avoids the need for *ad hoc* arguments based on time-dilation or mass-defect corrections. We would like to emphasize that, as we strove to calculate creation and annihilation operators, we were able to go beyond what semiclassical treatments are capable of and managed to have a proper discussion of the variance associated with the fractional frequency shift. With that, we showed that the variance of the fractional frequency shift will only provide a fundamental limitation in the short-term stability, and it should be seen as a —relatively small— correction to the quantum projection noise of a single measurement. Treating the possible imperfections of the trap, we agree with Yudin & Taichenachev that these terms will have an impact, but as they only change the effective trap frequencies, it will be absorbed in a proper calibration of the trap.

With our formalism, we were also able to treat the case of a spinless atom in a Penning trap, allowing us to see that, with the proper use of the mass defect, one

does not have contributions with opposite sign in the fractional frequency shift coming from the different motions. Therefore, we conclude that it is not possible to null the fractional frequency shift by adding magnetron motion.

### 3.6 Outlook: Further research directions

Finally, we would like to discuss which should be the next natural steps if one wants to study this relativistic effects further. Regarding relativistic corrections for clocks, it would be desirable to account for spin, this could be achieved along the lines of [55,56], but taking into account the gravitational field. With these treatment one could treat systems with spin, in particular for Penning traps where the interaction between the spin and the magnetic field is relevant. In this work, we treated the simple case of an ion, but more complicated systems such as atom clocks based on ion crystals [64] as well as neutral lattice clocks [65,66] are relevant. We hope that our treatment provides a solid basis for these applications too, and therefore, this could be another route for possible future studies.

Penning trap mass spectrometry has been used to detect metastable electronic states in highly charged ions [67]. Using this technique, another possibility to extend our work will be to model how the mass defect could be used as a tool for reading out the internal states.

# 4

## Quadrupole transitions with continuous dynamical decoupling(CDD)

### 4.1 Motivation and research problem

Optical clocks based on neutral atoms trapped in optical lattices have shown uncertainties of a few parts in  $10^{-18}$  [65]. At the same time, optical ion clocks [20] have shown systematic uncertainties below  $10^{-18}$  [21, 68–70]. Clocks at this level of uncertainty open the way to many applications, such as relativistic geodesy [24–30], tests of general relativity [31–33], and to explorations of physics beyond the standard model [34]. However, in order to exploit these applications, the statistical uncertainty of the clock must reach a certain level after some integration time, which will depend on the phenomena under investigation.

The statistical uncertainty for a given clock species can be improved by extending the probe time, which will ultimately be limited by the lifetime of the excited states. Nevertheless, in practice, it is usually limited by the coherence time of the clock laser [71, 72]. We can also improve the statistical uncertainty by interrogating many atoms simultaneously [73–76]. But increasing the number of ions stored in a Paul trap entails further obstacles to overcome. Depending on the ion species chosen, inhomogeneous or time-dependent frequency shifts, such as the Zeeman shift, the Quadrupole shift, or the radio frequency (rf) electric field-induced tensor ac Stark shift, pose a limitation. These effects can contribute to the decoherence of the state or broaden the joint linewidth of the ions, thus limiting the usable probe time. Several approaches exist to constrain these shifts even without exact knowledge of the electric field gradient. One approach consists in averaging over different transitions or directions to exploit the different scaling of the shift with the angular momentum component [77, 78]. Another method dynamically changes the static offset B-field

direction within the clock interrogation [79] to mimic the magic angle spinning technique of nuclear magnetic resonance spectroscopy [80].

In the field of quantum technology there have been ideas for protecting a quantum system from its environment, and recently, some of these have been transferred to atomic clocks. One of these ideas is known as dynamical decoupling protocols. These protocols have been studied both theoretically [81–92] and experimentally [93–100], and are based on tailoring the quantum properties of the system by applying external pulses to eliminate the effect of environmental perturbations. Here, we will investigate continuously applied time-periodic fields, also known as continuous dynamical decoupling (CDD) [100–111]. CDD has been shown to be useful in the application of qubit gates [112–114] and plays an important role in reducing environmental perturbations in nitrogen vacancy centers in diamonds, which are promising candidates for applications in the field of quantum information technologies [110, 115–117].

The application of these protocols to atomic clocks has been studied in several papers [92, 100, 110]. We will build on the work of Aharon *et al.* [92], where they motivate robust optical clock transitions by applying CDD. For these artificial optical quadrupole transitions, more complicated ion-laser interactions need to be addressed, which will be the focus of the current work.

In Sec. 4.2, we start by reformulating the description of CDD to easily treat the laser-ion interaction. We begin by recapitulating the dynamical decoupling principle for a particular spin manifold, which is subject to a Zeeman splitting controlled by a static dc magnetic field. Here, modulated external rf magnetic fields are employed to mitigate the amplitude-induced line shifts [92]. We continue by showing the effective Hamiltonian in the so-called doubly-dressed basis 4.2.1. Then, with the appropriate CDD parameters, we quantify the suppression of Zeeman and quadrupole shifts in the doubly-dressed basis 4.2.2. Having established the CDD formulation and notation, we proceed to accurately describe the laser-ion interaction in Sec. 4.3. We consider optical quadrupole transitions between two such spin manifolds and characterize the laser-ion interaction necessary to drive the above transitions 4.3.1, showing that there is no selection rule for transitions in the doubly-dressed basis; the only necessary condition to drive a particular transition will be the proper detuning of the laser. The suppression of Zeeman and quadrupole shifts will come at the cost of a reduction in the effective Rabi frequency for transitions in the doubly-dressed basis, and therefore, the characterization of these transitions will allow us to choose an appropriate candidate for a clock transition. We continue by considering the approximations made during the previous sections, namely, the rotating wave approximation during the derivation of the doubly-dressed basis, which is also known as Bloch-Siegert effect, and the cross-field effect, which consists in the effect that the rf fields applied for dynamic

decoupling to the ground states manifold have on the excited states manifold and vice versa. Both effects will be accounted for approximately using the so-called Magnus expansion 4.3.2. To gain further insight into this scheme, we study and characterize the particular case of a quadrupole transition between the  $S = 1/2$  and  $D = 5/2$  manifolds of  $^{40}\text{Ca}^+$  4.3.3, comparisons with experimental data for this example will be shown elsewhere [118]. We proceed by comparing our approximate solutions for a single layer of dressing, i.e., the dressed basis and the dressed basis corrected by the Bloch-Siegert effect approximately, with the true solutions of the Hamiltonian, the Floquet states in Sec. 4.4. In addition, we address whether it is possible to combine our CDD scheme with the implementation of a Mølmer-Sørensen gate in Sec. 4.5, in order to implement entanglement between two ions.

## 4.2 Dynamical decoupling

In this section, we will recapitulate the principle of dynamic decoupling for the suppression of Zeeman and quadrupole shifts of atomic levels by dressing with radio frequency (rf) magnetic fields [92, 100, 110]. The present work aims to characterize quadrupole transitions from a spin manifold of ground states to a manifold of excited states. We will first study how these magnetic fields affect one spin manifold, which will facilitate the discussion of the physical principle of dynamic decoupling. Furthermore, treating one manifold will separate the effects inherent to the problem of a single manifold and those that are connected to their cross coupling.

### 4.2.1 Doubly-dressed basis

We will consider a manifold of total spin  $S$  with basis states  $|M\rangle$  ( $|M| \leq S$ ) and quantization axis along  $z$ . If a static magnetic field  $B$  along the  $z$ -axis is present, the internal states  $|M\rangle$  will be shifted by a value proportional to their spin, due to the linear Zeeman effect. Therefore, the Hamiltonian will have the expression

$$H_{\text{dc}} = g\mu_B B S_z = \omega_0 S_z, \quad (4.1)$$

where  $g$  is the gyromagnetic factor, the corresponding Larmor frequency is  $\omega_0 = g\mu_B B$ , with  $\mu_B$  being the Bohr magnetron, and we set  $\hbar = 1$ . The eigenstates of this Hamiltonian will be referred to as bare states. A radio-frequency field  $B_{\text{rf}}(t)$  is applied in the  $x - y$  plane, which for the sake of generality we consider enclosing an angle  $\alpha$  with the  $x$ -axis. The rf field  $B_{\text{rf}}(t)$  is assumed to comprise frequency components at a fundamental frequency  $\omega_1$  and sideband frequencies  $\omega_1 \pm \omega_2$ , where  $\omega_2 < \omega_1$ , such

that the Hamiltonian for the rf fields is

$$H_{\text{rf}} = g(\Omega_1 \cos(\omega_1 t) - \Omega_2 \sin(\omega_1 t) \cos(\omega_2 t))(S_x \cos \alpha + S_y \sin \alpha), \quad (4.2)$$

where  $\Omega_1$  and  $\Omega_2$  are set by the amplitudes of the fundamental and sideband components of the rf-magnetic field, respectively. Therefore, the total Hamiltonian for the spin  $S$  manifold in the laboratory frame (LF) is

$$H^{\text{LF}} = H_{\text{dc}} + H_{\text{rf}}. \quad (4.3)$$

To help characterize the rf or dressing fields, we are going to introduce a series of transformations into several frames. We remind the reader that the transformations to rotating frames have been introduced in Sec. 2.2. In this sequence of transformations we will denote a unitary rotation around an axis  $\mathbf{n}$  about an angle  $\theta$  by

$$U_{\mathbf{n}}(\theta) = \exp(i\theta \mathbf{nS}), \quad (4.4)$$

and use the shorthand notation

$$\mathcal{R}_{\mathbf{n}}(\theta)A := U_{\mathbf{n}}(\theta)AU_{\mathbf{n}}^\dagger(\theta), \quad (4.5)$$

for the conjugation of an operator  $A$  with  $U_{\mathbf{n}}(\theta)$ , as we similarly did in chapter 2. As in the previous chapter, we use bold symbols to denote three-vectors.

First, we go into a frame rotating around the  $z$ -axis at the rf frequency  $\omega_1$  by transforming the operator defining the Schrödinger equation, i.e.,  $H^{\text{LF}} - i\frac{d}{dt}$ , as described in chapter 2,

$$\begin{aligned} \mathcal{R}_{\mathbf{z}}(\omega_1 t) \left[ H^{\text{LF}} - i\frac{d}{dt} \right] &= \Delta_1 S_z + \frac{g\Omega_1}{2} (S_x \cos \alpha + S_y \sin \alpha) \\ &+ \frac{g\Omega_2}{2} \cos(\omega_2 t) (S_y \cos \alpha - S_x \sin \alpha) - i\frac{d}{dt}. \end{aligned} \quad (4.6)$$

Here, we define the detuning of the rf-field with respect to the Larmor frequency  $\Delta_1 = \omega_0 - \omega_1$ . We also use a rotating wave approximation (RWA) and drop terms oscillating at  $2\omega_1$ , assuming  $2\omega_1 \gg g\Omega_1/2, \Delta_1$ <sup>1</sup>. Remember that the RWA has been introduced in Sec. 2.2. The effective contribution of these counter-rotating terms on the bare states is addressed in Sec. 4.3.2. The time-derivative on the left-hand side of Eq. (4.6) accounts for the terms that contribute to the transformed Hamiltonian due to the time dependence of the transformation, i.e.,  $\mathcal{R}_{\mathbf{z}}(\omega_1 t) \left[ H - i\frac{d}{dt} \right] = (\mathcal{R}_{\mathbf{z}}(\omega_1 t)H) - \omega_1 S_z - i\frac{d}{dt}$ . This notation is useful when dealing with sequences of transformations.

---

<sup>1</sup>To be precise one should consider the size of the eigenvalues of the operator  $S_x$  for the last inequality, nevertheless, for the cases we are going to treat in this chapter they are going to be small and therefore will not affect the inequality.

In the next step, the Hamiltonian is rewritten in the dressed state basis corresponding to the eigenstates of the time-independent part of the Hamiltonian on the right-hand side of Eq. (4.6), which correspond to the first line in the right-hand side. We achieve this by a rotation around an axis  $\mathbf{n}_1 = (-\sin \alpha, \cos \alpha, 0)$  and an angle  $\theta_1 \in [0, \pi]$  defined by  $\cos \theta_1 = \Delta_1/\bar{\omega}_0$ , where

$$\bar{\omega}_0 = (\Delta_1^2 + g^2\Omega_1^2/4)^{1/2}. \quad (4.7)$$

The Hamiltonian in this first dressed basis is calculated using the transformation

$$\mathcal{R}_{\mathbf{n}_1}(\theta_1)\mathcal{R}_{\mathbf{z}}(\omega_1 t) [H^{\text{LF}} - i\frac{d}{dt}] = \bar{\omega}_0 S_z + \frac{g\Omega_2}{2} \cos(\omega_2 t) (S_y \cos \alpha - S_x \sin \alpha) - i\frac{d}{dt}. \quad (4.8)$$

This Hamiltonian refers to a new time-dependent quantization axis enclosing an angle  $\theta_1$  with the  $z$ -axis. In Fig. 4.1 a) we find the representation of the quantization axis, with the corresponding energies of the eigenstates depicted in Fig. 4.1 b). These eigenstates, also called bare states, are separated by an energy splitting  $\hbar\omega_0$ , which corresponds to the Zeeman splitting. To compare with the dressed basis, we can observe the new quantization axis in Fig. 4.1 c) and the corresponding energies of the eigenstates, in the rotating frame, in Fig. 4.1 d). These eigenstates, also called dressed states, are separated by an energy splitting  $\hbar\bar{\omega}_0$ , which corresponds to a combined effect between the Zeeman splitting and the fundamental frequency  $\omega_1$  in the rf field.

The next dressing layer consists of the same two types of transformations as the first one. First, the system is transformed into a rotating frame with frequency  $\omega_2$  around the new quantization axis, where fast oscillating terms  $2\omega_2 \gg g\Omega_2/4, \Delta_2$  are neglected,

$$\mathcal{R}_{\mathbf{z}}(\omega_2 t)\mathcal{R}_{\mathbf{n}_1}(\theta_1)\mathcal{R}_{\mathbf{z}}(\omega_1 t) [H^{\text{LF}} - i\frac{d}{dt}] = \Delta_2 S_z + \frac{g\Omega_2}{2} (S_y \cos \alpha - S_x \sin \alpha) - i\frac{d}{dt}. \quad (4.9)$$

The detuning at the second dressing layer is  $\Delta_2 = \bar{\omega}_0 - \omega_2$ . Then, the time-independent Hamiltonian is diagonalized. The transformation that achieves this corresponds to a rotation about an axis  $\mathbf{n}_2 = (-\cos \alpha, -\sin \alpha, 0)$  by an angle  $\theta_2 \in [0, \pi]$ , where

$$\cos \theta_2 = \Delta_2/\bar{\bar{\omega}}_0, \quad (4.10)$$

and

$$\bar{\bar{\omega}}_0 = (\Delta_2^2 + g^2\Omega_2^2/16)^{1/2}. \quad (4.11)$$

This results in the final, doubly-dressed Hamiltonian

$$H = \mathcal{R}_{\mathbf{n}_2}(\theta_2)\mathcal{R}_{\mathbf{z}}(\omega_2 t)\mathcal{R}_{\mathbf{n}_1}(\theta_1)\mathcal{R}_{\mathbf{z}}(\omega_1 t) [H^{\text{LF}} - i\frac{d}{dt}] + i\frac{d}{dt} = \bar{\bar{\omega}}_0 S_z. \quad (4.12)$$

We add  $i\frac{d}{dt}$  in the last equation because we are transforming the operator defining the Schrödinger equation, i.e.,  $H - i\frac{d}{dt}$ , as explained in chapter 2, and we want to recover the Hamiltonian after the transformations. The quantization axis of the Hamiltonian in Eq. (4.12) is now again rotated at an angle  $\theta_2$  with respect to the previous one. In principle, further dressing layers can be added, which will correspond to a similar sequence of transformations. Applications of  $n$  layers of dressing have been discussed by Cai *et al.* [110].

We emphasize that the dressing procedure involves two RWAs, which are implicit in Eq. (4.12), and are based on  $2\omega_i \gg g\Omega_i/2^i$  for  $i = 1, 2$ . Thus, we have the hierarchy of time scales  $\bar{\omega}_0^{-1} > \omega_2^{-1} > \omega_1^{-1}$ . Nevertheless, the terms neglected during the RWA will be accounted for perturbatively using a Magnus expansion in Sec. 4.3.2.

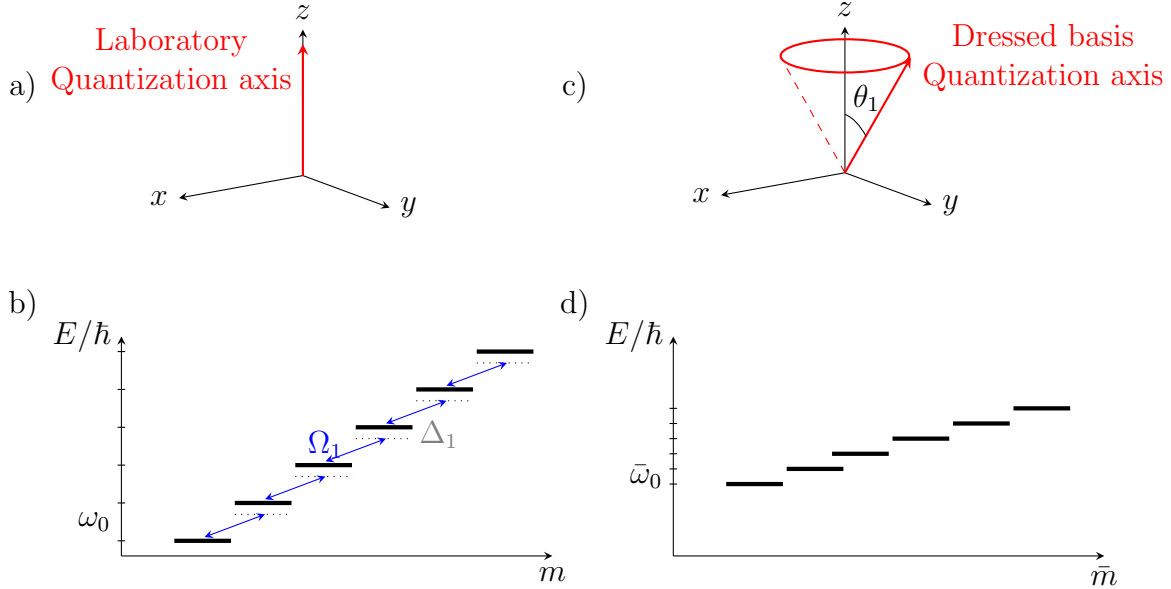


Figure 4.1: Sketch of dynamical decoupling effect on a given manifold. Figs. *a)* and *c)* correspond respectively to the quantization axis of Figs. *b)* and *d)*. In Fig. *b)* we show the level scheme of the bare basis, with coupling  $\Omega_1$  between the bare states driven by the time-dependent near-resonant magnetic field and the detuning  $\Delta_1 = \omega_0 - \omega_1$ . In Fig. *d)* the level scheme in the dressed basis quantization axis is displayed. Note that *c)* and *d)* are not to scale as  $\bar{\omega}_0 \ll \omega_0$ , due to  $\bar{\omega}_0 = (\Delta_1^2 + g^2\Omega_1^2/4)^{1/2}$ .

### 4.2.2 Suppression of Zeeman and quadrupole shifts

In this section, we discuss how the two layers of dressing help to suppress linear Zeeman and electric quadrupole shifts. We refer to the original work of Aharon *et al.* [92] for a detailed discussion. Both effects can be modeled by an additional term



$V^{\text{LF}}(t)$  added to the Hamiltonian in Eq. (4.3). This term may be time-dependent, but is assumed to fluctuate slowly on the time scales of the dressed states energy splitting  $\bar{\omega}_0^{-1}$ . In the doubly-dressed basis and in an interaction picture with respect to  $H$ , Eq. (4.12), such an additional term will be effectively described by

$$V^{\text{IP}} = \mathcal{R}_{\mathbf{z}}(\bar{\omega}_0 t) \mathcal{R}_{\mathbf{n}_2}(\theta_2) \mathcal{R}_{\mathbf{z}}(\omega_2 t) \mathcal{R}_{\mathbf{n}_1}(\theta_1) \mathcal{R}_{\mathbf{z}}(\omega_1 t) V^{\text{LF}} =: \mathcal{D}(\omega_i, g\Omega_i, t, \alpha) [V^{\text{LF}}]. \quad (4.13)$$

Remember that  $\alpha$  is the enclosed angle with the x-axis of the radio-frequency field in Eq. (4.2). The last (leftmost) rotation around  $z$  at frequency  $\bar{\omega}_0$  accounts for the interaction picture. We will abbreviate the complete sequence of transformations corresponding to the dynamic decoupling and the change to the interaction picture as  $\mathcal{D}(\omega_i, g\Omega_i, t, \alpha)$ . The goal of dynamic decoupling is to reduce  $V^{\text{IP}}$  by an appropriate choice of the driving parameters, which are the rf frequencies  $\omega_i$  and Rabi frequencies  $g\Omega_i$ , with  $i = 1, 2$ . This general reasoning can now be applied to linear-magnetic and electric-quadrupole shifts.

Let us first study the shift of the bare states created through magnetic field fluctuations. This shift can be described by

$$V_{\delta B}^{\text{LF}} = g\mu_B \delta \mathbf{B}(t) \mathbf{S}, \quad (4.14)$$

where  $\delta \mathbf{B}(t)$  is the time dependent part of the magnetic field, being the total magnetic field for the bare states  $\mathbf{B}(t) = (0, 0, B) + \delta \mathbf{B}(t)$ . To calculate the energy shift in the interaction picture after the transformations, Eq. (4.13), the changes of the spin vectors must be considered.

In a RWA one has  $\mathcal{R}_{\mathbf{z}}(\omega t) \mathbf{S} = S_z \mathbf{e}_z$ , therefore, applying the rotation and going to an interaction picture for one layer with a general direction of rotation  $\mathbf{n} = \cos \varphi \mathbf{e}_x + \sin \varphi \mathbf{e}_y$ , we obtain

$$\mathcal{R}_{\mathbf{z}}(\omega t) \mathcal{R}_{\mathbf{n}}(\theta) S_z = \cos \theta S_z + \frac{i}{2} \sin \theta (e^{it(\omega+\varphi)} S_+ - e^{-it(\omega+\varphi)} S_-) \simeq \cos \theta S_z. \quad (4.15)$$

The RWA drops all the terms oscillating at frequency  $\omega + \varphi$ . This can be applied for the two dressing layers, as in Eq. (4.13), obtaining

$$V_{\delta B}^{\text{IP}} = \mathcal{D}(\omega_i, g\Omega_i, t, \alpha) [V_{\delta B}^{\text{LF}}] = \cos \theta_1 \cos \theta_2 g\mu_B \delta B_z(t) S_z. \quad (4.16)$$

Under the assumption that  $\delta \mathbf{B}(t)$  fluctuates slowly on all relevant time scales, only the component along  $z$ , the direction of the dc field, matters. The terms in the  $x$  and  $y$  components of  $\delta \mathbf{B}(t)$  can be neglected in a RWA after the first rotation around  $z$  with frequency  $\omega_1$ . We would like to highlight that the same results are obtained if the RWA is applied after performing all the transformations and no RWA is applied

in between. This is a subtle but important point to make; if we want to make a transformation, apply a RWA, and afterwards, apply the inverse transformation, the result will be inconsistent, so either the relevant hierarchy of timescales regarding the different transformations needs to be confirmed, or realizing the RWA after all transformations has to give the same result when done properly. Eq. (4.16) shows that magnetic field fluctuations can be suppressed and even nulled by choosing the angle in the first and/or second stage of dressing to be  $\theta_{1(2)} = \pi/2$ , which is fulfilled by a set of resonant parameters  $\Delta_{1(2)} = 0$ , cf. Eq. (4.10).

A similar cancellation can be achieved for electric-quadrupole shifts. Such cancellation has been discussed previously in [92] and [100]. To the best of our knowledge, in the case of the continuous dynamical decoupling scheme considered here, no expression for the quadrupole shift Hamiltonian in the doubly-dressed basis has been derived. The quadrupole shift is described by the Hamiltonian

$$V_Q^{\text{LF}} = \text{Tr} \{QF(t)\}, \quad (4.17)$$

where  $Q_{ij} = \frac{3}{2}(S_i S_j + S_j S_i) - S(S+1)\mathbb{1}$ , with  $S(S+1) = \mathbf{S}^2$ ,  $F_{ij} = \frac{\partial E_j}{\partial x_i}$  and the components of the electric field are denoted by  $E_j$ . The quadrupole operator becomes, in a RWA,

$$\begin{aligned} \mathcal{R}_z(\omega t)Q &\simeq \frac{3}{2} \begin{pmatrix} S_x^2 + S_y^2 & 0 & 0 \\ 0 & S_x^2 + S_y^2 & 0 \\ 0 & 0 & 2S_z^2 \end{pmatrix} - S(S+1)\mathbb{1} \\ &= \frac{S(S+1) - 3S_z^2}{2} \begin{pmatrix} 1 & 0 & 0 \\ 0 & 1 & 0 \\ 0 & 0 & -2 \end{pmatrix}. \end{aligned} \quad (4.18)$$

The latter expression is useful for evaluating the quadrupole shift. This is further simplified when using the Laplace equation  $F_{xx} + F_{yy} + F_{zz} = 0$  in the quadrupole shift Hamiltonian

$$\mathcal{R}_z(\omega t)V_Q^{\text{LF}} = \text{Tr}\{\mathcal{R}_z(\omega t)[Q]F\} \simeq \frac{3F_{zz}}{2} (3S_z^2 - S(S+1)). \quad (4.19)$$

Thus, in the first layer of dressing, one has to evaluate

$$\begin{aligned} \mathcal{R}_z(\omega t)\mathcal{R}_n(\theta)S_z^2 &= \left[ \cos\theta S_z + \frac{i}{2} \sin\theta (e^{it(\omega+\varphi)} S_+ - e^{-it(\omega+\varphi)} S_-) \right]^2 \\ &\simeq \cos^2\theta S_z^2 + \frac{\sin^2\theta}{4} (S_+ S_- + S_- S_+) \\ &= \frac{\sin^2\theta}{2} S(S+1) - \frac{1 - 3\cos^2\theta}{2} S_z^2. \end{aligned} \quad (4.20)$$

Iterating this transformation once more yields the expression in the interaction picture

$$V_Q^{\text{IP}} = \mathcal{D}(\omega_i, g\Omega_i, t, \alpha) [V_Q^{\text{LF}}] = \frac{1}{4} (1 - 3 \cos^2 \theta_1) (1 - 3 \cos^2 \theta_2) \times \frac{3F_{zz}(t)}{2} [S(S+1) - 3S_z^2]. \quad (4.21)$$

The first line on the right-hand side of Eq. (4.21), whose magnitude is at most one, gives the reduction of the quadrupole shift due to dynamic decoupling. The last line is just the standard expression for the quadrupole shift of the non-degenerate levels in the RWA. With the so-called magic angle,  $\cos^2 \theta_{1(2)} = 1/3$ , the quadrupole shift can be erased in either the first or the second dressing layer.

Generally, with two layers of dressing, it is possible to erase both Zeeman and quadrupole shifts simultaneously by choosing  $\cos \theta_{1(2)} = 0$  and  $\cos^2 \theta_{2(1)} = 1/3$ . When determining which effect to cancel in the first layer and which in the second, it is important to consider time scales and time averaging. The first dressing layer involves a coarse grain of time over a scale of  $\omega_1^{-1}$ , while the second one averages over  $\omega_2^{-1} > \omega_1^{-1}$ . Therefore, it will be advantageous to cancel the faster fluctuations first.

### 4.3 Laser-ion interaction

After properly describing the effect of two layers of dressing in a given manifold, we will consider electric-quadrupole transitions between two Zeeman manifolds. We will start by characterizing the laser-ion interaction and finding the conditions that drive each transition. After that, we will take into account the counter-rotating terms neglected in the previous section as well as the so-called cross-field effect, which accounts for how the off-resonant fields applied to the ground manifold affect the excited manifold and vice versa. We will finish the section by applying this formalism to the particular case of  $^{40}\text{Ca}^+$  in order to visualize how these transitions will be spread in the frequency spectrum.

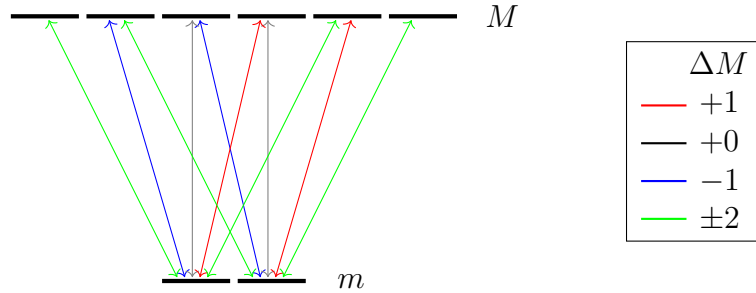


Figure 4.2: Shows the possible combinations allowed by the quadrupole selection rules in the bare basis states  $(m, M)$ .

### 4.3.1 Quadrupole transitions in doubly-dressed basis

We consider an ion with a manifold of ground states (s) and a manifold of excited states (d) that exhibit an electric, quadrupole-allowed, optical transition at frequency  $\omega_{sd}$ . The spin in the manifolds is denoted by  $S^\kappa$  ( $\kappa = s, d$ ) and the angular momentum operators are denoted by  $\mathbf{S}^\kappa$ , such that  $(\mathbf{S}^\kappa)^2 = S^\kappa(S^\kappa + 1)$ . The Zeeman states in the two manifolds will be expressed with lower case letters for the ground states,  $|m\rangle$  ( $|m| \leq S^s$ ) and upper case letters for the excited states,  $|M\rangle$  ( $|M| \leq S^d$ ). A schematic for this transition between the two manifolds can be seen in Fig. 4.2 for the case of  $^{40}\text{Ca}^+$ . The letters s and d are motivated for the manifolds  $S = 1/2$  and  $D = 5/2$  of  $^{40}\text{Ca}^+$ , which is the example we will work with.

The dc magnetic field along the laboratory axis  $z$  splits the Zeeman states by frequencies  $\omega_0^\kappa = g_\kappa \mu_B B$ , where  $g_\kappa$  is the gyromagnetic factor of spin manifold  $S^\kappa$ . Both manifolds are subject to the respective dynamical decoupling rf-dressing fields with angles  $\alpha_\kappa$ , rf frequencies  $\omega_i^\kappa$ , and Rabi frequencies  $g_\kappa \Omega_i^\kappa$ , for  $i = 1, 2$ , as explained in Sec. 4.2.1. Therefore, the Hamiltonian in the laboratory frame is

$$H^{\text{LF}} = H_{\text{dc}}^s + H_{\text{rf}}^s + H_{\text{dc}}^d + H_{\text{rf}}^d, \quad (4.22)$$

generalizing Eq. (4.3) to the case of two spin manifolds. We note that this neglects an unavoidable cross-coupling through an off-resonant driving of the s manifold by the rf dressing fields of the d manifold, and vice versa. This effect will be neglected in the following, and is treated in Sec. 4.3.2. In the doubly-dressed basis, this Hamiltonian becomes

$$H = \bar{\omega}_0^s S_z^s + \bar{\omega}_0^d S_z^d, \quad (4.23)$$

generalizing Eq. (4.12).

The electric-quadrupole interaction ( $E2$ ) of the ion with a laser of frequency  $\omega_L$  and vector potential  $\mathbf{A}(\mathbf{R}, t) = \mathbf{A}^+(\mathbf{R})e^{-i\omega_L t} + \text{c.c.}$  is  $V_{E2} = \frac{ie\omega_{sd}}{2} (r_i r_j \partial_i A_j(\mathbf{R}, t) - \text{h.c.})$ , see e.g. [119]. By expanding the s and d manifolds in the bare basis, and in a frame rotating at the optical transition frequency  $\omega_{sd}$ , one obtains, in optical RWA,

$$V_{E2}^{\text{LF}} = i \sum_{m, M} (\Omega_{mM} |M\rangle \langle m| e^{-i\Delta_L t} - \text{h.c.}). \quad (4.24)$$

The Rabi frequencies are  $\Omega_{mM} = \langle M | r_i r_j | m \rangle \partial_i A_j^+(\mathbf{R}) / \hbar$ . The matrix elements  $\langle M | r_i r_j | m \rangle$  imply the quadrupole selection rules  $|\Delta m| = |M - m| \leq 2$ , see e.g. figure 4.2. The laser detuning is  $\Delta_L = \omega_L - \omega_{sd}$ .

We are now in a position to discuss how the dynamical decoupling affects the quadrupole interaction. To do so, we need to switch to the doubly-dressed basis and

to an interaction picture with respect to (4.23), generalizing the procedure explained in the previous section to two spin manifolds. Denoting by  $\mathcal{D}^\kappa = \mathcal{D}^\kappa(\omega_i^\kappa, g^\kappa \Omega_i^\kappa, t, \alpha_\kappa)$  the dressing procedure of the spin manifold  $\kappa$ , where  $\mathcal{D}$  is defined in Eq. (4.13), the laser-ion interaction becomes

$$\begin{aligned} V_{E2}^{\text{IP}} &= \mathcal{D}^s \otimes \mathcal{D}^d [V_{E2}^{\text{LF}}] \\ &= i \sum_{\bar{m}, \bar{M}} \left( \sum_{m, M} \Omega_{mM} \langle \bar{M} | \mathcal{D}^s \otimes \mathcal{D}^d [ |M\rangle \langle m| ] | \bar{m} \rangle | \bar{M} \rangle \langle \bar{m} | e^{-i\Delta_L t} - \text{h.c.} \right). \end{aligned} \quad (4.25)$$

Here, we expanded the quadrupole interaction in the basis of doubly-dressed states. Now, we need to calculate the matrix elements corresponding to a given pair of dressed states, which we will write as

$$\langle \bar{M} | \mathcal{D}^s \otimes \mathcal{D}^d [ |M\rangle \langle m| ] | \bar{m} \rangle = \mathcal{U}_{\bar{M}M}^d(t) (\mathcal{U}_{\bar{m}m}^s(t))^*, \quad (4.26)$$

with

$$\mathcal{U}_{\bar{M}M}^d(t) = \langle \bar{M} | U_{\mathbf{z}}(\bar{\omega}_0^d t) U_{\mathbf{n}_2^d}(\theta_2^d) U_{\mathbf{z}}(\omega_2^d t) U_{\mathbf{n}_1^d}(\theta_1^d) U_{\mathbf{z}}(\omega_1^d t) | M \rangle, \quad (4.27)$$

and equivalently for  $\mathcal{U}_{\bar{m}m}^s(t)$  with  $d \leftrightarrow s$  and  $\bar{M}, M \leftrightarrow \bar{m}, m$ . As an example, we will evaluate the matrix elements for the d-states

$$\begin{aligned} &\langle \bar{M} | U_{\mathbf{z}}(\bar{\omega}_0 t) U_{\mathbf{n}_2}(\theta_2) U_{\mathbf{z}}(\omega_2 t) U_{\mathbf{n}_1}(\theta_1) U_{\mathbf{z}}(\omega_1 t) | M \rangle \\ &= \sum_{\bar{M}} \langle \bar{M} | U_{\mathbf{n}_2}(\theta_2) | \bar{M} \rangle \langle \bar{M} | U_{\mathbf{n}_1}(\theta_1) | M \rangle e^{i(\bar{M}\bar{\omega}_0 + \bar{M}\omega_2 + M\omega_1)t}, \end{aligned} \quad (4.28)$$

where we used the expansion of the identity  $\mathbf{1} = \sum_{\bar{M}} | \bar{M} \rangle \langle \bar{M} |$ . Finally, the remaining matrix elements of the unitary matrices corresponding to the rotations of the quantization axis are

$$\begin{aligned} \langle \bar{M} | U_{\mathbf{n}_1}(\theta_1) | M \rangle &= \langle \bar{M} | e^{i\theta_1(-\sin \alpha S_x + \cos \alpha S_y)} | M \rangle \\ &= \langle \bar{M} | e^{-i\alpha S_z} e^{i\theta_1 S_y} e^{i\alpha S_z} | M \rangle \\ &= e^{-i\alpha(\bar{M}-M)} d_{\bar{M}M}^S(\theta_1), \end{aligned} \quad (4.29)$$

and

$$\langle \bar{M} | U_{\mathbf{n}_2}(\theta_2) | \bar{M} \rangle = e^{-i(\alpha-\pi/2)(\bar{M}-\bar{M})} d_{\bar{M}\bar{M}}^S(\theta_2). \quad (4.30)$$

Here, the Wigner d-matrix is used, which is defined as [120]

$$\begin{aligned} d_{\bar{M}M}^S(\theta) &= \langle S\bar{M} | e^{-i\theta S_y} | SM \rangle \\ &= \sqrt{(S+\bar{M})!(S-\bar{M})!(S+M)!(S-M)!} \\ &\quad \times \sum_k \frac{(-1)^k \cos\left(\frac{\theta}{2}\right)^{2S+M-\bar{M}-2k} \left[-\sin\left(\frac{\theta}{2}\right)\right]^{\bar{M}-M+2k}}{(S+M-k)!k!(\bar{M}-M+k)!(S-\bar{M}-k)!}. \end{aligned} \quad (4.31)$$

The sum is over all  $k$  that do not make negative one of the factorials in the denominator. We can also use that  $d_{MM}^S(-\theta) = d_{M\bar{M}}^S(\theta)$ . With that, we get to the final expression for the laser-ion interaction in the doubly dressed basis

$$V_{E2}^{\text{IP}} = i \sum_{\bar{m}, \bar{M}} \left( \sum_{m, M} \sum_{\bar{m}, \bar{M}} \bar{\Omega}_{\bar{m}\bar{M}}^{mM, \bar{m}\bar{M}} |\bar{M}\rangle \langle \bar{m}| e^{i\Delta_{\bar{m}\bar{M}}^{mM, \bar{m}\bar{M}} t} - \text{h.c.} \right), \quad (4.32)$$

where we introduced the effective Rabi frequency

$$\begin{aligned} \bar{\Omega}_{\bar{m}\bar{M}}^{mM, \bar{m}\bar{M}} &= \Omega_{mM} e^{-i\alpha_d(\bar{M}-M) - i\frac{\pi}{2}(\bar{M}-\bar{M})} d_{M\bar{M}}(\theta_1^d) d_{\bar{M}\bar{M}}(\theta_2^d) \\ &\times e^{i\alpha_s(\bar{m}-m) + i\frac{\pi}{2}(\bar{m}-\bar{m})} d_{\bar{m}m}(\theta_1^s) d_{\bar{m}\bar{m}}(\theta_2^s). \end{aligned} \quad (4.33)$$

and the effective detuning

$$\Delta_{\bar{m}\bar{M}}^{mM, \bar{m}\bar{M}} = -\Delta_L + \bar{M}\bar{\omega}_0^d + \bar{M}\omega_2^d + M\omega_1^d - \bar{m}\bar{\omega}_0^s - \bar{m}\omega_2^s - m\omega_1^s. \quad (4.34)$$

We can see that the effect of  $\alpha_\nu$  is only a common phase for the Rabi frequencies. It is important to note that no RWA is applied in Eq. (4.32).

Thus, to drive a  $\bar{m} \leftrightarrow \bar{M}$  transition in the doubly-dressed basis, the laser detuning must be chosen such that  $\Delta_{\bar{m}\bar{M}}^{mM, \bar{m}\bar{M}} = 0$ , that is

$$\Delta_L = \bar{M}\bar{\omega}_0^d + \bar{M}\omega_2^d + M\omega_1^d - \bar{m}\bar{\omega}_0^s - \bar{m}\omega_2^s - m\omega_1^s \quad (4.35)$$

is satisfied for one set of indices  $(m, M, \bar{m}, \bar{M})$ . The magnitude of the effective Rabi frequency is

$$\left| \bar{\Omega}_{\bar{m}\bar{M}}^{mM, \bar{m}\bar{M}} \right| = |d_{M\bar{M}}(\theta_1^d)| |d_{\bar{M}\bar{M}}(\theta_2^d)| |d_{\bar{m}m}(\theta_1^s)| |d_{\bar{m}\bar{m}}(\theta_2^s)| |\Omega_{mM}| \leq |\Omega_{mM}|, \quad (4.36)$$

since the Wigner  $d$ -matrix is unitary, and therefore, all its elements are smaller than one in magnitude. To make efficient use of the laser power, it will be advantageous to choose  $(m, M, \bar{m}, \bar{M})$  such that the contribution of the Wigner  $d$ -matrix elements is as large as possible. In doing so,  $m$  and  $M$  have to respect the quadrupole selection rules, but not necessarily the pair  $(\bar{m}, \bar{M})$ .

### 4.3.2 Corrections to the bare frequencies

In this subsection, we want to study the consequence of accounting for the counter-rotating terms, also known as Bloch-Siegert effect, and the so-called cross-field effect, which accounts for the response that the excited states manifold (d) have due to the presence of the rf fields applied to the ground states manifold (s) and vice versa. We will do so using the so-called Magnus expansion [16], which allows us to treat these effects in a perturbative way, and is explained in chapter 2.

Let us start with the counter-rotating terms in the first RWA in Eq. (4.6). We consider the Hamiltonian

$$H_{\text{co}} = \frac{g}{4} \left( \Omega_1 (e^{i(2\omega_1 t - \alpha)} S_+ + e^{-i(2\omega_1 t - \alpha)} S_-) + i\Omega_2 \cos(\omega_2 t) (e^{i(2\omega_1 t - \alpha)} S_+ - e^{-i(2\omega_1 t - \alpha)} S_-) \right). \quad (4.37)$$

We will treat this term as a correction to the detuning, thus in a rotating frame with respect to  $H_{\text{det}} = \Delta_1 S_z$  this transforms into

$$H_{\text{co}}^{\text{RF}} = \mathcal{R}_{\mathbf{z}}(\Delta_1 t)[H_{\text{co}}] = c_{\text{co}}(t)S_+ + c_{\text{co}}^*(t)S_-, \quad (4.38)$$

where

$$c_{\text{co}}(t) = \frac{g}{4} (\Omega_1 + i\Omega_2 \cos(\omega_2 t)) e^{i((\omega_0 + \omega_1)t - \alpha_d)}. \quad (4.39)$$

Therefore,  $H_{\text{co}}^{\text{RF}}$  will contain only terms oscillating fast at time scales  $\omega_0 + \omega_1$  and at sideband frequencies  $\omega_2$  of these. The effect of these off-resonant driving terms, averaged over a time scale  $T \gg (\omega_0 + \omega_1)^{-1}$ , can be described by an effective Hamiltonian

$$\begin{aligned} H_{\text{co}}^{\text{eff}} &= -\frac{i}{2T} \int_0^T dt_1 \int_0^{t_1} dt_2 [H_{\text{co}}^{\text{RF}}(t_1), H_{\text{co}}^{\text{RF}}(t_2)] \\ &= -\frac{i}{T} \int_0^T dt_1 \int_0^{t_1} dt_2 (c_{\text{co}}(t_1)c_{\text{co}}^*(t_2) - \text{c.c.})S_z \\ &\simeq \omega_0 \frac{g^2}{8} \frac{(\Omega_1)^2 + (\Omega_2)^2}{\omega_0(\omega_0 + \omega_1)} S_z. \end{aligned} \quad (4.40)$$

Further corrections are of higher order in  $\Omega_i/|\omega_0 + \omega_1| \ll 1$ . The form of the effective Hamiltonian (first line) corresponds to the first non-vanishing term in the Magnus expansion of the time-evolution operator corresponding to the Hamiltonian in Eq. (4.38). Therefore, the counter-rotating terms can be accounted for by suitably shifted bare frequencies that absorb the contributions of  $H_{\text{co}}^{\text{eff}}$ .

We continue by treating the non-resonant rf dressing fields of the d (s) spin manifold affecting the s (d) manifold. Here, only the former case is covered. The corresponding Hamiltonian on the s manifold is

$$H_{\text{d} \rightarrow \text{s}} = g_s (\Omega_1^{\text{d}} \cos(\omega_1^{\text{d}} t) - \Omega_2^{\text{d}} \sin(\omega_1^{\text{d}} t) \cos(\omega_2^{\text{d}} t)) (S_x^{\text{s}} \cos \alpha_d + S_y^{\text{s}} \sin \alpha_d). \quad (4.41)$$

In a rotating frame with respect to the dc Hamiltonian  $H_{\text{dc}}^{\text{s}} = \omega_0^{\text{s}} S_z^{\text{s}}$ , we obtain

$$H_{\text{d} \rightarrow \text{s}}^{\text{RF}} = \mathcal{R}_{\mathbf{z}}(\omega_0^{\text{s}} t)[H_{\text{d} \rightarrow \text{s}}] = c_{\text{cf}}(t)S_+ + c_{\text{cf}}^*(t)S_-, \quad (4.42)$$

where

$$c_{\text{cf}}(t) = \frac{g_s}{2} (\Omega_1^{\text{d}} \cos(\omega_1^{\text{d}} t) - \Omega_2^{\text{d}} \sin(\omega_1^{\text{d}} t) \cos(\omega_2^{\text{d}} t)) e^{i(\omega_0^{\text{s}} t - \alpha_d)}. \quad (4.43)$$

Thus,  $H_{d \rightarrow s}^{\text{RF}}$  will contain only terms oscillating fast at time scales  $\omega_0^s \pm \omega_1^d$  and at side-band frequencies  $\omega_2^d$  of these. The effect of these off-resonant driving terms, averaged over a time scale  $T \gg (\omega_0^s \pm \omega_1^d)^{-1}$ , can be described by an effective Hamiltonian

$$\begin{aligned} H_{d \rightarrow s}^{\text{eff}} &= -\frac{i}{2T} \int_0^T dt_1 \int_0^{t_1} dt_2 [H_{d \rightarrow s}^{\text{RF}}(t_1), H_{d \rightarrow s}^{\text{RF}}(t_2)] \\ &= -\frac{i}{T} \int_0^T dt_1 \int_0^{t_1} dt_2 (c_{\text{cf}}(t_1)c_{\text{cf}}^*(t_2) - \text{c.c.})S_z^s \\ &\simeq \omega_0^s \frac{g_s^2}{4} \frac{(\Omega_1^d)^2 + (\Omega_2^d)^2}{(\omega_0^s)^2 - (\omega_1^d)^2} S_z^s. \end{aligned} \quad (4.44)$$

Corrections to this are of higher order in  $\Omega_i^d/|\omega_0^s \pm \omega_1^d| \ll 1$ . The same result holds for the effect on the other manifold with  $s \leftrightarrow d$ . Thus, the cross-driving can be accounted for by suitably shifted bare frequencies absorbing the contributions of  $H_{d(s) \rightarrow s(d)}^{\text{eff}}$ . Therefore, if we combine the Bloch-Siegert effect and the cross-field effect we obtain an effective Zeeman splitting for the bare  $s$  manifold

$$\omega_{0\text{eff}}^s = \omega_0^s \left( 1 + \frac{g_s^2}{4} \frac{(\Omega_1^d)^2 + (\Omega_2^d)^2}{(\omega_0^s)^2 - (\omega_1^d)^2} + \frac{g_s^2}{8} \frac{(\Omega_1^s)^2 + (\Omega_2^s)^2}{\omega_0^s(\omega_0^s + \omega_1^s)} \right). \quad (4.45)$$

Once more via the replacement  $s \leftrightarrow d$  we can recover the effective shift for the  $d$  manifold.

These corrections will be taken into account in the next section when we study the particular case of  $^{40}\text{Ca}^+$ , and are indeed relevant to achieve agreement between theoretical predictions and experimental data.

### 4.3.3 Application to $^{40}\text{Ca}^+$

In this section, we will apply the above expressions to the case of the  $S_{1/2}$  to  $D_{5/2}$  transition in a  $^{40}\text{Ca}^+$  ion and compare them to measurements on the decoupled system. The experiment has been developed in the laboratory group of Prof. Dr. Piet Schmidt at PTB by Lennart Pelzer, Dr. Ludwig Krinner and Kai Dietze. For this experiment we will have the total spin of the manifolds  $S^s = \frac{1}{2}$  and  $S^d = \frac{5}{2}$ . The goal is to derive the frequency spectrum and the relative coupling strengths with the parameters given in Table 4.1, for each possible transition with a set of indices  $(m, M, \bar{m}, \bar{M}, \bar{\bar{m}}, \bar{\bar{M}})$ .

Before showing the results for two layers of dressing, we first want to gain some insight by explaining just one particular transition  $(\bar{m}, \bar{M})$  in the case of a single layer of dressing, with the parameters given in the first part of Table 4.1. We need to translate the equations for the effective Rabi frequency (4.33) and the effective



Dressing	Parameters	Value
1 <sup>st</sup> layer	$g_s \mu_b B_z$	$2\pi \times 10$ MHz
	$\Omega_1^s$	$2\pi \times 46\,805$ Hz
	$\Omega_1^d$	$2\pi \times 115\,600$ Hz
	$\omega_1^s$	$2\pi \times 10\,002\,090$ Hz
	$\omega_1^d$	$2\pi \times 5\,994\,834$ Hz
2 <sup>nd</sup> layer	$\Omega_2^s$	$2\pi \times 3469$ Hz
	$\Omega_2^d$	$2\pi \times 6809$ Hz
	$\omega_2^s$	$2\pi \times 72\,050$ Hz
	$\omega_2^d$	$2\pi \times 160\,589$ Hz

Table 4.1: Case study of double dressing for a  $^{40}\text{Ca}^+$  ion for the  $S_{1/2}$  and  $D_{5/2}$  manifolds. The upper part of the table refers to the variables in the first layer of dressing and the lower part of the second layer of dressing. For this calculations we will use the known values of the gyromagnetic factors  $g_s = 2.00225664$  [121] and  $g_d = 1.2003340$  [122].

detuning (4.34) for the case of a single dressing. This can be achieved by fixing  $\omega_2^{\text{d(s)}} = 0$  and  $\Omega_2^{\text{d(s)}} = 0$ , which implies

$$\bar{\Omega}_{\bar{m}\bar{M}}^{mM} = \Omega_{mM} e^{i(\alpha_d M - \alpha_s m) + i\frac{\pi}{2}(\bar{M} - \bar{m})} d_{M\bar{M}}(\theta_1^d) d_{\bar{m}m}(\theta_1^s) \quad (4.46)$$

and

$$\Delta_{\bar{m}\bar{M}}^{mM} = -\Delta_L + \bar{M}\bar{\omega}_0 + M\omega_1^d - \bar{m}\bar{\omega}_0 - m\omega_1^s, \quad (4.47)$$

where we go to an interaction picture with respect to the Hamiltonian in the first dressed basis (4.8).

The results are illustrated in Fig. 4.3, where Fig. 4.3 a) depicts a transition in the first dressed basis with indices  $(\bar{m}, \bar{M}) = (-1/2, -1/2)$ . This transition can be driven in 10 different ways through the possible transitions in the bare basis for the appropriate laser detuning. Using different transitions in the bare basis will imply different effective Rabi frequencies. These effective Rabi frequencies are shown in Fig. 4.3 b). The colors refer to the different possible selection rules shown in Fig. 4.2.

Due to the fact that the first dressed basis has no selection rules, each transition in the doubly-dressed basis can be driven through  $6 \times 2$  combinations of the first dressed basis, which will result in the desired transition in the doubly-dressed basis. Therefore, since there are also no selection rules between the doubly-dressed basis, a fixed initial state in the doubly-dressed basis  $|\bar{m}\rangle$  will have  $6 \times 12 \times 10$  possible transitions. For the transitions with an initial state  $|\bar{m}\rangle = |-1/2\rangle$ , Fig. 4.4 a) depicts the effective Rabi frequencies relative to the Rabi frequencies of the transitions in the bare basis, i.e.,  $\left| \bar{\Omega}_{\bar{m}\bar{M}}^{mM} / \Omega_{mM} \right|$ . This ratio is plotted against the laser detuning, that shows for which

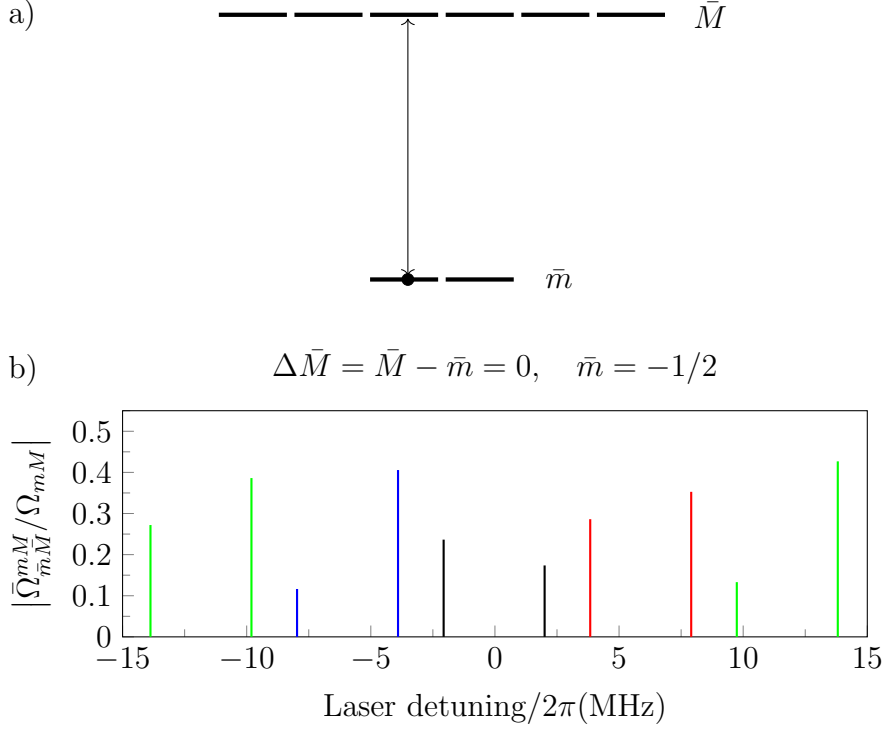


Figure 4.3: Fig. a) shows a particular transition in the dressed basis basis with indices  $\bar{M} = -1/2 \leftrightarrow \bar{m} = -1/2$ . This transition can be driven using different combinations of underlying states  $(m, M)$  in the bare basis, shown in Fig. 4.2, through an appropriate laser detuning. The color code for the allowed transitions is the same as in Fig. 4.2. Since the dressed states are a time dependent superposition of the bare basis states, as shown in Fig. 4.1, their transition strength depends on the selection rules of the bare basis. Fig. b) depicts the effective Rabi frequencies relative to the Rabi frequencies of the transitions in the bare basis, i.e.,  $|\bar{\Omega}_{\bar{m}\bar{M}}^{mM}/\Omega_{mM}|$ . This ratio is plotted against the laser detuning, which shows for which values the transitions occur.

values the transitions are resonant. The shaded area corresponds to the region defined by the pair  $(m, M) = (-0.5, -1.5)$ , shown in more detail in Fig. 4.4 b). Similarly, Fig. 4.4 c) shows the tuple  $(m, M, \bar{m}, \bar{M}) = (-0.5, -1.5, -0.5, -2.5)$ , where we can see the transition with higher effective Rabi frequency. Here, we can also observe that there are no selection rules for  $\Delta\bar{M}$ . Noticeably, the relative Rabi frequencies have different weights, making the characterization of these transitions necessary to make efficient use of the laser power. Efficient use of laser power can be achieved by choosing a transition with high effective Rabi frequency and, ideally, a small effective Rabi frequency of the nearest neighboring transitions. As we can see, such an optimization becomes simply a matter of engineering after the characterization of the transitions.

For the case of a single layer of dressing we compared the theoretical results with the experimental data. After accounting approximately for the counter-rotating terms and for the cross-field effect using Magnus expansion, we managed to obtain an agreement between theory and experiment. With that, we verified the equations derived throughout this chapter for the case of one layer of dressing. This comparison can be found in detail in our article [118].

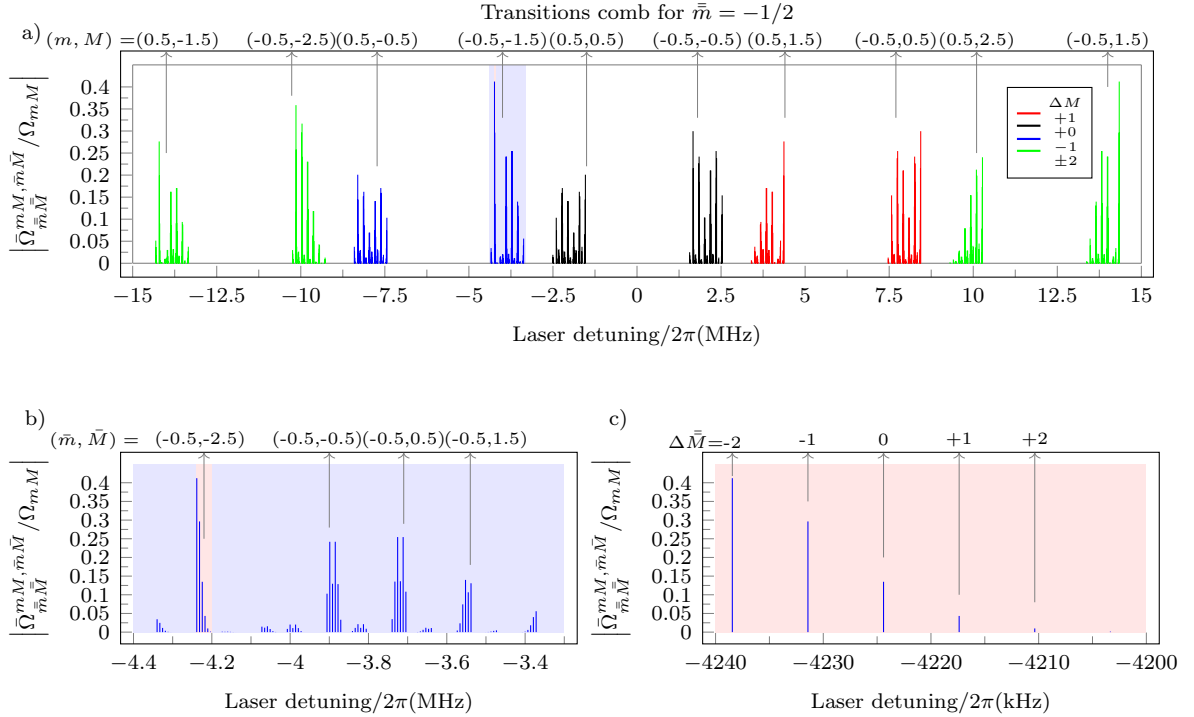


Figure 4.4: In this figure we show the ratio of the Rabi frequencies  $\left| \frac{\bar{\Omega}_{\bar{m}\bar{M}}^{mM, \bar{m}\bar{M}}}{\Omega_{mM}} \right|$  for all possible transitions from a doubly-dressed ground state  $|\bar{m}\rangle$  to a doubly-dressed excited state  $|\bar{M}\rangle$  at different laser detuning. Each color represents a different selection rule for the pair  $(m, M)$ . The green color stands for  $\pm 2$  transitions, the blue color for  $-1$  transitions, the red color for  $+1$  transitions and finally the black color stands for  $+0$  transitions. We initialized the ground doubly-dressed state in the state  $|\bar{m}\rangle = -1/2$ .

## 4.4 Dressed states vs Floquet states

In this section, we compare the description of a single layer of dressing in terms of dressed states with another perspective based on Floquet states. As mentioned already in chapter 2, we expect the dressed states to be an approximation of the Floquet states.

For this case our Hamiltonian will be equivalent to Eq. (4.2) with  $\Omega_2 = 0$

$$H_{\text{rf}} = g\Omega_1 \cos(\omega_1 t)(S_x \cos \alpha + S_y \sin \alpha). \quad (4.48)$$

Using QuTiP [123], we numerically calculate the Floquet states and compare them with the first dressed basis. Additionally, we also want to compare the Floquet basis with the first dressed basis including the counter-rotating terms in an approximate way, as shown in Sec. 4.3.2, which we will refer to as corrected dressed states. We will show these comparisons for the cases of total spin  $S = 1/2$  and  $S = 5/2$ , which are the relevant cases in our study. Taking into account several frequencies at the same time is computationally and theoretically, from the point of view of Floquet theory, a lot more demanding and goes beyond the scope of this work. Therefore, we will not be able to study the so-called cross-field effect as it will involve the presence of two different frequencies.

Before showing the numerical results, we want to give some analytical insight into our problem. With this goal, let us study the expression of the Hamiltonian after going to the rotating frame, and under the RWA, similar to Eq. (4.6), we obtain

$$\mathcal{R}_{\mathbf{z}}(\omega_1 t) [H^{\text{LF}} - i \frac{d}{dt}] = \Delta_1 S_z + \frac{g\Omega_1}{2} (S_x \cos \alpha + S_y \sin \alpha) - i \frac{d}{dt}. \quad (4.49)$$

By fixing  $\alpha = 0$  and  $\Delta_1 = 0$ , we have, simply, a Hamiltonian proportional to  $S_x$  and therefore, the effect of the dynamical decoupling is such that the eigenstates of our problem in a rotating frame at the frequency  $\omega_1$  are just the eigenstates of  $S_x$ . Of course, the dressed states will now be generated by a  $\pi/2$  rotation transforming  $S_x$  into  $S_z$ , but, to make the discussion easier, we will refer to the dressed states as the eigenstates of  $S_x$  in the rotating frame. The Floquet states will be calculated numerically from the total Hamiltonian, therefore, in order to compare them, the fact that the dressed states are in a rotating frame must be taken into account.

The values for the numerical simulations presented in this section are shown in Table 4.1, additionally, we fixed  $\alpha = 0$ ,  $\Delta_1 = 0$  and the results are plotted for the duration of one period  $T^{\text{s(d)}} = \frac{2\pi}{\omega_1^{\text{s(d)}}}$ . We first study the case of the manifold  $S = 1/2$ , which presents a symmetry between its two eigenstates, and therefore we are only going to present the results for  $\bar{m} = 1/2$ . Fig. 4.5 shows the infidelity, i.e.,  $1 - |\langle \bar{m} | u_{m_f}(t) \rangle|^2$ , where  $u_{m_f}(t)$  corresponds to the Floquet state with an average value of  $S_x$  close to  $m_f$ , and of course we will choose  $\bar{m} = m_f = 1/2$  for comparison. We can see how accounting for the counter-rotating terms using the Magnus expansion improves the fidelity considerably.

Coming back to the insight gained before, we are dealing with a Hamiltonian that, in a rotating frame and under the RWA, takes the form of  $S_x$ . Therefore, to see

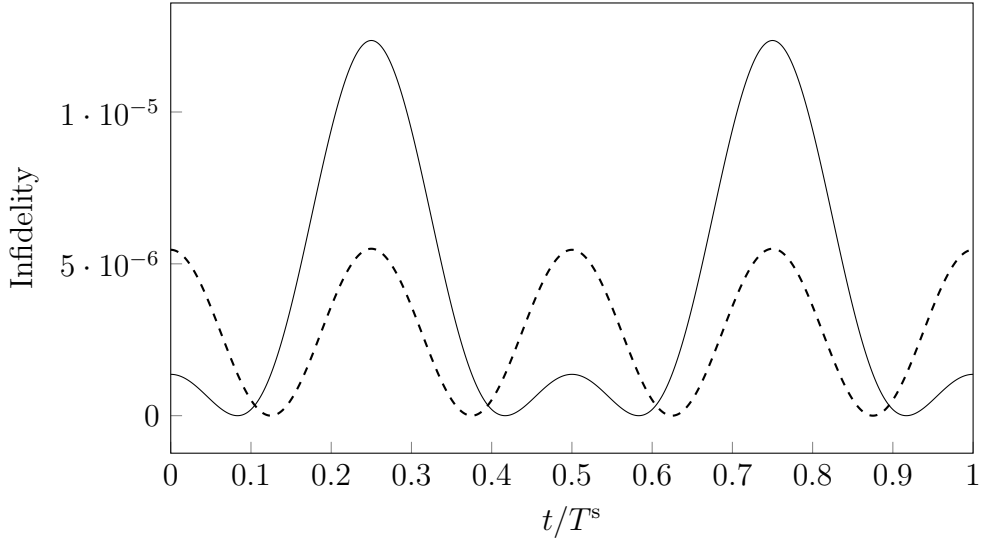


Figure 4.5: In this figure we show the infidelity,  $1 - |\langle \bar{m} | u_{m_f}(t) \rangle|^2$ , with  $\bar{m} = m_f = 1/2$  (solid line) during one period  $T^s = \frac{2\pi}{\omega_1^s}$ . We also show the infidelity between the same Floquet state and the corresponding corrected dressed state (dashed line) including Bloch-Siegert shifts.

how much they differ, it will be useful to study the average of  $S_z$ . This is motivated because the corrections using Magnus expansion to the dressed states were absorbed in the Zeeman splitting. The average of  $S_z$  is shown in Fig. 4.6, where we can see that the Floquet states, in the rotating frame, can be envisioned in the Bloch sphere as states pointing in the direction  $x$  but have some fluctuations around a particular value of  $S_z$ , which is shifted from the equator. For the case of  $S = 1/2$  both eigenstates are shifted by the same magnitude but in opposite directions in the equator, as can be seen in Figs. 4.6 a) and b). Something worth highlighting is that, if we take into account the counter-rotating terms, i.e., the corrected dressed states, they correspond to the time-independent part of the Floquet states, as can be seen in Fig. 4.6, where the time average of the Floquet state corresponds to the corrected dressed state, up to the level of  $10^{-6}$ . This statement is also justified by Fig. 4.5, where we can see how the infidelity oscillates around an average value for the corrected dressed states.

We can now study the same effects for the total spin  $S = 5/2$  manifold. For this case we have a symmetry between  $M_f \leftrightarrow -M_f$ , and therefore, we will show the plots only for the positive eigenvalues of the operator  $S_x$  of the Floquet states. The infidelity is shown in Fig. 4.7 for the cases of  $M_f = 1/2$  (orange),  $M_f = 3/2$  (cyan) and  $M_f = 5/2$  (purple). We can observe again that the Magnus expansion leads to higher fidelity, as expected from studying the previous manifold. We observe numerically that we have better fidelity for higher values of  $M_f$ . We have checked this feature as well for the case of a spin manifold  $S = 3/2$ . Similarly to the previous

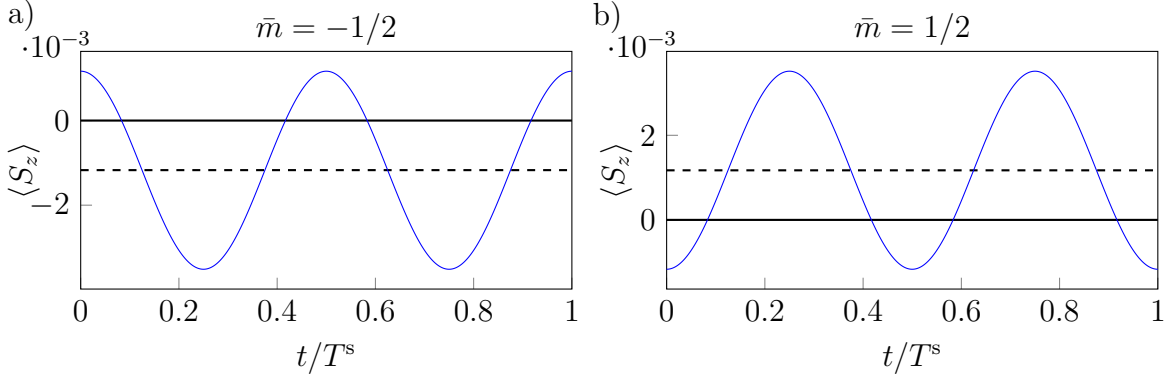


Figure 4.6: Figs. a) and b) show the average of  $S_z$  of the dressed states (solid black line), the corrected dressed states (dashed black line) and the Floquet states (solid blue line) during one period  $T^s = \frac{2\pi}{\omega_1^s}$ , for the cases of  $\bar{m} = -1/2$  and  $\bar{m} = 1/2$ , respectively.

case, Fig. 4.8 shows the value of  $S_z$  for the Floquet states, the dressed states and the corrected dressed states. Also for the  $S = 5/2$  manifold, the corrected dressed states correspond to the time-independent part of the Floquet states. We can observe once more that the fluctuations are also bigger for this manifold. The magnitude of the fidelity for all states in this manifold is smaller than for the previous manifold, we associate this with a higher dimension of the Hilbert space. By algebraically calculating the Floquet states one could gain further insight on why this is the case, as well as why there is better fidelity for higher values of  $M_f$ , but this goes beyond the intention of this chapter.

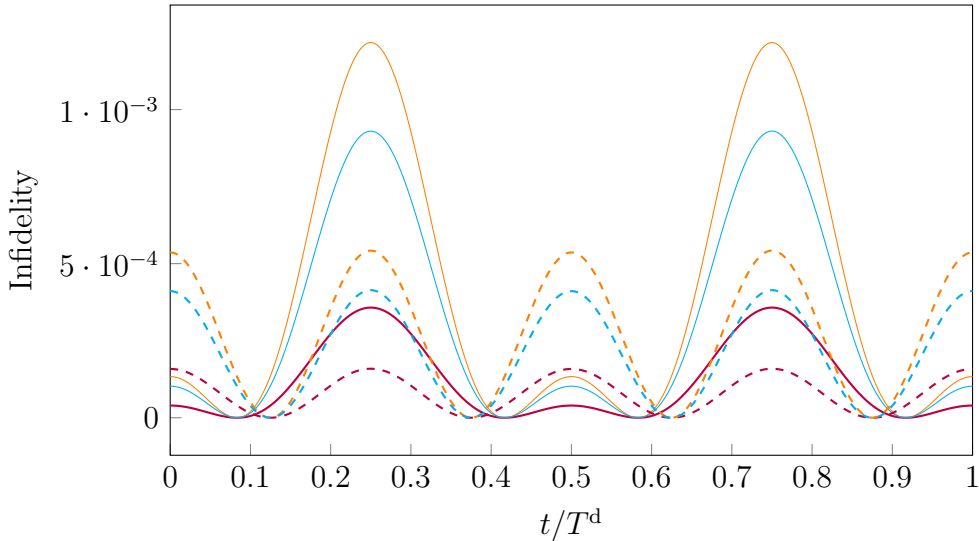


Figure 4.7: In this figure we show the infidelity,  $1 - |\langle \bar{M} | u_{M_f}(t) \rangle|^2$ , with  $\bar{M} = M_f$  (solid line) during one period  $T^d = \frac{2\pi}{\omega_1^d}$  for the cases of  $\bar{M} = 1/2$  (orange),  $\bar{M} = 3/2$  (cyan) and  $\bar{M} = 5/2$  (purple). We also show the infidelity between the same Floquet state and the corresponding corrected dressed state (dashed lines).

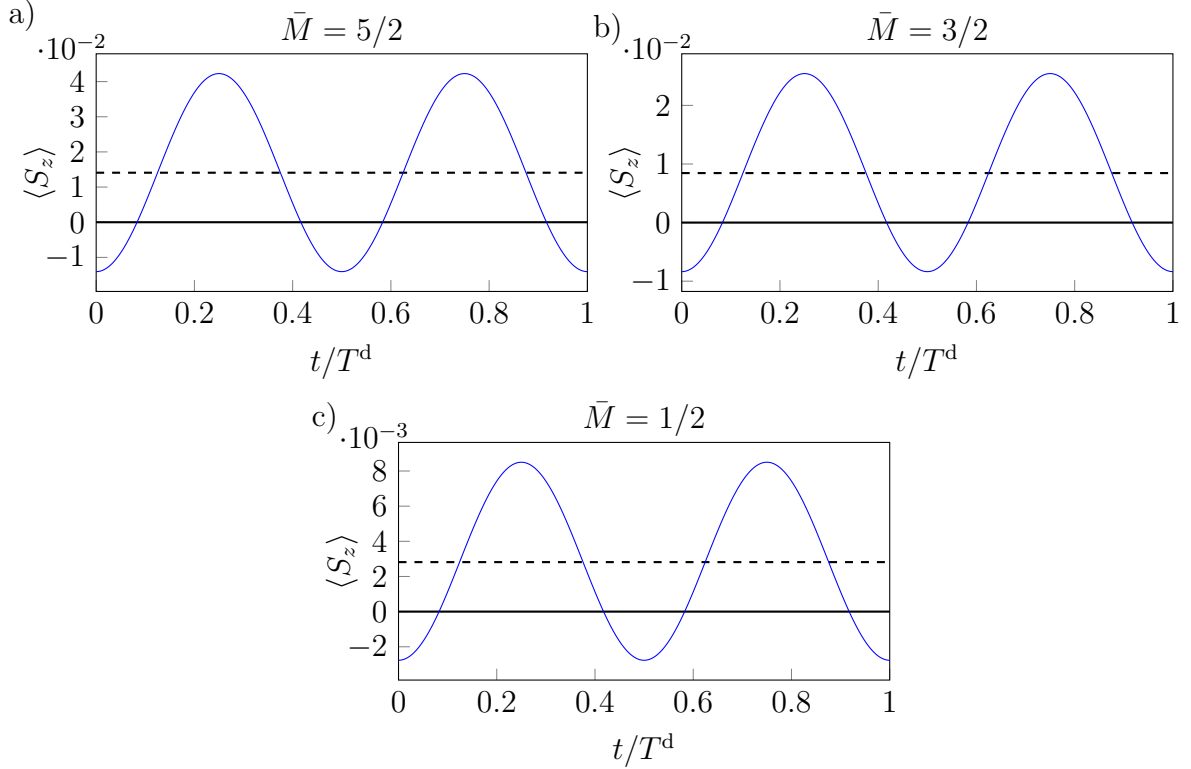


Figure 4.8: Figs. a), b) and c) show the average of  $S_z$  of the dressed states (solid black line), the corrected dressed states (dashed black line) and the Floquet states (solid blue line) during one period  $T^d = \frac{2\pi}{\omega_1^d}$ , for the cases of  $\bar{M} = 5/2$ ,  $\bar{M} = 3/2$  and  $\bar{M} = 1/2$ , respectively.

## 4.5 Mølmer-Sørensen gates.

After having a reduction of the magnetic field oscillations and the quadrupole shift as a consequence of the continuous dynamical decoupling, we ask ourselves if it would be feasible to, on top of that mechanism, create a Mølmer-Sørensen (MS) gate to produce entanglement between two ions. For creating the gate, it is necessary to drive the appropriate sideband transitions. In the previous treatment, the ion was assumed to be in a particular position  $\mathbf{R}_0 = \mathbf{0}$ . If we now consider the trap structure, the position of the ion will be described by a position operator  $\hat{\mathbf{R}}$ , affecting the expression of the vector potential, which will manifest the sideband transitions. The treatment can be found e.g. in [7]. Assuming that the laser field is a plane wave  $E(\hat{\mathbf{R}}, t) = E_0 e^{ik\hat{\mathbf{R}}} e^{i\omega_L t}$ , we obtain  $\mathbf{A}^+(\hat{\mathbf{R}}) e^{-i\omega_L t} = \frac{E_0}{i\omega} e^{ik\hat{\mathbf{R}}} e^{-i\omega t}$ . For simplicity, we will consider the motion along the direction  $\hat{x}$  and use the relation

$$k\hat{x} = \eta(\hat{a}u^*(t) + \hat{a}^\dagger u(t)), \quad (4.50)$$

where  $\eta$  is the Lamb Dicke parameter,  $u(t)$  is related with the motion of the ion and defined in Eq. (3.38), and  $\hat{a}$  is the ladder operator of the confinement and is defined in Eq. (3.43). We can make an expansion around the position of the atom assuming that we are in the Lamb Dicke regime,  $\eta \ll 1$ . We obtain, in a frame rotating at the optical transition frequency  $\omega_{sd}$ ,

$$V_{MS}^{\text{LF}} = i \sum_{m,M} \left\{ \Omega_{mM} |M\rangle\langle m| e^{-i\Delta_L t} (1 + i\bar{\eta}(\hat{a}e^{-i\nu t} + \hat{a}^\dagger e^{i\nu t})) - \text{h.c.} \right\}, \quad (4.51)$$

where  $\bar{\eta}$  is the effective Lamb Dicke parameter for which we will assume that the information about the trap parameters and the weight of the modes of motion is encoded.  $\nu$  is the trapping frequency, which fulfills the relations  $\omega_1^s \approx 5\nu$  and  $\nu \approx 20\omega_2^s$  for our case study. Nevertheless,  $(\omega_2^s \ll \nu \ll \omega_1^s)$  should always be fulfilled for the nature of our problem.

The transformations to go to the second dressed basis are independent of the ladder operators, and therefore, they will be encoded in the common denominator for the carrier and sideband transitions.

To drive MS gates we must keep in mind the hierarchy of time scales. The resonant condition with a sideband transition is  $\Delta_L = \bar{M}\bar{\omega}_0^d + \bar{M}\omega_2^d + M\omega_1^d - \bar{m}\bar{\omega}_0^s - \bar{m}\omega_2^s - m\omega_1^s \pm \nu$ . As we do not want to drive the sideband transition, we will assume a certain detuning  $\delta$  from resonance to be present, therefore, in order to drive the gate, the true laser detuning will be  $\Delta_L \pm \delta$ . This  $\delta$  usually needs to fulfill  $\delta \ll \nu$ , but in this study, in a first approach, it will have to fulfill  $\delta \ll \bar{\omega}_0$  as well, if we want to create a gate at the level of the doubly-dressed basis. Expressing the above expression including the dressing, after the appropriate transformations in the doubly-dressed basis and in the interaction picture with respect to Eq. (4.23) we obtain

$$V_{MS}^{\text{IP}} = - \sum_{\bar{m}, \bar{M}} \sum_{m, M} \sum_{\bar{m}, \bar{M}} \bar{\eta} \bar{\Omega}_{\bar{m}, \bar{M}}^{m, M, \bar{m}, \bar{M}} |M\rangle\langle \bar{m}| (\hat{a}e^{-i(\omega_c + \delta + \nu)t} + \hat{a}^\dagger e^{-i(\omega_c + \delta - \nu)t}) + \text{h.c.}, \quad (4.52)$$

where we defined the carrier frequency as  $\omega_c = \Delta_L + \bar{M}\bar{\omega}_0^d + \bar{M}\omega_2^d + M\omega_1^d - \bar{m}\bar{\omega}_0^s - \bar{m}\omega_2^s - m\omega_1^s$ . In the last expression we did not write the carrier contribution, for which we will have to ensure that it is off resonant for any indices. In a MS-gate without dressing, the carrier is off resonant under the condition  $\delta \ll \nu$ , which will be fulfilled as soon as we choose to be close to resonant to one particular sideband transition for a given set of indices. With the CDD, neglecting the carrier is not as straightforward as before due to the comb of possible transitions that can be seen in Fig. 4.4. As we could be resonant with a different carrier, the comb structure needs to be considered before neglecting all of the carrier transitions.



We want to see which terms are going to be relevant once we fix a particular sideband transition to be used as the gate. With a particular detuning  $\delta$ , if we fix the indices  $(m_0, M_0, \bar{m}_0, \bar{M}_0, \bar{\bar{m}}_0, \bar{\bar{M}}_0)$  we will be able to neglect all other contributions in a RWA. In order to show that, let us write the more relevant contributions, which will be the neighbors with the same indices except that they will have  $\bar{M} \neq \bar{\bar{M}}_0$ , as the smallest frequency will be  $\bar{\omega}_0^d$ . The total expression with the first relevant terms, using the appropriate laser detuning, can be written as

$$V_{MS}^{\text{IP}} \approx - \sum_{\bar{M}} \left\{ \bar{\eta} \bar{\Omega}_{m_0 \bar{m}_0 \bar{M} \bar{M}_0}^{m_0 M_0, \bar{m}_0 \bar{M}_0} |\bar{M}_0\rangle \langle \bar{m}_0| \hat{a} e^{-i(\delta + (\bar{M} - \bar{M}_0) \bar{\omega}_0^d)t} + h.c. \right\}. \quad (4.53)$$

Therefore, we can neglect the neighbors in a RWA if the following relation is fulfilled  $\bar{\eta} \bar{\Omega}_{m_0 \bar{m}_0 \bar{M} \bar{M}_0}^{m_0 M_0, \bar{m}_0 \bar{M}_0} \ll \bar{\omega}_0^d$ , but, in general, for driving a MS-gate one of the requirements is that  $\bar{\eta} \bar{\Omega}_{m_0 \bar{m}_0 \bar{M} \bar{M}_0}^{m_0 M_0, \bar{m}_0 \bar{M}_0} \ll \delta$ . Taking into account that in our study we also have to fulfill  $\delta \ll \bar{\omega}_0$ , in order not to drive the neighboring sidebands, we will be able to eliminate all the neighbors with a RWA, obtaining a final expression

$$V_{MS}^{\text{IP}} \approx - \bar{\eta} \bar{\Omega}_{m_0 \bar{m}_0 \bar{M} \bar{M}_0}^{m_0 M_0, \bar{m}_0 \bar{M}_0} |\bar{M}_0\rangle \langle \bar{m}_0| \hat{a} e^{-i\delta t} + h.c.. \quad (4.54)$$

From now on we will define the sideband Rabi frequency for a fixed sideband transition as  $\Omega_s = \bar{\eta} \bar{\Omega}_{m_0 \bar{m}_0 \bar{M} \bar{M}_0}^{m_0 M_0, \bar{m}_0 \bar{M}_0}$ .

In order to drive MS gates we will assume  $N$  ions in a two level system approximation. With this in mind, we will approximate each particle to a two level system defining  $\sigma_x = |\bar{M}\rangle \langle \bar{m}| + |\bar{m}\rangle \langle \bar{M}|$ . Via the Magnus expansion, the evolution operator for the above Hamiltonian can be found in the second order,

$$U(t) = e^{\sum_{j=1}^N \sigma_x^{(j)} (\alpha_j(t) a^\dagger - \alpha_j^*(t) a)} e^{-i \sum_{j,n=1}^N \sigma_x^{(j)} \sigma_x^{(n)} \Phi(t)}, \quad (4.55)$$

with

$$\alpha(t) = \frac{\Omega_s}{\delta} (e^{-i\delta t} - 1) \quad (4.56)$$

the time-dependent displacement. Requiring  $\alpha(T_g) = 0$ , gives a condition on the gate time  $T_g$ .

$$\Phi(t) = \frac{\Omega_s^2}{\delta} \left[ t - \frac{1}{\delta} \sin(\delta t) \right] \quad (4.57)$$

is the geometric phase. For these calculations, we assumed that the sideband Rabi frequency is the same for all particles. For the case of  $\delta \gg \Omega_s$ , the Rabi frequency of the gate will be  $\Omega_g = \frac{\Omega_s^2}{\delta}$ . For the gate to make a complete cycle we need

$$T_g \Omega_g = 2\pi K, \quad (4.58)$$

where  $K$  stands for the number of loops. The gate duration will be approximately

$$T_g = 2\pi K \frac{\delta}{\Omega_s^2}. \quad (4.59)$$

In order to erase the displacement, we will also need to fulfill

$$\delta T_g = 2n\pi, \quad (4.60)$$

for an integer  $n$ .

With the example treated in the previous section we ask ourselves which  $T_g$  will be realistic with the parameters of the problem. Combining the previous mentioned conditions, we want the detuning  $\delta$  from the sideband transition to fulfill  $\Omega_s \ll \delta \ll \bar{\omega}_0$ , therefore, we will assume for a case study  $3\Omega_s = \delta$  and  $3\delta = \bar{\omega}_0$ . We want to highlight at this point that the properties of the comb, e.g., the different weights of the transitions will permit us to allow less stringent conditions. Nevertheless, with the previous mentioned condition and using Eq. (4.59) assuming one loop, i.e.,  $K = 1$ , we obtain

$$T_g = 2\pi \frac{\delta}{\Omega_s^2} = 2\pi \frac{9}{\delta} = 2\pi \frac{27}{\bar{\omega}_0} \approx 3.375\text{ms}. \quad (4.61)$$

While this will not be a competitive gate for quantum computing applications, it may well be sufficient for applications in ion clocks. For ion clocks the gate time has to be compared with the interrogation time. Assuming an interrogation time of one second, the gate will be 300 times faster than the interrogation time. The extra time of the gate will add to the dark time of the interrogation scheme.

## 4.6 Conclusion

In conclusion, we recapitulated the treatment of continuous dynamical decoupling, which consists in applying an rf magnetic field perpendicular to the quantization axis. We considered first one manifold, showing how it could be used for suppressing Zeeman and quadrupole shifts. We managed to find a time-dependent frame in which the effective Hamiltonian is time independent. Therefore, in that frame, and after RWAs, we can find an effective basis for that Hamiltonian; we called this basis the dressed basis (doubly-dressed basis if applying two layers of dressing). Afterwards, we showed how it can be applied to two manifolds. We strove to write this mechanism

with a formalism that allowed us to write the interaction between the laser and the ion in an easier and intuitive way.

With this formalism, we properly characterized the laser-ion interaction to drive quadrupole transitions between two manifolds, showing that there are no selection rules for the dressed basis or doubly-dressed basis. Effectively, this mechanism creates a comb of possible transitions, which was not so intuitive to predict from the general problem. After this characterization, one can drive the same transition in the doubly-dressed basis using a different laser detuning, which is based on making the same transition through different combinations of transitions in the bare and dressed bases. We addressed the RWAs done in the first section as well as the cross-field effect, i.e., how the off-resonant fields applied to the ground manifold affect the excited manifold and vice versa. We did so by treating them in an approximate way using the Magnus expansion. Both effects can be effectively interpreted as a shift of the Zeeman splitting for both manifolds. This approximation proved useful to match theoretical and experimental data. After properly characterizing the CDD mechanism, we applied it to the particular case of a quadrupole transition between the  $S = 1/2$  and  $D = 5/2$  manifolds of  $^{40}\text{Ca}^+$ . For this case, we managed to show the comb of possible transitions and give intuition for the mechanism in a given example.

To gain more insight into our problem, we focused on only one layer of dressing and one manifold. With that, we managed to compare the approximate solutions, i.e., the dressed basis and the dressed basis accounting for the counter-rotating terms, with the exact solution of the problem: the Floquet states. With this treatment, we showed that the corrected dressed states are the time-independent part of the Floquet states, which encourages the use of the corrected dressed states as a sufficiently good approximation for our system.

We finished the chapter by studying the possibility of constructing MS-gates on the level of the doubly-dressed basis, showing which gate times will be feasible with this mechanism and concluding that further engineering needs to be done in order to implement MS-gates on top of the CDD scheme with reasonable gate times.

## 4.7 Outlook: Further research directions

We would like to finish by contemplating further improvements that can be done to this work or further directions of investigation. If one uses the CDD for a particular pair of manifolds in a particular ion, once the actual parameters of the problem are known, we can find the best possible transition by studying the comb of transitions and choosing which properties do we want to optimize. Nevertheless, the opposite is also true, we can try to play with the parameters of the problem in order to find

adequate properties of a given transition. We did work within this concept, but it proved to be a more intricate problem than expected considering the number of variables involved in the problem.

Another work could consist on modeling the laser pulse and trying to optimize it in order to have a more efficient transition. In this regard, we simulated Ramsey sequences with different pulses and further work could be done in this direction.

For further insight on how good of an approximation the dressed states are, or even to actually use the real solution to the complete CDD scheme, the Floquet states, further work needs to be done in order to implement more than one frequency. It is not evident how to do that. One starting point could be the generalized Floquet theory, explained in the work of Peter Hänggi [3]. Another option is trying to come up with some approximate treatment, as the different order of magnitude between the frequencies makes it harder to treat or even simulate.

Finally, more work needs to be done to apply MS-gates. We would like to highlight that we did not consider any technical noise for the sideband transitions. Therefore, this approach gives us an order of magnitude that may be feasible to achieve after a reasonable amount of experimental work. If properly considering the noise and the experimental difficulties lead to a non-competitive gate we will have to consider a different approach. One way of reducing the gate time is to apply only one layer of dressing. With one layer of dressing, we will have access to faster gates by about an order of magnitude. Of course, before considering applying only one layer of dressing we should try to engineer an appropriate transition in the doubly-dressed basis by exploiting the selection rules and using the parameters of the problem.

# 5

## Summary and closing statements

This thesis aimed to provide an insight into the treatment of systematic shifts in the context of atomic clocks and precision measurements, contributing to extend the theoretical tools and understanding that need to go hand in hand with experimental improvements.

We started by introducing the mathematical methods required to treat various effects studied during our work. Afterwards, the first part of the thesis focused on providing an adequate treatment of *relativistic corrections* from an *ab initio* derivation. We succeed in fully characterizing the external and internal dynamics of an electromagnetically bound, charged two-particle system in external electromagnetic and gravitational fields, including leading order relativistic corrections. We focused on the case of an ion in a Paul trap, but the advantage of our treatment is that it provides a suitable tool that can be applied to several different systems. Of course, it needs to be developed and adapted to any particular problem, but the underlying general Hamiltonian derived in the first part of chapter 3 will serve as a basis for several problems. With our treatment, we managed to recover semiclassical results from the literature for the case of trapped ions in a Paul trap, which allowed us to gain further insight into those effects and to extend the quantum states that can be considered. Moreover, we managed to properly describe the dominant effects and imperfections in the trap, addressing and closing open questions on the role of time dilation and mass defect in ion clocks. We finished the first part by treating a particular case of a transition between two clock states with zero nuclear, electronic, and total angular momentum in a Penning trap. This leads to an interesting result in which the contribution of the magnetron motion to the fractional frequency shift, which normally had a different sign than the rest of the contributions, changes sign once the mass defect is considered, closing the argument about the attempt to cancel the fractional frequency shift by adding magnetron motion to the system.

The second part of the thesis is focused on implementing a particular mechanism,

the continuous dynamical decoupling, to null or reduce the shifts related to *environmental perturbations*. The continuous dynamical decoupling consists in employing a modulated external rf magnetic field to effectively erase unwanted effects. Even though it is not a new mechanism in the literature, we managed to present it in a form and notation that allowed us to easily apply the laser-ion interaction to drive quadrupole transitions, fully understanding the underlying mechanism and the role of various layers of dressing. After applying the mechanism to two manifolds simultaneously, and accounting perturbatively for some approximations we performed during the calculations, we characterized the transition between two manifolds and studied quadrupole transitions between the  $S = 1/2$  and  $D = 5/2$  manifolds of  $^{40}\text{Ca}^+$  as a particular example. The suppression of the shift comes at the cost of a reduced Rabi frequency. The transitions present themselves in the form of a comb, which requires some engineering to select the best candidate for a clock transition. We showed interestingly, for the case of one layer of dressing, that the corrected dressed states correspond to the time-independent part of the Floquet states, which are the appropriate basis for describing the time-periodic Hamiltonian. We finished by discussing the implementation of a Mølmer-Sørensen gate to achieve entanglement between two ions at the level of the doubly-dressed basis.

We hope that this thesis provides some clarity to several topics in the field as well as opens further research directions, such as

- The implementation of spin in the derivation of an *ab initio* Hamiltonian starting from the Dirac equation, this has been done before, but not accounting for a gravitational field so far.
- Expanding our Hamiltonian in order to study more complicated systems as ion crystals or lattice clocks.
- Properly consider the mass defect as a tool for reading out internal states in Penning trap mass spectrometry.
- Further study on how to calculate Floquet states in a system with more than one frequency and compare them with the corrected dressed states.
- Engineering a way of implementing a Mølmer-Sørensen gate with the underlying continuous dynamical decoupling using the comb properties.

The list of interesting projects for research could carry on, showing how extensive the field is. Nevertheless, the field is being driven by experts all over the world in several different directions, which foresees an exciting and promising future.

# A

## Hamiltonian for ion in external electromagnetic fields with first-order relativistic corrections

In this appendix, we will show the full derivation of the multipolar light-atom Hamiltonian including first-order relativistic corrections, i.e., we will only keep terms up to order  $c^{-2}$ . Specifically, we consider a hydrogenlike atomic ion as an electromagnetically bound two-body system composed of a core (charge  $e_1$ , coordinates  $\mathbf{r}_1$ ) and an electron ( $e_2, \mathbf{r}_2$ ) as represented in Fig. 3.1, in external electromagnetic fields. The changes due to gravity will be included in a different appendix. For the case of a neutral atom, Sonnleitner & Barnett [49] recently gave a derivation of the multipolar light-atom Hamiltonian with relativistic corrections. The individual steps of the derivation can be found in textbooks [124], [125] and [126], or as individual articles (for example [57] and [127]). We choose to follow the work of Sonnleitner & Barnett because they have a transparent and comprehensive derivation. The treatment of this problem has of course a long history, as can be seen in the references from [49]. In contrast to Sonnleitner & Barnett, we will allow for a non-vanishing net charge  $Q = e_1 + e_2 \neq 0$ . The approach we will follow here, is also present in the work of the Bachelor thesis [128] by Simon Eilers, co-author of the article developed within this topic.

## A.1 Classical, approximately relativistic Lagrangian for charges in external radiation fields

The starting point for the derivation is the classical Lagrangian for two particles interacting with electromagnetic potentials  $\phi_{\text{tot}}$  and  $\mathbf{A}_{\text{tot}}$ ,

$$L = - \sum_{i=1,2} m_i c^2 \sqrt{1 - \dot{\mathbf{r}}_i^2 / c^2} + \frac{\epsilon_0}{2} \int d^3\mathbf{x} \left( (\partial_t \mathbf{A}_{\text{tot}} + \nabla \phi_{\text{tot}})^2 - c^2 (\nabla \times \mathbf{A}_{\text{tot}})^2 \right) + \int d^3\mathbf{x} (\mathbf{j} \cdot \mathbf{A}_{\text{tot}} - \rho \phi_{\text{tot}}), \quad (\text{A.1})$$

where  $m_i$  is the mass of the  $i$ -th particle with corresponding position  $\mathbf{r}_i$  and velocity  $\dot{\mathbf{r}}_i$ . The charge and current densities are defined as

$$\rho(\mathbf{x}, t) = \sum_{i=1,2} e_i \delta(\mathbf{x} - \mathbf{r}_i(t)) \quad \text{and} \quad \mathbf{j}(\mathbf{x}, t) = \sum_{i=1,2} e_i \dot{\mathbf{r}}_i(t) \delta(\mathbf{x} - \mathbf{r}_i(t)), \quad (\text{A.2})$$

where,  $\delta$  refers to the Dirac delta function.

We refer to the potentials created by the two particles,  $\mathcal{A}$  and  $\phi$ , as internal potentials, and consider all other contributions,  $\mathbf{A}$  and  $\Phi$ , as external, such that  $\mathbf{A}_{\text{tot}} = \mathcal{A} + \mathbf{A}$  and  $\phi_{\text{tot}} = \phi + \Phi$ . For both external and internal potentials we will choose the Coulomb gauge, i.e.,  $\mathcal{A} = \mathcal{A}^\perp$  and  $\mathbf{A} = \mathbf{A}^\perp$ . This will allow to express contributions with internal potentials in the form of the more conventional Coulomb potential of charged particles.

The first term of the Lagrangian corresponds to the Lagrangian for the point particles, which describes the dynamics due to their kinetic energy. The integral in the first line represents the Lagrangian of the electromagnetic field, which describes the dynamics due to the field energy of the electromagnetic potentials. Lastly, the second line consists of the interaction between the electromagnetic field and the particles, it contains the mutual electrostatic interaction between the particles and the interaction with an external scalar potential.

After inserting the potentials, expanding the squares in Eq. (A.1) and recalling the relation  $\int d\mathbf{x} a^\perp \cdot b^\parallel = 0$ , our Lagrangian becomes

$$L = - \sum_{i=1,2} m_i c^2 \sqrt{1 - \dot{\mathbf{r}}_i^2 / c^2} + \frac{\epsilon_0}{2} \int d^3\mathbf{x} \left( (\partial_t \mathcal{A}^\perp + \nabla \phi)^2 + 2 (\partial_t \mathbf{A}^\perp) \cdot (\partial_t \mathcal{A}^\perp) - c^2 (\nabla \times \mathcal{A}^\perp)^2 + (\partial_t \mathbf{A}^\perp)^2 - 2c^2 (\nabla \times \mathbf{A}^\perp) (\nabla \times \mathcal{A}^\perp) - c^2 (\nabla \times \mathbf{A}^\perp)^2 \right) + \int d^3\mathbf{x} (\mathbf{j} \cdot (\mathcal{A}^\perp + \mathbf{A}^\perp) - \rho(\phi + \Phi)), \quad (\text{A.3})$$



where we also neglect the effect of  $\nabla\Phi$  as only the internal potential is relevant for the particle dynamics. A similar argument can be seen in [126] (p.141).

Using that the internal potentials satisfy Maxwell's equations in the Coulomb gauge

$$\nabla^2\phi = -\rho/\varepsilon_0, \quad \left(\nabla^2 - \frac{1}{c^2}\frac{\partial^2}{\partial t^2}\right)\mathcal{A}^\perp = -\mu_0\mathbf{j}^\perp, \quad (\text{A.4})$$

where  $\mathbf{j}^\perp = \mathbf{j} - \mathbf{j}^\parallel = \mathbf{j} - \varepsilon_0\nabla\frac{\partial}{\partial t}\phi$ , we can calculate the second term of the Lagrangian

$$\frac{\varepsilon_0}{2}\int d^3\mathbf{x}(\partial_t\mathcal{A}^\perp + \nabla\phi)^2 = \frac{\varepsilon_0}{2}\int d^3\mathbf{x}\left((\partial_t\mathcal{A}^\perp)^2 + (\nabla\phi)^2\right). \quad (\text{A.5})$$

By making the integration by parts and using Maxwell's equation, we obtain

$$\frac{\varepsilon_0}{2}\int d^3\mathbf{x}\left((\partial_t\mathcal{A}^\perp)^2 - \phi\nabla^2\phi\right) = \frac{1}{2}\int d^3\mathbf{x}\left(\varepsilon_0(\partial_t\mathcal{A}^\perp)^2 + \rho\phi\right). \quad (\text{A.6})$$

Using the relation  $-\frac{\varepsilon_0 c^2}{2}\int d^3\mathbf{x}(\nabla\times\mathcal{A}^\perp)^2 = -\frac{1}{2\mu_0}\int d^3\mathbf{x}\mathcal{A}^\perp\cdot(\nabla\times(\nabla\times\mathcal{A}^\perp))$ , the third term of (A.3) becomes

$$-\frac{1}{2\mu_0}\int d^3\mathbf{x}\mathcal{A}^\perp\cdot(\nabla\times(\nabla\times\mathcal{A}^\perp)) = -\frac{1}{2}\int d^3\mathbf{x}\mathcal{A}^\perp\cdot\mathbf{j}^\perp + \frac{\varepsilon_0}{2}\int d^3\mathbf{x}\mathcal{A}^\perp\cdot(\partial_t^2\mathcal{A}^\perp), \quad (\text{A.7})$$

where we used the relation  $\nabla^2 A = \nabla(\nabla\cdot A) - \nabla\times(\nabla\times A)$  and once more, Maxwell's equation.

Using the previous results, we can rewrite the Lagrangian (A.3) in the form

$$\begin{aligned} L = & \sum_{i=1,2} \frac{m_i \dot{\mathbf{r}}_i^2}{2} \left(1 + \frac{\dot{\mathbf{r}}_i^2}{4c^2}\right) + \frac{1}{2}\int d^3\mathbf{x}\left(\varepsilon_0(\partial_t\mathcal{A}^\perp)^2 + \rho\phi\right) + \frac{\varepsilon_0}{2}\int d^3\mathbf{x}\left((\partial_t\mathcal{A}^\perp)^2\right. \\ & \left.+ 2(\partial_t\mathcal{A}^\perp)\cdot(\partial_t\mathcal{A}^\perp) - 2c^2(\nabla\times\mathcal{A}^\perp)(\nabla\times\mathcal{A}^\perp) - c^2(\nabla\times\mathcal{A}^\perp)^2\right) \\ & - \frac{1}{2}\int d^3\mathbf{x}\mathcal{A}^\perp\cdot\mathbf{j}^\perp + \frac{\varepsilon_0}{2}\int d^3\mathbf{x}\mathcal{A}^\perp\cdot(\partial_t^2\mathcal{A}^\perp) \\ & + \int d^3\mathbf{x}(\mathbf{j}\cdot(\mathcal{A}^\perp + \mathbf{A}^\perp) - \rho(\phi + \Phi)), \end{aligned} \quad (\text{A.8})$$

where we made a Taylor expansion of the first term and erased the term  $-\sum_i m_i c^2$ , which represents the negative rest energy of the particles, this can be done as changing by a constant the Lagrangian expression does not change the dynamics of the problem. Finally, using the relation  $\mathcal{A}^\perp\cdot\partial_t^2\mathcal{A}^\perp + (\partial_t\mathcal{A}^\perp)^2 = \partial_t^2(\mathcal{A}^\perp)^2/2$ , we obtain

$$L = L_{\text{Darwin}} + L_{\text{field}} + L_{\text{int}} + L_{\text{cross}},$$

$$L_{\text{Darwin}} = \sum_{i=1,2} \frac{m_i \dot{\mathbf{r}}_i^2}{2} \left( 1 + \frac{\dot{\mathbf{r}}_i^2}{4c^2} \right) + \frac{1}{2} \int d^3\mathbf{x} (\mathbf{j}^\perp \cdot \mathcal{A}^\perp - \rho\phi), \quad (\text{A.9})$$

$$L_{\text{field}} = \frac{\varepsilon_0}{2} \int d^3\mathbf{x} \left( (\partial_t \mathbf{A}^\perp)^2 - c^2 (\nabla \times \mathbf{A}^\perp)^2 \right), \quad (\text{A.10})$$

$$L_{\text{int}} = \int d^3\mathbf{x} (\mathbf{j}^\perp \cdot \mathbf{A}^\perp - \rho\Phi), \quad (\text{A.11})$$

$$L_{\text{cross}} = \frac{\varepsilon_0}{4} \int d^3\mathbf{x} \frac{\partial^2}{\partial t^2} (\mathcal{A}^\perp)^2 + \varepsilon_0 \int d^3\mathbf{x} (\partial_t \mathbf{A}^\perp \cdot \partial_t \mathcal{A}^\perp - c^2 (\nabla \times \mathbf{A}^\perp) (\nabla \times \mathcal{A}^\perp)). \quad (\text{A.12})$$

The first contribution (A.9) is the well-known Darwin Lagrangian [124, 129], which describes the approximately relativistic motion of the particles and their interaction with the fields generated by their respective counterparts. This contribution can be rewritten by inserting the equations of the generated fields by the particles

$$\phi(\mathbf{x}, t) = \frac{1}{4\pi\varepsilon_0} \int d^3\mathbf{x}' \frac{\rho(\mathbf{x}', t)}{|\mathbf{x} - \mathbf{x}'|}, \quad (\text{A.13})$$

$$\mathcal{A}^\perp(\mathbf{x}, t) = \frac{\mu_0}{8\pi} \sum_{i=1,2} e_i \left( \frac{\dot{\mathbf{r}}_i}{|\mathbf{x} - \mathbf{r}_i|} + \frac{(\mathbf{x} - \mathbf{r}_i)(\dot{\mathbf{r}}_i \cdot (\mathbf{x} - \mathbf{r}_i))}{|\mathbf{x} - \mathbf{r}_i|^3} \right), \quad (\text{A.14})$$

that can be found in [49], and using the definitions for  $\rho$  and  $\mathbf{j}$ , obtaining

$$\begin{aligned} L_{\text{Darwin}} = & \frac{m_1 \dot{\mathbf{r}}_1^2}{2} + \frac{m_1 \dot{\mathbf{r}}_1^4}{8c^2} + \frac{m_2 \dot{\mathbf{r}}_2^2}{2} + \frac{m_2 \dot{\mathbf{r}}_2^4}{8c^2} - \frac{1}{4\pi\varepsilon_0} \frac{e_1 e_2}{r} \left( 1 - \frac{\dot{\mathbf{r}}_1 \cdot \dot{\mathbf{r}}_2}{2c^2} \right) \\ & + \frac{e_1 e_2}{4\pi\varepsilon_0} \frac{(\dot{\mathbf{r}}_1 \cdot \mathbf{r})(\dot{\mathbf{r}}_2 \cdot \mathbf{r})}{2r^3 c^2}, \end{aligned} \quad (\text{A.15})$$

where  $\mathbf{r} = \mathbf{r}_1 - \mathbf{r}_2$  and  $r = |\mathbf{r}|$ .

The second contribution  $L_{\text{field}}$  describes the dynamics of the external fields and  $L_{\text{int}}$  their interaction with the charged particles.

Finally,  $L_{\text{cross}}$  can be neglected in our problem. This is justified as the first term is of order  $c^{-4}$  and the second term is a cross talk between the transverse electric and magnetic fields generated by the moving charges and the external fields. Those terms appear whenever the back-action of fields generated by a (moving) charged particle on itself is considered. A more thorough argumentation can be found in [49].

## A.2 From classical Lagrangian to quantum Hamiltonian in minimal-coupling form

After deducing the classical Lagrangian, the next step is to derive the classical and quantum Hamiltonian.

To obtain the classical Hamiltonian, we need the canonical momenta associated with the particle coordinates  $\mathbf{r}_i$  and the external field  $\mathbf{A}^\perp$ ,

$$\mathbf{p}_i = \frac{\partial}{\partial \dot{\mathbf{r}}_i} L = m_i \dot{\mathbf{r}}_i + \frac{m_i \dot{\mathbf{r}}_i^2}{2c^2} \dot{\mathbf{r}}_i + \frac{e_1 e_2}{8\pi \varepsilon_0 c^2 r} \left( \dot{\mathbf{r}}_j + \frac{\mathbf{r} (\dot{\mathbf{r}}_j \cdot \mathbf{r})}{r^2} \right) + e_i \mathbf{A}^\perp(\mathbf{r}_i), \quad (\text{A.16})$$

$$\mathbf{\Pi}^\perp = \frac{\partial}{\partial \dot{\mathbf{A}}^\perp} L = \varepsilon_0 \dot{\mathbf{A}}^\perp, \quad (\text{A.17})$$

where  $i, j \in \{1, 2\}$  and  $i \neq j$ .

Now we can calculate the classical Hamiltonian

$$H = \sum_{i=1,2} \mathbf{p}_i \dot{\mathbf{r}}_i + \int d^3\mathbf{x} \mathbf{\Pi}^\perp \cdot \dot{\mathbf{A}}^\perp - L. \quad (\text{A.18})$$

Expressing it in terms of the conjugate variables, taking only corrections up to  $\mathcal{O}(c^{-2})$ , and defining  $\bar{\mathbf{p}}_i = \mathbf{p}_i - e_i \mathbf{A}^\perp(\mathbf{r}_i)$ , we obtain

$$\begin{aligned} H = & \sum_{i=1,2} \left( \frac{\bar{\mathbf{p}}_i^2}{2m_i} - \frac{\bar{\mathbf{p}}_i^4}{8m_i^3 c^2} \right) + \frac{e_1 e_2}{4\pi r \varepsilon_0} - \frac{e_1 e_2}{8\pi \varepsilon_0 r c^2 m_1 m_2} \left( \bar{\mathbf{p}}_1 \cdot \bar{\mathbf{p}}_2 + \frac{(\bar{\mathbf{p}}_1 \cdot \mathbf{r})(\bar{\mathbf{p}}_2 \cdot \mathbf{r})}{r^2} \right) \\ & + \frac{\varepsilon_0}{2} \int d^3\mathbf{x} \left( \left( \frac{\mathbf{\Pi}^\perp}{\varepsilon_0} \right)^2 + c^2 (\nabla \times \mathbf{A}^\perp)^2 \right) + \sum_{i=1,2} e_i \Phi(\mathbf{r}_i). \end{aligned} \quad (\text{A.19})$$

Starting from the classical Hamiltonian, the quantum mechanical Hamiltonian can be derived by imposing the canonical commutation relations

$$[\hat{r}_{i,k}, \hat{p}_{j,l}] = i\hbar \delta_{i,j} \delta_{k,l}, \quad (\text{A.20})$$

$$\left[ \hat{A}_k^\perp(\mathbf{x}), \hat{\Pi}_l^\perp(\mathbf{x}') \right] = i\hbar \delta_{k,l} \delta^\perp(\mathbf{x} - \mathbf{x}'), \quad (\text{A.21})$$

where  $i, j \in \{1, 2\}$  are related to the particles and  $k, l \in \{1, 2, 3\}$  are related to the operators' components. Therefore, for the quantum Hamiltonian, the correct ordering during the canonical quantization becomes relevant. This applies to a term originating from  $\int d^3\mathbf{x} \mathbf{j} \cdot \mathcal{A}^\perp$ . Using the symmetric version of  $\mathcal{A}^\perp$  that can be found in [49], we obtain the approximately relativistic Hamiltonian operator for two charged particles minimally coupled to the electromagnetic field

$$\begin{aligned}
 H_{[\text{min.c.}]} = & \sum_{i=1,2} \left( \frac{\hat{\mathbf{p}}_i^2}{2m_i} - \frac{\hat{\mathbf{p}}_i^4}{8m_i^3 c^2} \right) + \frac{e_1 e_2}{4\pi \hat{r} \varepsilon_0} + \frac{\varepsilon_0}{2} \int d^3 \mathbf{x} \left( \left( \frac{\hat{\mathbf{\Pi}}^\perp}{\varepsilon_0} \right)^2 + c^2 (\nabla \times \hat{\mathbf{A}}^\perp)^2 \right) \\
 & - \frac{e_1 e_2}{16\pi \varepsilon_0 c^2 m_1 m_2} \left( \hat{\mathbf{p}}_1 \cdot \frac{1}{\hat{r}} \hat{\mathbf{p}}_2 + (\hat{\mathbf{p}}_1 \cdot \hat{\mathbf{r}}) \frac{1}{\hat{r}^3} (\hat{\mathbf{r}} \cdot \hat{\mathbf{p}}_2) + (1 \leftrightarrow 2) \right) + \sum_{i=1,2} e_i \Phi(\hat{\mathbf{r}}_i),
 \end{aligned} \tag{A.22}$$

where  $(1 \leftrightarrow 2)$  denotes the preceding term with indices 1 and 2 switched. In the main text, see e.g., Eq. (3.3), we did not write the dynamics of the field as it will not affect the dynamics of our particles, but of course it will be present in the Hamiltonian.

### A.3 Power-Zienau-Woolley transformation to a multipolar Hamiltonian in center of mass coordinates for charged composite particles

The Hamiltonian given in equation (A.22) describes the approximately relativistic dynamics of charged composite particles of spin zero in the presence of external radiation fields. To try to separate the relative and central dynamics, we want to express our Hamiltonian into a multipolar form. We will achieve this by using a Power-Zienau-Woolley (PZW) transformation, which was developed by Power, Zienau and Woolley [130–132].

As we can see in [126], the PZW transformation is performed by the unitary operator  $\hat{U} = e^{-\frac{i}{\hbar} \hat{\Lambda}}$ , where the generating function  $\hat{\Lambda}$  is defined as

$$\hat{\Lambda}(t) = \int d^3 \mathbf{x} \hat{\mathcal{P}}(\mathbf{x}, t) \cdot \hat{\mathbf{A}}(\mathbf{x}, t), \tag{A.23}$$

where  $\hat{\mathcal{P}}(\mathbf{x}, t)$  is the polarization density and is defined as

$$\hat{\mathcal{P}}(\mathbf{x}, t) = \sum_{i=1,2} e_i \left( \hat{\mathbf{r}}_i(t) - \hat{\mathbf{R}}(t) \right) \int_0^1 d\lambda \delta \left( \mathbf{x} - \hat{\mathbf{R}}(t) - \lambda \left( \hat{\mathbf{r}}_i(t) - \hat{\mathbf{R}}(t) \right) \right), \tag{A.24}$$

with the center of mass coordinate  $\hat{\mathbf{R}} = \frac{m_1 \hat{\mathbf{r}}_1 + m_2 \hat{\mathbf{r}}_2}{M}$  and  $M = m_1 + m_2$  being the total mass. This expression differs from the one given in [126], that is because in the end we will want to express the result in the center of mass coordinates.

The interpretation of  $\mathcal{P}$  as the polarization field is supported by

$$\nabla \cdot \hat{\mathcal{P}}(\mathbf{x}, t) = -\hat{\rho}(\mathbf{x}, t), \tag{A.25}$$

such that the displacement field is  $\mathbf{D} = \varepsilon_0 \mathbf{E} + \mathcal{P} = -\mathbf{\Pi} + \mathcal{P}$ . We also obtain

$$\partial_t \hat{\mathcal{P}}(\mathbf{x}, t) = \hat{\mathbf{j}}(\mathbf{x}, t) - \nabla \times \hat{\mathcal{M}}(\mathbf{x}, t) + \nabla \times \left( \dot{\hat{\mathbf{R}}} \times \hat{\mathcal{P}}(\mathbf{x}, t) \right), \quad (\text{A.26})$$

where the magnetization  $\hat{\mathcal{M}}$  is defined as

$$\begin{aligned} \hat{\mathcal{M}}(\mathbf{x}, t) = \sum_{i=1,2} e_i \left( \hat{\mathbf{r}}_i(t) - \hat{\mathbf{R}}(t) \right) \times \left( \dot{\hat{\mathbf{r}}}_i(t) - \dot{\hat{\mathbf{R}}}(t) \right) \int_0^1 d\lambda \lambda \delta(\mathbf{x} - \hat{\mathbf{R}}(t) \\ - \lambda \left( \hat{\mathbf{r}}_i(t) - \hat{\mathbf{R}}(t) \right)). \end{aligned} \quad (\text{A.27})$$

The last term in (A.26) is the so-called Röntgen current [58] and describes the magnetization  $\hat{\mathcal{M}}_{\text{Röntgen}}(\mathbf{x}, t) = \hat{\mathcal{P}}(\mathbf{x}, t) \times \dot{\hat{\mathbf{R}}}(t)$  generated by an electric polarization when the center of mass has a velocity  $\dot{\hat{\mathbf{R}}}$ .

The PZW transformation leads to the transformed multipolar Hamiltonian  $\hat{H}_{[\text{mult.}]} = \hat{U} \hat{H}_{[\text{min.c.}]} \hat{U}^\dagger$ . Taking into account that the function  $\hat{\Lambda}$  only depends on the variables  $\hat{\mathbf{r}}_1$ ,  $\hat{\mathbf{r}}_2$  and  $\hat{\mathbf{A}}^\perp$ , we find that the only terms that change in the Hamiltonian are the canonical momenta associated with the particle coordinates  $\mathbf{r}_i$  and the external field  $\mathbf{A}^\perp$

$$\hat{\mathbf{p}}'_i = \hat{U} \hat{\mathbf{p}}_i \hat{U}^\dagger = \hat{\mathbf{p}}_i + \frac{i}{\hbar} \left[ \hat{\mathbf{p}}_i, \hat{\Lambda} \right] = \hat{\mathbf{p}}_i + \frac{i}{\hbar} \left[ \hat{\mathbf{p}}_i, \hat{\Lambda} \right] = \hat{\mathbf{p}}_i + \nabla_{\hat{\mathbf{r}}_i} \hat{\Lambda}, \quad (\text{A.28})$$

$$\hat{\mathbf{\Pi}}'^\perp = \hat{U} \hat{\mathbf{\Pi}}^\perp \hat{U}^\dagger = \hat{\mathbf{\Pi}}^\perp + \frac{i}{\hbar} \left[ \hat{\mathbf{\Pi}}^\perp, \hat{\Lambda} \right] = \hat{\mathbf{\Pi}}^\perp + \frac{i}{\hbar} \left[ \hat{\mathbf{\Pi}}^\perp, \hat{\mathcal{A}}^\perp \right] \hat{\mathcal{P}} = \hat{\mathbf{\Pi}}^\perp + \hat{\mathcal{P}}, \quad (\text{A.29})$$

where  $\nabla_{\hat{\mathbf{r}}_i}$  denotes derivation with respect to the position of the  $i$ th particle.

These new variables are no longer the conjugate variables as before. Performing the integral with respect to  $d^3\mathbf{x}$  shows that  $\Lambda = \sum_j e_j \int_0^1 d\lambda \hat{\mathbf{r}}_j \cdot \hat{\mathbf{A}}^\perp \left( \hat{\mathbf{R}} + \lambda \hat{\mathbf{r}}_j \right)$ , where  $\hat{\mathbf{r}}_j := \hat{\mathbf{r}}_j - \hat{\mathbf{R}}$ . Expanding to first order in  $\hat{\mathbf{r}}_j$  (electric dipole approximation), we obtain

$$\begin{aligned} \nabla_{\hat{\mathbf{r}}_i} \hat{\mathbf{r}}_j \cdot \hat{\mathbf{A}}^\perp \left( \hat{\mathbf{R}} + \lambda \hat{\mathbf{r}}_j \right) &= \left( \delta_{ij} - \frac{m_i}{M} \right) \hat{\mathbf{A}}^\perp \left( \hat{\mathbf{R}} + \lambda \hat{\mathbf{r}}_j \right) + \left( \lambda \delta_{ij} + (1 - \lambda) \frac{m_i}{M} \right) \\ &\quad \times \left[ \left( \hat{\mathbf{r}}_j \cdot \nabla \right) \hat{\mathbf{A}}^\perp \left( \hat{\mathbf{R}} + \lambda \hat{\mathbf{r}}_j \right) + \hat{\mathbf{r}}_j \times \left( \nabla \times \hat{\mathbf{A}}^\perp \left( \hat{\mathbf{R}} + \lambda \hat{\mathbf{r}}_j \right) \right) \right] \\ &\simeq \left( \delta_{ij} - \frac{m_i}{M} \right) \left[ \hat{\mathbf{A}}^\perp(\hat{\mathbf{R}}) + \lambda \left( \hat{\mathbf{r}}_j \cdot \nabla \right) \hat{\mathbf{A}}^\perp(\hat{\mathbf{R}}) \right] \\ &\quad + \left( \lambda \delta_{ij} + (1 - \lambda) \frac{m_i}{M} \right) \left[ \left( \hat{\mathbf{r}}_j \cdot \nabla \right) \hat{\mathbf{A}}^\perp(\hat{\mathbf{R}}) + \hat{\mathbf{r}}_j \times \left( \nabla \times \hat{\mathbf{A}}^\perp(\hat{\mathbf{R}}) \right) \right] \\ &= \left( \delta_{ij} - \frac{m_i}{M} \right) \hat{\mathbf{A}}^\perp \left( \hat{\mathbf{R}} \right) + 2 \left( \lambda \delta_{ij} + \left( \frac{1}{2} - \lambda \right) \frac{m_i}{M} \right) \left[ \left( \hat{\mathbf{r}}_j \cdot \nabla \right) \hat{\mathbf{A}}^\perp(\hat{\mathbf{R}}) \right] \\ &\quad + \left( \lambda \delta_{ij} + (1 - \lambda) \frac{m_i}{M} \right) \left[ \hat{\mathbf{r}}_j \times \left( \nabla \times \hat{\mathbf{A}}^\perp(\hat{\mathbf{R}}) \right) \right]. \end{aligned} \quad (\text{A.30})$$

Integrating over  $\lambda$

$$\begin{aligned}
\nabla_{\hat{\mathbf{r}}_i} \hat{\Lambda} &= \sum_j e_j \left[ \left( \delta_{ij} - \frac{m_i}{M} \right) \hat{\mathbf{A}}^\perp(\hat{\mathbf{R}}) + \delta_{ij} \left( (\hat{\mathbf{r}}_j \cdot \nabla) \hat{\mathbf{A}}^\perp(\hat{\mathbf{R}}) \right) \right. \\
&\quad \left. + \left( \frac{\delta_{ij}}{2} + \frac{m_i}{2M} \right) \left( \hat{\mathbf{r}}_j \times \left( \nabla \times \hat{\mathbf{A}}^\perp(\hat{\mathbf{R}}) \right) \right) \right] \\
&= e_i \left[ \hat{\mathbf{A}}^\perp(\hat{\mathbf{R}}) + \left( (\hat{\mathbf{r}}_i \cdot \nabla) \hat{\mathbf{A}}^\perp(\hat{\mathbf{R}}) \right) + \frac{1}{2} \left( \hat{\mathbf{r}}_i \times \left( \nabla \times \hat{\mathbf{A}}^\perp(\hat{\mathbf{R}}) \right) \right) \right] \\
&\quad - (e_1 + e_2) \left[ \frac{m_i}{M} \hat{\mathbf{A}}^\perp(\hat{\mathbf{R}}) \right] + \frac{e_1 \hat{\mathbf{r}}_1 + e_2 \hat{\mathbf{r}}_2}{2} \left[ \frac{m_i}{M} \times \left( \nabla \times \hat{\mathbf{A}}^\perp(\hat{\mathbf{R}}) \right) \right], \quad (\text{A.31})
\end{aligned}$$

which leads to the Hamiltonian

$$\begin{aligned}
H_{[\text{mult.}]} &= \sum_{i=1,2} \left( \frac{\hat{\mathbf{p}}_i'^2}{2m_i} - \frac{\hat{\mathbf{p}}_i'^4}{8m_i^3 c^2} \right) + \frac{e_1 e_2}{4\pi \hat{r} \varepsilon_0} + \sum_{i=1,2} e_i \Phi(\hat{\mathbf{r}}_i) \\
&\quad + \frac{\varepsilon_0}{2} \int d^3 \mathbf{x} \left( \left( \frac{\hat{\Pi}^\perp + \hat{\mathcal{P}}}{\varepsilon_0} \right)^2 + c^2 \left( \nabla \times \hat{\mathbf{A}}^\perp \right)^2 \right) \\
&\quad - \frac{e_1 e_2}{16\pi \varepsilon_0 c^2 m_1 m_2} \left( \hat{\mathbf{p}}_1' \cdot \frac{1}{\hat{r}} \hat{\mathbf{p}}_2' + (\hat{\mathbf{p}}_1' \cdot \hat{\mathbf{r}}) \frac{1}{\hat{r}^3} (\hat{\mathbf{r}} \cdot \hat{\mathbf{p}}_2') + \text{H.c.} \right), \quad (\text{A.32})
\end{aligned}$$

where

$$\begin{aligned}
\hat{\mathbf{p}}_i' &= \hat{\mathbf{p}}_i - e_i \hat{\mathbf{A}}^\perp(\hat{\mathbf{r}}_i) + e_i \left[ \hat{\mathbf{A}}^\perp(\hat{\mathbf{R}}) + \left( (\hat{\mathbf{r}}_i \cdot \nabla) \hat{\mathbf{A}}^\perp(\hat{\mathbf{R}}) \right) + \frac{1}{2} \left( \hat{\mathbf{r}}_i \times \left( \nabla \times \hat{\mathbf{A}}^\perp(\hat{\mathbf{R}}) \right) \right) \right] \\
&\quad - (e_1 + e_2) \left[ \frac{m_i}{M} \hat{\mathbf{A}}^\perp(\hat{\mathbf{R}}) \right] + \frac{e_1 \hat{\mathbf{r}}_1 + e_2 \hat{\mathbf{r}}_2}{2} \left[ \frac{m_i}{M} \times \left( \nabla \times \hat{\mathbf{A}}^\perp(\hat{\mathbf{R}}) \right) \right], \quad (\text{A.33})
\end{aligned}$$

and  $i \neq j$ . Noticing that  $\hat{\mathbf{A}}^\perp(\hat{\mathbf{R}}) + \left( (\hat{\mathbf{r}}_i \cdot \nabla) \hat{\mathbf{A}}^\perp(\hat{\mathbf{R}}) \right) \simeq \hat{\mathbf{A}}^\perp(\hat{\mathbf{r}}_i)$ , we can reexpress the last equation as

$$\hat{\mathbf{p}}_i' = \hat{\mathbf{p}}_i + \frac{1}{2} \left( e_i \hat{\mathbf{r}}_i + e_j \hat{\mathbf{r}}_j + \frac{m_i}{M} (e_i + e_j) \hat{\mathbf{r}}_i \right) \times \left( \nabla \times \hat{\mathbf{A}}^\perp(\hat{\mathbf{R}}) \right) - (e_1 + e_2) \left[ \frac{m_i}{M} \hat{\mathbf{A}}^\perp(\hat{\mathbf{R}}) \right]. \quad (\text{A.34})$$

To get a more compact form we will define the dipole moment  $\hat{\mathbf{d}} = \sum_{i=1,2} e_i (\hat{\mathbf{r}}_i - \hat{\mathbf{R}})$  and the total charge  $Q = e_1 + e_2$ , obtaining

$$\begin{aligned}
\hat{\mathbf{p}}_i' &= \hat{\mathbf{p}}_i + \frac{1}{2} \left( \hat{\mathbf{d}} + \frac{m_i Q}{M} \hat{\mathbf{r}}_i \right) \times \left( \nabla \times \hat{\mathbf{A}}^\perp(\hat{\mathbf{R}}) \right) - \frac{Q m_i}{M} \hat{\mathbf{A}}^\perp(\hat{\mathbf{R}}) \\
&= \hat{\mathbf{p}}_i - \frac{m_i}{M} Q \hat{\mathbf{A}}^\perp(\hat{\mathbf{R}}) + \frac{1}{2} \left( \hat{\mathbf{d}} + \frac{Q m_i}{M} \hat{\mathbf{r}}_i \right) \times \hat{\mathbf{B}}(\hat{\mathbf{R}}). \quad (\text{A.35})
\end{aligned}$$

Before going to the center of mass and relative coordinates, we will rewrite the external scalar potential and the polarization in a more comprehensible way, to this goal we will apply once more the dipole approximation for these terms

$$\begin{aligned}
\sum_{i=1,2} e_i \Phi(\hat{\mathbf{r}}_i) &= \sum_{i=1,2} e_i \Phi(\hat{\mathbf{R}} + (\hat{\mathbf{r}}_i - \hat{\mathbf{R}})) \\
&= \sum_{i=1,2} e_i \Phi(\hat{\mathbf{R}}) - \sum_{i=1,2} e_i (\hat{\mathbf{r}}_i - \hat{\mathbf{R}}) \cdot \mathbf{E}^{\parallel}(\hat{\mathbf{R}}) + \mathcal{O}\left(\left(\hat{\mathbf{r}}_i - \hat{\mathbf{R}}\right)^2\right) \\
&= Q\Phi(\hat{\mathbf{R}}) - \hat{\mathbf{d}} \cdot \mathbf{E}^{\parallel} + \mathcal{O}\left(\left(\hat{\mathbf{r}}_i - \hat{\mathbf{R}}\right)^2\right), \tag{A.36}
\end{aligned}$$

$$\begin{aligned}
\hat{\mathcal{P}}(\mathbf{x}) &= \sum_{i=1,2} e_i (\hat{\mathbf{r}}_i - \hat{\mathbf{R}}) \int_0^1 d\lambda \delta(\mathbf{x} - \hat{\mathbf{R}}) + \mathcal{O}\left(\left(\hat{\mathbf{r}}_i - \hat{\mathbf{R}}\right)^2\right) \\
&= \sum_{i=1,2} e_i (\hat{\mathbf{r}}_i - \hat{\mathbf{R}}) \delta(\mathbf{x} - \hat{\mathbf{R}}) + \mathcal{O}\left(\left(\hat{\mathbf{r}}_i - \hat{\mathbf{R}}\right)^2\right) \\
&= \hat{\mathbf{d}} \delta(\mathbf{x} - \hat{\mathbf{R}}) + \mathcal{O}\left(\left(\hat{\mathbf{r}}_i - \hat{\mathbf{R}}\right)^2\right). \tag{A.37}
\end{aligned}$$

## A.4 Change to the center of mass $\mathbf{R}$ and relative $\mathbf{r}$ coordinates

Without relativistic corrections, the COM and relative coordinates are the natural choice as they separate the external and internal DOF, respectively. Therefore, the goal of this section is to express the Hamiltonian in these coordinates and study how internal and external DOF couple due to the relativistic corrections.

These coordinates are the center of mass and the relative coordinate  $(\hat{\mathbf{R}}, \hat{\mathbf{r}})$  and their corresponding momenta  $(\hat{\mathbf{P}}, \hat{\mathbf{p}})$  defined by

$$\hat{\mathbf{R}} = \frac{m_1 \hat{\mathbf{r}}_1 + m_2 \hat{\mathbf{r}}_2}{M}, \quad \hat{\mathbf{P}} = \hat{\mathbf{p}}_1 + \hat{\mathbf{p}}_2, \tag{A.38}$$

$$\hat{\mathbf{r}} = \hat{\mathbf{r}}_1 - \hat{\mathbf{r}}_2, \quad \hat{\mathbf{p}} = \frac{m_2 \hat{\mathbf{p}}_1 - m_1 \hat{\mathbf{p}}_2}{M}. \tag{A.39}$$

This gives us the relations  $\hat{\mathbf{p}}_{1,2} = \frac{m_{1,2}}{M} \hat{\mathbf{P}} \pm \hat{\mathbf{p}}$ , where the  $\pm$  refers to  $+$  for the subscript 1 and  $-$  otherwise. Substituting them in the previous expressions (A.35), and defining the relative mass  $\mu = \frac{m_1 m_2}{M}$ , we obtain

$$\hat{\mathbf{p}}'_{1,2} = \frac{m_{1,2}}{M} \left( \hat{\mathbf{P}} - Q \hat{\mathbf{A}}^{\perp}(\hat{\mathbf{R}}) \right) \pm \hat{\mathbf{p}} + \frac{1}{2} \left( \hat{\mathbf{d}} \pm \frac{Q\mu}{2M} \hat{\mathbf{r}} \right) \times \hat{\mathbf{B}}(\hat{\mathbf{R}}). \tag{A.40}$$

We will substitute these expressions in the previous Hamiltonian (A.32) and neglect terms of the form

$$\frac{\hat{\mathbf{d}} \times \hat{\mathbf{B}}(\hat{\mathbf{R}})}{2m_i c^2} \propto \frac{|\hat{\mathbf{d}} \cdot \hat{\mathbf{E}}(\hat{\mathbf{R}})|}{m_i c^2} \frac{1}{2c}, \quad \text{or} \quad \hat{\mathbf{p}}_i \frac{\hat{\mathbf{d}} \times \hat{\mathbf{B}}(\hat{\mathbf{R}})}{2m_i m_j c^2} \propto \frac{|\hat{\mathbf{p}}_i|}{m_i c} \frac{|\hat{\mathbf{d}} \cdot \hat{\mathbf{E}}(\hat{\mathbf{R}})|}{m_j c^2}, \quad (\text{A.41})$$

that can be consistently neglected as they are of higher order in  $c^{-2}$ , which can be seen from  $|\hat{\mathbf{d}} \cdot \hat{\mathbf{E}}(\hat{\mathbf{R}})| \ll e^2 / (4\pi\epsilon_0 r) \ll m_i c^2$ . It is worth highlighting here that because we allowed a non-vanishing total charge  $Q$  a considerable number of extra terms appear in the Hamiltonian compared to [49]. Later, we realized that most of these terms are absorbed if we wrote the Hamiltonian in the center of mass coordinates minimally coupled to the electromagnetic field, i.e., writing it in terms of  $\hat{\mathbf{P}} = \hat{\mathbf{P}} - Q\hat{\mathbf{A}}^\perp(\hat{\mathbf{R}})$ . Therefore, the Hamiltonian in the center of mass coordinates becomes

$$\hat{H} = \hat{H}_{\text{com}} + \hat{H}_{\text{int}} + \hat{H}_{\text{emf}} + \hat{H}_{\text{pol}} + \hat{H}_{\text{at-emf}} + \hat{H}_{\text{mass defect}} + \hat{H}_X, \quad (\text{A.42})$$

$$\hat{H}_{\text{com}} = \frac{\hat{\mathbf{P}}^2}{2M} \left( 1 - \frac{\hat{\mathbf{P}}^2}{4M^2 c^2} \right), \quad (\text{A.43})$$

$$\begin{aligned} \hat{H}_{\text{int}} = & \frac{\hat{\mathbf{p}}^2}{2\mu} \left( 1 - \frac{m_1^3 + m_2^3}{M^3} \frac{\hat{\mathbf{p}}^2}{4\mu^2 c^2} \right) \\ & + \frac{e_1 e_2}{4\pi\epsilon_0} \left[ \frac{1}{\hat{r}} + \frac{1}{2\mu M c^2} \left( \hat{\mathbf{p}} \cdot \frac{1}{\hat{r}} \hat{\mathbf{p}} + (\hat{\mathbf{p}} \cdot \hat{\mathbf{r}}) \frac{1}{\hat{r}^3} (\hat{\mathbf{r}} \cdot \hat{\mathbf{p}}) \right) \right], \end{aligned} \quad (\text{A.44})$$

$$\hat{H}_{\text{emf}} = \frac{1}{2} \int d^3\mathbf{x} \left( \epsilon_0 \hat{\mathbf{E}}^{\perp 2} + \frac{1}{\mu_0} \hat{\mathbf{B}}^2 \right), \quad (\text{A.45})$$

$$\hat{H}_{\text{pol}} = \frac{1}{2\epsilon_0} \int d^3\mathbf{x} \hat{\mathcal{P}}^{\perp 2}, \quad (\text{A.46})$$

$$\begin{aligned} \hat{H}_{\text{at-emf}} = & Q\Phi(\hat{\mathbf{R}}) - \hat{\mathbf{d}} \cdot \hat{\mathbf{E}}(\hat{\mathbf{R}}) + \left[ \frac{1}{2M} \hat{\mathbf{P}} \cdot (\hat{\mathbf{d}} \times \hat{\mathbf{B}}(\hat{\mathbf{R}})) + \text{H.c.} \right] \\ & - \frac{m_1 - m_2}{4m_1 m_2} \left[ \hat{\mathbf{p}} \cdot (\hat{\mathbf{d}} \times \hat{\mathbf{B}}(\hat{\mathbf{R}})) + \text{H.c.} \right] + \frac{Q}{4M} \left[ \hat{\mathbf{p}} \cdot (\hat{\mathbf{r}} \times \hat{\mathbf{B}}(\hat{\mathbf{R}})) + \text{H.c.} \right] \\ & + \frac{1}{8\mu} (\hat{\mathbf{d}} \times \hat{\mathbf{B}}(\hat{\mathbf{R}}))^2 - \frac{Q(m_1 - m_2)}{4M^2} (\hat{\mathbf{d}} \times \hat{\mathbf{B}}(\hat{\mathbf{R}})) (\hat{\mathbf{r}} \times \hat{\mathbf{B}}(\hat{\mathbf{R}})) \\ & + \frac{\mu Q^2}{8M^2} (\hat{\mathbf{r}} \times \hat{\mathbf{B}}(\hat{\mathbf{R}}))^2, \end{aligned} \quad (\text{A.47})$$

$$\hat{H}_{\text{mass defect}} = -\frac{\hat{\mathbf{P}}^2}{2M} \frac{1}{M c^2} \left( \frac{\hat{\mathbf{p}}^2}{2\mu} + \frac{e_1 e_2}{4\pi\epsilon_0 \hat{r}} \right) = -\frac{\hat{\mathbf{P}}^2}{2M} \otimes \frac{\hat{H}_{\text{int}}^{(0)}}{M c^2}, \quad (\text{A.48})$$

$$\begin{aligned} \hat{H}_X = & -\frac{1}{2M^2 c^2} \left[ \frac{1}{\mu} (\hat{\mathbf{P}} \cdot \hat{\mathbf{p}})^2 + \frac{e_1 e_2}{4\pi\epsilon_0 \hat{r}^3} (\hat{\mathbf{P}} \cdot \hat{\mathbf{r}})^2 \right] \\ & + \frac{m_1 - m_2}{2\mu M^2 c^2} \left[ \frac{1}{\mu} (\hat{\mathbf{P}} \cdot \hat{\mathbf{p}}) \hat{\mathbf{p}}^2 + \frac{e_1 e_2}{8\pi\epsilon_0} \left( \hat{\mathbf{P}} \cdot \frac{1}{\hat{r}} \hat{\mathbf{p}} + \hat{\mathbf{P}} \cdot \hat{\mathbf{r}} \frac{1}{\hat{r}^3} \hat{\mathbf{r}} \cdot \hat{\mathbf{p}} + \text{H.c.} \right) \right]. \end{aligned} \quad (\text{A.49})$$



The Hamiltonian  $\hat{H}_{\text{com}}$  describes the Hamiltonian minimally coupled to the electromagnetic field for the COM with first relativistic corrections.  $\hat{H}_{\text{int}}$  describes the internal Hamiltonian with its first relativistic corrections; in the main text, this Hamiltonian will be written in a two-level approximation.  $\hat{H}_{\text{emf}}$  is the electromagnetic field Hamiltonian, which gives the energy of the radiation field.  $\hat{H}_{\text{pol}}$  is a self-energy that is known to contribute to the Lamb shift and may be absorbed in any renormalized energy pertaining to the internal motion, as is discussed in [127].  $\hat{H}_{\text{at-emf}}$  contains the interaction of the atom and the electromagnetic field, in the first line we have the electric monopole and dipole interactions, and the minimally-coupled Röntgen term. In the second line we have the magnetic-dipole interaction, the third and fourth lines contain diamagnetic interaction terms. The  $Q$ -dependent terms can be interpreted as modifying the electric dipole  $\hat{\mathbf{d}}$  by  $\hat{\mathbf{d}}' = \hat{\mathbf{d}} + (\mu/M)Q\hat{\mathbf{r}}$  in the limit  $m_1 \ll m_2$ . They cancel the implicit  $Q$ -dependence of  $\hat{\mathbf{d}}$  such that  $\hat{\mathbf{d}}'$  is equal to the dipole moment of a neutral atom (if  $m_1 \ll m_2$ ) [133]. Terms contributing also for neutral systems ( $Q = 0$ ) are reported and discussed in [127].  $\hat{H}_{\text{mass defect}}$  contains the coupling between internal and external DOF that we are interested in, connecting the kinetic energy with  $\hat{H}_{\text{int}}^{(0)}$ , which refers to the internal Hamiltonian without relativistic corrections. Finally,  $\hat{H}_X$  contains extra couplings between internal and external DOF; but in this case, this coupling appears because with relativistic corrections, the COM coordinates are not the adequate choice of coordinates to study our Hamiltonian, as will be shown in the next section.

## A.5 Separation of central and relative dynamics

Since a system's energy content is part of its inertia, the appropriate way to discuss this problem should be to express the Hamiltonian in the center of energy frame, but this is not a canonical transformation, as explained in [49]. Nevertheless, there exists a choice of coordinates via a canonical transformation that allows the separation of COM and relative dynamics up to our order of approximation, as shown by Close and Osborn [57] for the case of neutral systems  $Q = 0$ . It consists of *relativistic* variants of the COM and relative coordinates, as by themselves they no longer separate the two DOF fully.

For a composite system with net charge  $Q \neq 0$ , we generalize this transformation by seeking for new coordinates  $\hat{\tilde{\mathbf{R}}}$  and  $\hat{\tilde{\mathbf{r}}}$  with respective momenta  $\hat{\tilde{\mathbf{P}}}$  and  $\hat{\tilde{\mathbf{p}}}$ , which fulfill

$$\begin{aligned}
 \hat{\mathbf{R}} &= \hat{\tilde{\mathbf{R}}} + \frac{m_1 - m_2}{2M^2c^2} \left[ \left( \frac{\hat{\tilde{\mathbf{P}}}^2}{2\mu} \hat{\tilde{\mathbf{r}}} + \text{H.c.} \right) + \frac{e_1 e_2}{4\pi\epsilon_0 \hat{r}} \hat{\tilde{\mathbf{r}}} \right] \\
 &\quad - \frac{1}{4M^2c^2} \left[ \left( \hat{\tilde{\mathbf{r}}} \cdot \hat{\tilde{\mathbf{P}}} \right) \hat{\tilde{\mathbf{p}}} + \left( \hat{\tilde{\mathbf{P}}} \cdot \hat{\tilde{\mathbf{p}}} \right) \hat{\tilde{\mathbf{r}}} + \text{H.c.} \right], \\
 \hat{\mathbf{P}} &= \hat{\tilde{\mathbf{P}}} + f \left( \hat{\tilde{\mathbf{R}}}, \hat{\tilde{\mathbf{P}}}, \hat{\tilde{\mathbf{r}}}, \hat{\tilde{\mathbf{p}}} \right), \\
 \hat{\mathbf{r}} &= \hat{\tilde{\mathbf{r}}} + \frac{m_1 - m_2}{2\mu M^2c^2} \left[ \left( \hat{\tilde{\mathbf{r}}} \cdot \hat{\tilde{\mathbf{P}}} \right) \hat{\tilde{\mathbf{p}}} + \text{H.c.} \right] - \frac{\hat{\tilde{\mathbf{r}}} \cdot \hat{\tilde{\mathbf{P}}}}{2M^2c^2} \hat{\tilde{\mathbf{P}}}', \\
 \hat{\mathbf{p}} &= \hat{\tilde{\mathbf{p}}} + \frac{\hat{\tilde{\mathbf{p}}} \cdot \hat{\tilde{\mathbf{P}}}'}{2M^2c^2} \hat{\tilde{\mathbf{P}}}' - \frac{m_1 - m_2}{2M^2c^2} \left[ \frac{\hat{\tilde{\mathbf{P}}}^2}{\mu} \hat{\tilde{\mathbf{P}}}' + \frac{e_1 e_2}{4\pi\epsilon_0} \left( \frac{1}{\hat{r}} \hat{\tilde{\mathbf{P}}}' - \frac{\hat{\tilde{\mathbf{P}}} \cdot \hat{\tilde{\mathbf{r}}}}{\hat{r}^3} \hat{\tilde{\mathbf{r}}} \right) \right]. \tag{A.50}
 \end{aligned}$$

Here, we include a minimal coupling of the COM DOF to the electromagnetic field  $\hat{\tilde{\mathbf{P}}}' = \hat{\tilde{\mathbf{P}}} - Q\hat{\mathbf{A}}^\perp(\hat{\tilde{\mathbf{R}}})$ . To still have a canonical transformation, the definition of the COM momentum involves an ansatz function  $f(\hat{\tilde{\mathbf{R}}}, \hat{\tilde{\mathbf{P}}}, \hat{\tilde{\mathbf{r}}}, \hat{\tilde{\mathbf{p}}})$ . Enforcing canonical commutation relations  $[\hat{\tilde{\mathbf{R}}}_k, \hat{\tilde{\mathbf{P}}}_l] = [\hat{\tilde{\mathbf{r}}}_k, \hat{\tilde{\mathbf{p}}}_l] = i\hbar\delta_{kl}$  and  $[\hat{\tilde{\mathbf{R}}}_k, \hat{\tilde{\mathbf{r}}}_l] = [\hat{\tilde{\mathbf{R}}}_k, \hat{\tilde{\mathbf{p}}}_l] = [\hat{\tilde{\mathbf{P}}}_k, \hat{\tilde{\mathbf{p}}}_l] = [\hat{\tilde{\mathbf{P}}}_k, \hat{\tilde{\mathbf{r}}}_l] = 0$ , we find

$$\begin{aligned}
 f \left( \hat{\tilde{\mathbf{R}}}, \hat{\tilde{\mathbf{P}}}, \hat{\tilde{\mathbf{r}}}, \hat{\tilde{\mathbf{p}}} \right) &= \frac{m_1 - m_2}{2M^2c^2} Q \left[ \left( \frac{\hat{\tilde{\mathbf{P}}}^2}{2\mu} \nabla_{\hat{\tilde{\mathbf{R}}} } \left( \hat{\tilde{\mathbf{r}}} \cdot \hat{\mathbf{A}}^\perp(\hat{\tilde{\mathbf{R}}}) \right) + \text{H.c.} \right) \right. \\
 &\quad \left. + \frac{e_1 e_2}{4\pi\epsilon_0 \hat{r}} \nabla_{\hat{\tilde{\mathbf{R}}} } \left( \hat{\tilde{\mathbf{r}}} \cdot \hat{\mathbf{A}}^\perp(\hat{\tilde{\mathbf{R}}}) \right) \right] \\
 &\quad - \frac{Q}{4M^2c^2} \left[ \hat{\tilde{\mathbf{r}}} \cdot \hat{\tilde{\mathbf{P}}}' \nabla_{\hat{\tilde{\mathbf{R}}} } \left( \hat{\tilde{\mathbf{p}}} \cdot \hat{\mathbf{A}}^\perp(\hat{\tilde{\mathbf{R}}}) \right) + \hat{\tilde{\mathbf{P}}}' \cdot \hat{\tilde{\mathbf{p}}} \nabla_{\hat{\tilde{\mathbf{R}}} } \left( \hat{\tilde{\mathbf{r}}} \cdot \hat{\mathbf{A}}^\perp(\hat{\tilde{\mathbf{R}}}) \right) + \text{H.c.} \right]. \tag{A.51}
 \end{aligned}$$

In principle, every function  $g(\hat{\tilde{\mathbf{R}}}, \hat{\tilde{\mathbf{P}}}, \hat{\tilde{\mathbf{r}}}, \hat{\tilde{\mathbf{p}}}) = f(\hat{\tilde{\mathbf{R}}}, \hat{\tilde{\mathbf{P}}}, \hat{\tilde{\mathbf{r}}}, \hat{\tilde{\mathbf{p}}}) + h(\hat{\tilde{\mathbf{R}}})$  that fulfills  $\frac{\partial h_i}{\partial \hat{\tilde{\mathbf{R}}}_j} = 0$  is also a suitable choice besides  $f$ . We chose  $h$  to be zero in order to reproduce for  $Q = 0$  the coordinates used in [49]. In the main text, Eqs. (3.6) and (3.7), we used the notation of the usual COM coordinates to refer to the relativistic corrected ones. The only difference is that the vector potential  $\hat{\mathbf{A}}^\perp(\hat{\tilde{\mathbf{R}}})$  and the scalar Newtonian potential  $\phi(\hat{\tilde{\mathbf{R}}})$  should be evaluated in terms of the non-relativistic COM coordinates, but as both change slowly over the size of the atom, this correction is negligible and we can use the relativistic corrected variables instead.

# B

## Hamiltonian for ions in gravitational fields

In Appendix A we derived the multipolar light-atom Hamiltonian including first-order relativistic corrections, i.e., only keeping terms up to order  $c^{-2}$ , for a hydrogenlike atomic ion as an electromagnetically bound two-body system in external electromagnetic fields. For the case of  $Q = 0$  Schwartz & Giulini [50] included a weak gravitational field. Therefore, after our work in the previous appendix, there is still a gap of including the gravitational field and allowing a total charge  $Q \neq 0$ , which will be the aim of this appendix, and will be done by extending the work in [50].

Adapting the calculations to account for gravity was a work done by Simon Eilers, a master student co-author of the paper involving this work. The goal of this appendix is to summarize his work, that has been presented as part of his Master thesis [134], in order to have a complete derivation in the current thesis.

Schwartz & Giulini considered the interaction of the composite system with a weak gravitational field described by the Eddington-Robertson metric  $g_{\mu\nu}$ , which is defined by the Minkowski metric plus first-order relativistic corrections induced by a weak and static scalar potential  $\phi(\mathbf{r})$ . The weak condition is fulfilled for  $\phi(\mathbf{r})/c^2 \ll 1$ . Here,  $\mu = 0$  or  $\nu = 0$  correspond to time components of the metric and  $\mu, \nu \in \{1, 2, 3\}$  correspond to space components. In isotropic coordinates, and for a particle in a position  $\mathbf{r}$ , it reads

$$g_{\mu\nu}(\mathbf{r}) = \begin{pmatrix} -1 - 2\frac{\phi(\mathbf{r})}{c^2} - 2\beta\frac{\phi^2(\mathbf{r})}{c^4} + \mathcal{O}(c^{-6}) & \mathcal{O}(c^{-5}) \\ \mathcal{O}(c^{-5}) & \left(1 - 2\gamma\frac{\phi(\mathbf{r})}{c^2}\right)\mathbf{1} + \mathcal{O}(c^{-4}) \end{pmatrix}, \quad (\text{B.1})$$

where  $\beta$  and  $\gamma$  are the so-called Eddington-Robertson parameters and will allow us to test theories beyond general relativity, for which they have a value of 1.

## B.1 Classical Lagrangian

Our starting point is the classical Lagrangian for two particles interacting with the electromagnetic and gravitational fields

$$L = - \sum_{i=1,2} m_i c \sqrt{-g_{\mu\nu}(\mathbf{r}_i) \dot{r}_i^\mu \dot{r}_i^\nu} + \int d^3\mathbf{r} \sqrt{-g(\mathbf{r})} \left( J^\mu(\mathbf{r}) A_{\text{tot},\mu}(\mathbf{r}) - \frac{1}{4\mu_0} F_{\text{tot},\mu\nu}(\mathbf{r}) F_{\text{tot}}^{\mu\nu}(\mathbf{r}) \right), \quad (\text{B.2})$$

which corresponds to Eq. 3.1 in the main text, with the difference that we now state explicitly that  $F_{\text{tot}}$  and  $A_{\text{tot}}$  correspond, respectively, to the total electromagnetic four-potential and the total field strength tensor as in Appendix A. Of course, the difference from the previous appendix, a part from the inclusion of gravity, is that we are now in spacetime coordinates and therefore we have  $r_i^\mu = (ct, \mathbf{r}_i)$ ,  $A_{\text{tot},\mu} = (\phi_{\text{tot}}/c, \mathbf{A}_{\text{tot}})$  and  $F_{\text{tot},\mu\nu} = \partial_\mu A_{\text{tot},\nu} - \partial_\nu A_{\text{tot},\mu}$ . Do not confuse  $\phi_{\text{tot}}$  of the previous section with the gravitational potential defined in this section  $\phi$ .

It is worth noticing that, considering the relation between the electric current and its density, namely,  $J^\mu = j^\mu / \sqrt{-g(\mathbf{r})}$  combined with the prefactor of the integral in Eq. (B.2) makes the electromagnetic interaction insensitive to gravity, and therefore, will have the same expression as in Appendix A. Finally, after solving the Maxwell equations similar to the previous section and combining the results, we obtain

$$L = \sum_{i=1,2} \left( \frac{m_i \dot{\mathbf{r}}_i^2}{2} + \frac{m_i \dot{\mathbf{r}}_i^4}{8c^2} \right) - \left( 1 + (\gamma + 1) \frac{\phi(\mathbf{r}_1) + \phi(\mathbf{r}_2)}{2c^2} \right) \frac{e_1 e_2}{4\pi\epsilon_0 r} + \frac{e_1 e_2}{8\pi\epsilon_0 c^2} \left( \frac{\dot{\mathbf{r}}_1 \cdot \dot{\mathbf{r}}_2}{r} + \frac{(\dot{\mathbf{r}}_1 \cdot \mathbf{r})(\dot{\mathbf{r}}_2 \cdot \mathbf{r})}{r^3} \right) - \sum_{i=1,2} \left( m_i \phi(\mathbf{r}_i) + \frac{2\gamma + 1}{2} \frac{m_i \phi(\mathbf{r}_i)}{c^2} \dot{\mathbf{r}}_i^2 + (2\beta - 1) \frac{m_i \phi^2(\mathbf{r}_i)}{2c^2} \right) + \frac{\epsilon_0}{2} \int d^3\mathbf{x} \left[ \left( 1 - (\gamma + 1) \frac{\phi}{c^2} \right) (\partial_t \mathbf{A}^\perp)^2 - c^2 \left( 1 + (\gamma + 1) \frac{\phi}{c^2} \right) (\nabla \times \mathbf{A}^\perp)^2 \right] + \int d^3\mathbf{x} \left( \mathbf{j}^\perp \cdot \mathbf{A}^\perp - \rho \Phi \right). \quad (\text{B.3})$$

As we can see, the coupling between the charge density and the scalar potential  $\rho\Phi$  will be the only new term which exclusively depends on  $Q$  after inserting the explicit form of  $\rho$ , and therefore, will be the only term that differs from the derivation in [50].

## B.2 Minimal-coupling Hamiltonian and multipolar Hamiltonian

Going from the classical Lagrangian to the minimal-coupling Hamiltonian is done similarly as in Appendix A. The only difference is that Eqs. (A.16) and (A.17) are slightly altered to

$$\mathbf{p}_i = m_i \dot{\mathbf{r}}_i \left( 1 + \frac{\dot{\mathbf{r}}_i^2}{2c^2} - (2\gamma + 1) \frac{\phi(\mathbf{r}_i)}{c^2} \right) + \frac{e_1 e_2}{8\pi \varepsilon_0 c^2 r} \left( \dot{\mathbf{r}}_j + \frac{\mathbf{r}(\dot{\mathbf{r}}_j \cdot \mathbf{r})}{r^2} \right) + e_i \mathbf{A}^\perp(\mathbf{r}_i), \quad (\text{B.4})$$

$$\mathbf{\Pi}^\perp = \varepsilon_0 \left( 1 - (\gamma + 1) \frac{\phi}{c^2} \right) \dot{\mathbf{A}}^\perp. \quad (\text{B.5})$$

Following the same steps as in the case without gravity, we quantize the classical Hamiltonian by imposing canonical commutation relations, as in Eqs. (A.20) and (A.21), and we obtain in minimal-coupling form

$$\begin{aligned} \hat{H}_{[\text{min.c.}]} = & \sum_{i=1,2} \left( \frac{\hat{\mathbf{p}}_i^2}{2m_i} - \frac{\hat{\mathbf{p}}_i^4}{8m_i^3 c^2} \right) + \left( 1 + (\gamma + 1) \frac{\phi(\hat{\mathbf{r}}_1) + \phi(\hat{\mathbf{r}}_2)}{2c^2} \right) \frac{e_1 e_2}{4\pi \varepsilon_0 \hat{r}} \\ & - \frac{e_1 e_2}{16\pi \varepsilon_0 c^2 m_1 m_2} \left[ \hat{\mathbf{p}}_1 \cdot \frac{1}{\hat{r}} \hat{\mathbf{p}}_2 + \hat{\mathbf{p}}_1 \cdot \hat{\mathbf{r}} \frac{1}{\hat{r}^3} \hat{\mathbf{r}} \cdot \hat{\mathbf{p}}_2 + (1 \leftrightarrow 2) \right] \\ & + \sum_{i=1,2} \left( m_i \phi(\hat{\mathbf{r}}_i) + \frac{2\gamma + 1}{2m_i c^2} \hat{\mathbf{p}}_i \cdot \phi(\hat{\mathbf{r}}_i) \hat{\mathbf{p}}_i + (2\beta - 1) \frac{m_i \phi^2(\hat{\mathbf{r}}_i)}{2c^2} \right) \\ & + \frac{\varepsilon_0}{2} \int d^3 \mathbf{x} \left( 1 + (\gamma + 1) \frac{\phi}{c^2} \right) \left[ \left( \frac{\hat{\mathbf{\Pi}}^\perp}{\varepsilon_0} \right)^2 + c^2 (\nabla \times \hat{\mathbf{A}}^\perp)^2 \right] + \sum_{i=1,2} e_i \Phi(\hat{\mathbf{r}}_i), \end{aligned} \quad (\text{B.6})$$

where  $\hat{\mathbf{p}}_i = \mathbf{p}_i - e_i \mathbf{A}^\perp(\mathbf{r}_i)$  and  $(1 \leftrightarrow 2)$  denotes the preceding term with indices 1 and 2 switched.

We expand the gravitational potential  $\phi(\hat{\mathbf{r}}_i)$  around the center of mass coordinate  $\hat{\mathbf{R}}$  and assume that the potential does not vary over the extension of the ion, as done in [50], leading to

$$\phi(\hat{\mathbf{r}}_1) = \phi(\hat{\mathbf{r}}_2) = \phi(\hat{\mathbf{R}}) + \mathcal{O}(c^{-2}). \quad (\text{B.7})$$

With that, one can make the same steps as in Appendix A, including the dipole approximation, to obtain the multipolar Hamiltonian

$$\begin{aligned}
\hat{H}_{[\text{mult.}]} = & \sum_{i=1,2} \left( \frac{\hat{\mathbf{p}}_i'^2}{2m_i} - \frac{\hat{\mathbf{p}}_i'^4}{8m_i^3 c^2} \right) + \left( 1 + (\gamma + 1) \frac{\phi(\hat{\mathbf{R}})}{c^2} \right) \frac{e_1 e_2}{4\pi \varepsilon_0 \hat{r}} - \frac{e_1 e_2}{16\pi \varepsilon_0 c^2 m_1 m_2} \left[ \hat{\mathbf{p}}_1' \cdot \frac{1}{\hat{r}} \hat{\mathbf{p}}_2' \right. \\
& + \hat{\mathbf{p}}_1' \cdot \hat{\mathbf{r}} \frac{1}{\hat{r}^3} \hat{\mathbf{r}} \cdot \hat{\mathbf{p}}_2' + (1 \leftrightarrow 2) \left. \right] + \sum_{i=1,2} \left( m_i \phi(\hat{\mathbf{R}}) + \frac{2\gamma + 1}{2m_i c^2} \hat{\mathbf{p}}_i' \cdot \phi(\hat{\mathbf{R}}) \hat{\mathbf{p}}_i' \right. \\
& + (2\beta - 1) \frac{m_i \phi^2(\hat{\mathbf{R}})}{2c^2} \left. \right) + \frac{\varepsilon_0}{2} \int d^3 \mathbf{x} \left( 1 + (\gamma + 1) \frac{\phi(\hat{\mathbf{R}})}{c^2} \right) \left[ \left( \frac{\hat{\boldsymbol{\Pi}}^\perp + \hat{\boldsymbol{\mathcal{P}}^\perp}{\varepsilon_0} \right)^2 \right. \\
& \left. + c^2 (\nabla \times \hat{\mathbf{A}}^\perp)^2 \right] + Q\Phi(\hat{\mathbf{R}}) - \hat{\mathbf{d}} \cdot \hat{\mathbf{E}}(\hat{\mathbf{R}}), \tag{B.8}
\end{aligned}$$

where  $\hat{\mathbf{p}}_i'$  is defined as in Eq. (A.35).

### B.3 Hamiltonian in center of mass frame

By transforming the Hamiltonian to the center of mass and relative coordinates in the same spirit as in Appendix A, we obtain

$$\hat{H} = \hat{H}_{\text{com}} + \hat{H}_{\text{int}} + \hat{H}_{\text{emf}} + \hat{H}_{\text{pol}} + \hat{H}_{\text{at-emf}} + \hat{H}_{\text{mass defect}} + \hat{H}_{\text{metric}} + \hat{H}_{\text{X}}, \tag{B.9}$$

$$\begin{aligned}
\hat{H}_{\text{com}} = & \frac{\hat{\mathbf{P}}^2}{2M} \left( 1 - \frac{\hat{\mathbf{P}}^2}{4M^2 c^2} \right) + M \phi(\hat{\mathbf{R}}) \left( 1 + (2\beta - 1) \frac{\phi(\hat{\mathbf{R}})}{2c^2} \right) \\
& + \frac{2\gamma + 1}{2M_0 c^2} \hat{\mathbf{P}} \cdot \phi(\hat{\mathbf{R}}) \hat{\mathbf{P}}, \tag{B.10}
\end{aligned}$$

$$\hat{H}_{\text{emf}} = \frac{1}{2} \int d^3 \mathbf{x} \left( 1 + (\gamma + 1) \frac{\phi(\hat{\mathbf{R}})}{c^2} \right) \left( \varepsilon_0 \hat{\mathbf{E}}^{\perp 2} + \frac{1}{\mu_0} \hat{\mathbf{B}}^2 \right), \tag{B.11}$$

$$\hat{H}_{\text{pol}} = \frac{1}{2\varepsilon_0} \int d^3 \mathbf{x} \left( 1 + (\gamma + 1) \frac{\phi(\hat{\mathbf{R}})}{c^2} \right) \hat{\boldsymbol{\mathcal{P}}}^{\perp 2}, \tag{B.12}$$

$$\hat{H}_{\text{mass defect}} = \left( M \phi(\hat{\mathbf{R}}) - \frac{\hat{\mathbf{P}}^2}{2M} \right) \left( \frac{\hat{\mathbf{p}}^2}{2\mu} + \frac{e_1 e_2}{4\pi \varepsilon_0 \hat{r}} \right) = \left( M \phi(\hat{\mathbf{R}}) - \frac{\hat{\mathbf{P}}^2}{2M} \right) \otimes \frac{\hat{H}_{\text{int}}^{(0)}}{M c^2}, \tag{B.13}$$

$$\hat{H}_{\text{metric}} = \gamma \frac{\phi(\hat{\mathbf{R}})}{c^2} \left( 2 \frac{\hat{\mathbf{p}}^2}{2\mu} + \frac{e_1 e_2}{4\pi \varepsilon_0 \hat{r}} \right), \tag{B.14}$$

where we only write explicitly the terms that differ from Appendix A and the new contribution  $\hat{H}_{\text{metric}}$ .

The changes in the Hamiltonian  $\hat{H}_{\text{com}}$  describe the gravitational potential energy and the relativistic interaction between the kinetic COM minimally coupled to the

electromagnetic field and the gravitational field. The changes in  $\hat{H}_{\text{emf}}$  and  $\hat{H}_{\text{pol}}$  can be interpreted as having the electromagnetic field minimally coupled to gravity when expressing them in local coordinates.  $\hat{H}_{\text{mass defect}}$  now also contains another coupling between internal and external DOF, namely, connecting the gravitational potential with  $\hat{H}_{\text{int}}^{(0)}$ , which refers to the internal Hamiltonian without relativistic corrections. Finally,  $\hat{H}_{\text{metric}}$  contains gravitational corrections that have their origin in the correct measure of the coordinates  $\hat{\mathbf{r}}$  and  $\hat{\mathbf{p}}$  with respect to the metric  $g_{\mu\nu}$  [50]. The Hamiltonian  $\hat{H}_X$  that we removed in Appendix A by implementing relativistically corrected coordinates, will not depend on gravity, and therefore, the transformation to these coordinates will be the same.

This closes the gap between our work in the previous appendix and the work of Schwartz & Giulini, where we now include the gravitational corrections for the relativistic Hamiltonian of a charged composite system.





# C

## Equation of motion for a trapped ion

As mentioned in the main text there are several ways of calculating the quasienergies of the quasienergy eigenstates. The goal of this appendix is to use the approach of solving the inhomogeneous Mathieu equation. By doing so, we will also solve the case where we have imperfections in the trap.

The treatment will follow the derivation in [61] (Appendix A), applied to our particular case, where they solve the general problem in the classical and quantum cases. We also redirect the interested reader to [61] for a treatment of the quantization (section III), where also the inhomogeneous equation is solved.

We want to find the quasideigenenergies corresponding to the Hamiltonian for a trapped ion

$$\hat{H} = \frac{\hat{\mathbf{P}}^2}{2M} + Q \left( \Phi_{\text{dc}}(\hat{\mathbf{R}}) + \Phi_{\text{ac}}(\hat{\mathbf{R}}, t) \right) + M\phi_0 + M\mathbf{g} \cdot \hat{\mathbf{R}}, \quad (\text{C.1})$$

which combines all the cases studied in the main text, i.e., mass defect, spurious dc potential, gravity contribution and imperfections in the trap. This last contribution will be effective once we substitute the trap potential, choosing the center of coordinates to be the zero of the ac potential and its eigenvectors to be the basis. Following from Eq. (3.74)

$$\hat{H} = \frac{\hat{\mathbf{P}}^2}{2M} + Q \left( \Phi_{\text{dc}}(\hat{\mathbf{0}}) - \mathbf{E}_{\text{dc}} \cdot \hat{\mathbf{R}} + \frac{1}{2} \hat{\mathbf{R}}^T U \hat{\mathbf{R}} + \Phi_{\text{ac}}(\hat{\mathbf{R}}, t) \right) + M\phi_0 + M\mathbf{g} \cdot \hat{\mathbf{R}}, \quad (\text{C.2})$$

where remember  $U = U_0 \text{diag}(\alpha_1, \alpha_2, \alpha_3) + W$  with dimensionless coefficients  $\alpha_i$  and a purely off-diagonal perturbation  $W$ . Contrary to Eq. (3.74) we wrote the minus sign in

front of the linear contribution to be consistent with the spurious dc field introduced in the main text. From this Hamiltonian, we derive the equation of motion for a trapped ion

$$\frac{\partial^2 \vec{u}}{\partial \tau^2} + \left[ A + \frac{4Q}{M\Omega^2} W - 2K \cos(2\tau) \right] \vec{u} = -\frac{4}{M\Omega^2} (-Q\mathbf{E}_{\text{dc}} + M\mathbf{g}), \quad (\text{C.3})$$

where we used the matrix  $K$  to avoid confusion with the total charge  $Q$ , the matrices  $A$  and  $K$  are diagonal  $A = \text{diag}(\mathbf{a}_1, \mathbf{a}_2, \mathbf{a}_3)$ ,  $K = \text{diag}(\mathbf{q}_1, \mathbf{q}_2, \mathbf{q}_3)$  and  $\tau = \frac{\Omega t}{2}$ .

To solve the equation of motion, we need to start by solving the homogeneous part.

## C.1 Homogeneous solution

We will treat the term  $\frac{4Q}{M\Omega^2} W$  as a perturbation of  $A$ , therefore, the homogeneous case becomes

$$\frac{\partial^2 \vec{u}}{\partial \tau^2} + [A - 2K \cos(2\tau)] \vec{u} = 0. \quad (\text{C.4})$$

We seek for solutions in the form of a sum of two linearly independent complex solutions

$$\vec{u} = \sum_{n=-\infty}^{\infty} \vec{C}_{2n} [b e^{i(2n+\beta)\tau} + c e^{-i(2n+\beta)\tau}], \quad (\text{C.5})$$

where  $b$  and  $c$  are complex constants determined by the initial conditions, which for stable modes must fulfill the condition  $b = c^*$ ,  $\vec{C}_{2n}$  are all real, and  $\beta$  is the so-called characteristic exponent, which in general may be complex as is discussed in [61]. Combining (C.4) with (C.5), we obtain the recursive relation

$$K \vec{C}_{2n-2} = R_{2n} \vec{C}_{2n} - K \vec{C}_{2n+2}, \quad (\text{C.6})$$

where  $R_{2n} = A - (2n + \beta)^2 \mathbf{1}$ . As the matrices  $A$  and  $K$  are diagonal, we get three independent equations, following the same reasoning as in [7]. The lowest order approximation in the case  $|a_j| \ll 1$ ,  $q_j^2 \ll 1$ ,  $\forall j \in \{1, 2, 3\}$  can be found by assuming  $C_{\pm 4} \simeq 0$ , getting

$$\beta_j = \sqrt{\mathbf{a}_j + \frac{\mathbf{q}_j^2}{2}}, \quad (\text{C.7})$$

which gives a quasienergy eigenvalue for a Fock state  $(n_1, n_2, n_3)$  of

$$E = \sum_{j=1}^3 \frac{\hbar\Omega}{2} \beta_j (n_j + \frac{1}{2}). \quad (\text{C.8})$$

The next step is to consider  $W$  as a perturbation of the matrix  $A$  in Eq. (C.4). We will define the small parameter  $\epsilon = \frac{4}{M\Omega^2}$  and for clearness in notation we will also define the variables  $\xi_j = \beta_j^2$ , considering for the perturbation the following expansions

$$\vec{C}_{2n} = \sum_{l=0}^{\infty} \vec{C}_{2n}^{(l)} \epsilon^l, \quad \xi_j = \sum_{l=0}^{\infty} \xi_j^{(l)} \epsilon^l. \quad (\text{C.9})$$

Introducing them in (C.5) we obtain the same recursive relation (C.6), changing  $R_{2n}$  to  $R_{2n} = A + \epsilon QW - (2n + \beta)^2 \mathbb{1}$ . Keeping only the terms up to first order on  $\epsilon$ , we obtain

$$\left( A - \xi^{(0)} \mathbb{1} + \frac{K^2}{2} \right) \vec{C}_0^{(0)} + \epsilon \left[ \left( A - \xi^{(0)} \mathbb{1} + \frac{K^2}{2} \right) \vec{C}_0^{(1)} + (QW - \xi^{(1)} \mathbb{1}) \vec{C}_0^{(0)} \right] = 0. \quad (\text{C.10})$$

The first part of the previous equation vanishes, therefore, the part proportional to  $\epsilon$  has to vanish as well. Without loss of generality, we will assume  $\vec{C}_0^{(1)} = (a, b, c)$  and solve the equation. With that we obtain, for the case of non-degenerate eigenvalues,  $\xi^{(1)} = 0$  and a correction to the eigenvector  $\vec{C}_0$ . Therefore, our principal axes compared with the non-perturbed case are rotated by an amount proportional to the terms in the perturbation  $W$ . For example, the corrected  $\beta_x$  eigenvector is

$$\vec{C}_0 = (1, 0, 0) - \frac{4}{M\Omega^2} \left( 0, \frac{QW_{xy}}{\beta_y^{2(0)} - \beta_x^{2(0)}}, \frac{QW_{xz}}{\beta_z^{2(0)} - \beta_x^{2(0)}} \right). \quad (\text{C.11})$$

In the case of degenerate eigenvalues, we can assume without loss of generality  $\xi_x^{(0)} = \xi_y^{(0)} = \xi^{(0)}$ . The excess field will break the degeneracy, implying two different eigenvectors with two different corrections. To apply the perturbation in this case, we can assume  $\vec{C}_0^{(0)} = (\alpha, \gamma, 0)$  and  $\vec{C}_0^{(1)} = (a, b, c)$ , where this  $a$ ,  $b$  and  $c$  do not need to be the same as before, and  $\alpha^2 + \gamma^2 = 1$ . Without losing generality, we can assume  $\gamma > 0$  and we get two pair solutions

$$\xi^{(1)} = \pm QW_{xy}, \quad \alpha = \pm \frac{1}{\sqrt{2}}. \quad (\text{C.12})$$

Therefore, we see that in the case of degenerate eigenvalues, the perturbation  $\epsilon QW$  gives a correction to the eigenvalues  $\beta_x^2$  and  $\beta_y^2$ . Being a correction to the eigenvalues of the trap implies that it will be accounted for during the trap calibration.

The correction to the eigenvector will be

$$\vec{C}_0^{(1)} = -(0, 0, Q \frac{W_{xz}\alpha + W_{yz}\gamma}{\beta_z^{2(0)} - \beta^{2(0)}}). \quad (\text{C.13})$$

## C.2 Quasienergie values for the inhomogeneous case

After solving the homogeneous case, we need to find a periodic solution of equation (C.3) in order to have a complete solution. Inserting a solution of the form  $\vec{u}_\pi = \sum_{n \in \mathbb{Z}} \vec{B}_{2n} e^{i2n\tau}$ , and considering that the effect of  $W$  has already been treated as a perturbation of  $A$ , the lowest-order correction can be found under the assumptions  $B_{\pm 4} \simeq 0$ , obtaining

$$\vec{u}_\pi = -\frac{4}{M\Omega^2} \left[ 1 - \frac{1}{2} K e^{2\tau i} \right] \left( \bar{\beta}^2 \right)^{-1} (-Q\mathbf{E}_{\text{dc}} + M\mathbf{g}), \quad (\text{C.14})$$

where we defined the matrix  $\bar{\beta} = \text{diag}(\beta_x, \beta_y, \beta_z)$ . As can be found in [61] (section C), the new wavefunction will be

$$\psi(\vec{u}) = \exp \left\{ i \dot{\vec{u}}_\pi \cdot \vec{x} + i \alpha_\pi(\tau) \right\} \varphi(\vec{x}), \quad (\text{C.15})$$

where  $\varphi$  is the wavefunction whose energy is given by the solution of the homogeneous case,  $\vec{x} = \vec{u} - \vec{u}_\pi$ , and  $\alpha$  has the expression

$$\alpha_\pi(\tau) = \int_0^\tau \frac{1}{2} \left[ \left( \dot{\vec{u}}_\pi \right)^2 + \vec{u}_\pi \cdot \left( \ddot{\vec{u}}_\pi - \frac{4}{M\Omega^2} (-Q\mathbf{E}_{\text{dc}} + M\mathbf{g}) \right) \right] d\tau'. \quad (\text{C.16})$$

Under the usual approximation  $|q_j| \ll 1 \forall j \in \{1, 2, 3\}$ , that we can find in [35], we obtain an energy contribution due to the periodic solution

$$E_{\text{dc,g}} = - \sum_{i=1}^3 \frac{\hbar\Omega}{4} \left( \frac{4}{M\Omega^2} \right)^2 \frac{1}{\beta_i^2} (QE_{\text{dc},i} - Mg_i)^2. \quad (\text{C.17})$$

In [61] they worked with  $\hbar = 1$ ,  $M = 1$  and other rescaled variables, therefore we need to multiply by  $\frac{M\Omega}{2\hbar}$  in order to recover the energy units, ending up with an energy contribution from the periodic solution of

$$E_{\text{dc,g}} = - \sum_{i=1}^3 \frac{2}{M\Omega^2} \frac{1}{\beta_i^2} (QE_{\text{dc},i} - Mg_i)^2. \quad (\text{C.18})$$

After applying the Feynman-Hellman theorem (3.32) we recover the result in Eq. (3.69) that was also calculated via the averages of creation and annihilation operators.



# List of Figures

3.1	In this figure we show the coordinates and positions that we will use in the following derivation. $O$ stands for the center of coordinates, $\mathbf{r}_1$ and $\mathbf{r}_2$ are the positions of the two particles of charges $e_1$ and $e_2$ , respectively, and $(\mathbf{R}, \mathbf{r})$ is the center of mass coordinate system. . . .	23
3.2	<b>Simple Ramsey interrogation scheme:</b> For clarity, we show in this figure the Ramsey interrogation scheme in a frame rotating around $z$ with the laser frequency $\omega_L$ . In a) we can see the series of transformations introduced in the main text, the two $\pi/2$ rotations $\hat{U}_R(0)$ and $\hat{U}_R(\omega_L T_R)$ and the free evolution $\hat{U}(T_R)$ , but now in the rotating frame and where we assumed the simplified case in which the free evolution corresponds to the Hamiltonian $\hat{H} = \frac{\hbar\omega_0}{2}\hat{\sigma}_z$ , here $\phi = (\omega_0 - \omega_L)T_R$ . At the end of the Ramsey sequence $\langle\sigma_z\rangle$ is measured. In b) we see the representation of the Ramsey interrogation scheme on the Bloch sphere.	31
3.3	Redshift $\frac{g^2}{\omega_i^2 c^2}$ (red dotted line) and total fractional frequency shift, i.e., redshift plus second-order Doppler shift $\frac{\hbar\omega_i(\bar{n}+1/2)}{2Mc^2}$ , for $\bar{n} = 0$ (solid lines) and $\bar{n} = 1$ (dashed lines) for $\text{Al}^+$ (thick blue lines), $\text{Yb}^+$ (thin green lines), and neutral $\text{Sr}$ (thick orange lines) versus trapping frequency $\omega_i$ . Here, we considered for simplicity a static confinement $\mathbf{q}_i = 0$ . . . . .	42
4.1	Sketch of dynamical decoupling effect on a given manifold. Figs. <i>a</i> ) and <i>c</i> ) correspond respectively to the quantization axis of Figs. <i>b</i> ) and <i>d</i> ). In Fig. <i>b</i> ) we show the level scheme of the bare basis, with coupling $\Omega_1$ between the bare states driven by the time-dependent near-resonant magnetic field and the detuning $\Delta_1 = \omega_0 - \omega_1$ . In Fig. <i>d</i> ) the level scheme in the dressed basis quantization axis is displayed. Note that <i>c</i> ) and <i>d</i> ) are not to scale as $\bar{\omega}_0 \ll \omega_0$ , due to $\bar{\omega}_0 = (\Delta_1^2 + g^2\Omega_1^2/4)^{1/2}$ . . .	58
4.2	Shows the possible combinations allowed by the quadrupole selection rules in the bare basis states $(m, M)$ . . . . .	61

- 4.3 Fig. *a*) shows a particular transition in the dressed basis with indices  $\bar{M} = -1/2 \leftrightarrow \bar{m} = -1/2$ . This transition can be driven using different combinations of underlying states  $(m, M)$  in the bare basis, shown in Fig. 4.2, through an appropriate laser detuning. The color code for the allowed transitions is the same as in Fig. 4.2. Since the dressed states are a time dependent superposition of the bare basis states, as shown in Fig. 4.1, their transition strength depends on the selection rules of the bare basis. Fig. *b*) depicts the effective Rabi frequencies relative to the Rabi frequencies of the transitions in the bare basis, i.e.,  $|\bar{\Omega}_{\bar{m}\bar{M}}^{mM}/\Omega_{mM}|$ . This ratio is plotted against the laser detuning, which shows for which values the transitions occur. . . . . 68
- 4.4 In this figure we show the ratio of the Rabi frequencies  $|\bar{\Omega}_{\bar{m}\bar{M}}^{mM, \bar{m}\bar{M}}/\Omega_{mM}|$  for all possible transitions from a doubly-dressed ground state  $|\bar{m}\rangle$  to a doubly-dressed excited state  $|\bar{M}\rangle$  at different laser detuning. Each color represents a different selection rule for the pair  $(m, M)$ . The green color stands for  $\pm 2$  transitions, the blue color for  $-1$  transitions, the red color for  $+1$  transitions and finally the black color stands for  $+0$  transitions. We initialized the ground doubly-dressed state in the state  $|\bar{m}\rangle = -1/2$ . . . . . 69
- 4.5 In this figure we show the infidelity,  $1 - |\langle \bar{m} | u_{m_f}(t) \rangle|^2$ , with  $\bar{m} = m_f = 1/2$  (solid line) during one period  $T^s = \frac{2\pi}{\omega_1^s}$ . We also show the infidelity between the same Floquet state and the corresponding corrected dressed state (dashed line) including Bloch-Siegert shifts. . . . . 71
- 4.6 Figs. *a*) and *b*) show the average of  $S_z$  of the dressed states (solid black line), the corrected dressed states (dashed black line) and the Floquet states (solid blue line) during one period  $T^s = \frac{2\pi}{\omega_1^s}$ , for the cases of  $\bar{m} = -1/2$  and  $\bar{m} = 1/2$ , respectively. . . . . 72
- 4.7 In this figure we show the infidelity,  $1 - |\langle \bar{M} | u_{M_f}(t) \rangle|^2$ , with  $\bar{M} = M_f$  (solid line) during one period  $T^d = \frac{2\pi}{\omega_1^d}$  for the cases of  $\bar{M} = 1/2$  (orange),  $\bar{M} = 3/2$  (cyan) and  $\bar{M} = 5/2$  (purple). We also show the infidelity between the same Floquet state and the corresponding corrected dressed state (dashed lines). . . . . 72
- 4.8 Figs. *a*), *b*) and *c*) show the average of  $S_z$  of the dressed states (solid black line), the corrected dressed states (dashed black line) and the Floquet states (solid blue line) during one period  $T^d = \frac{2\pi}{\omega_1^d}$ , for the cases of  $\bar{M} = 5/2$ ,  $\bar{M} = 3/2$  and  $\bar{M} = 1/2$ , respectively. . . . . 73



# List of Tables

4.1	Case study of double dressing for a $^{40}\text{Ca}^+$ ion for the $S_{1/2}$ and $D_{5/2}$ manifolds. The upper part of the table refers to the variables in the first layer of dressing and the lower part of the second layer of dressing. For this calculations we will use the known values of the gyromagnetic factors $g_s = 2.00225664$ [121] and $g_d = 1.2003340$ [122]. . . . .	67
-----	---	----



# Bibliography

- [1] Marius Schulte. *Entanglement in Ramsey interferometry, optical atomic clocks and trapped ions*. PhD thesis, Leibniz University Hannover, 2020. (cit. on page. [iii](#)).
- [2] G. Floquet. Sur les équations différentielles linéaires à coefficients périodiques. *Annales scientifiques de l'École Normale Supérieure*, 12, 1883. (cit. on pages [5](#) and [11](#)).
- [3] Peter Hänggi. Driven quantum systems. In Thomas Dittrich, Peter Hänggi, Gert-Ludwig Ingold, Bernhard Kramer, Gerd Schön, and Wilhelm Zwerger, editors, *Quantum transport and dissipation*, chapter 5. Wiley-VCH, Weinheim New York, 1998. (cit. on pages [5](#) and [78](#)).
- [4] Hideo Sambe. Steady states and quasienergies of a quantum-mechanical system in an oscillating field. *Phys. Rev. A*, 7, 1973. (cit. on pages [5](#), [6](#), [15](#), [21](#), and [46](#)).
- [5] Martin Holthaus. Floquet engineering with quasienergy bands of periodically driven optical lattices. *Journal of Physics B: Atomic, Molecular and Optical Physics*, 49(1), 2015. (cit. on pages [5](#), [6](#), and [15](#)).
- [6] R. J. Glauber. The quantum mechanics of trapped wavepackets. In *Laser Manipulation of Atoms and Ions*. North-Holland, Amsterdam, 1992. (cit. on pages [5](#), [21](#), [33](#), and [34](#)).
- [7] D. Leibfried, R. Blatt, C. Monroe, and D. Wineland. Quantum dynamics of single trapped ions. *Rev. Mod. Phys.*, 75, 2003. (cit. on pages [5](#), [21](#), [33](#), [34](#), [35](#), [73](#), and [100](#)).
- [8] Ya. B. Zel'Dovich. The Quasienergy of a Quantum-mechanical System Subjected to a Periodic Action. *Soviet Journal of Experimental and Theoretical Physics*, 24, 1967. (cit. on pages [5](#), [6](#), [14](#), and [21](#)).
- [9] V. I. Ritus. Shift and Splitting of Atomic Energy Levels by the Field of an Electromagnetic Wave. *Soviet Journal of Experimental and Theoretical Physics*, 24, 1967. (cit. on pages [5](#), [6](#), [14](#), and [21](#)).

- [10] S. H. Autler and C. H. Townes. Stark effect in rapidly varying fields. *Phys. Rev.*, 100, 1955. (cit. on page. 6).
- [11] Jon H. Shirley. Solution of the schrödinger equation with a hamiltonian periodic in time. *Phys. Rev.*, 138, 1965. (cit. on page. 6).
- [12] A G Fainshtein, N L Manakov, and L P Rapoport. Some general properties of quasi-energetic spectra of quantum systems in classical monochromatic fields. *Journal of Physics B: Atomic and Molecular Physics*, 11(14), 1978. (cit. on page. 6).
- [13] Milena Grifoni and Peter Hänggi. Driven quantum tunneling. *Physics Reports*, 304(5), 1998. (cit. on page. 6).
- [14] Shih-I Chu and Dmitry A. Telnov. Beyond the floquet theorem: generalized floquet formalisms and quasienergy methods for atomic and molecular multi-photon processes in intense laser fields. *Physics Reports*, 390(1), 2004. (cit. on page. 6).
- [15] James S. Howland. Quantum stability. In Erik Balslev, editor, *Schrödinger Operators The Quantum Mechanical Many-Body Problem*, Berlin, Heidelberg, 1992. Springer Berlin Heidelberg. (cit. on page. 6).
- [16] Wilhelm Magnus. On the exponential solution of differential equations for a linear operator. *Communications on Pure and Applied Mathematics*, 7(4), 1954. (cit. on pages 8 and 64).
- [17] S Blanes, F Casas, J A Oteo, and J Ros. A pedagogical approach to the magnus expansion. *European Journal of Physics*, 31(4), 2010. (cit. on page. 8).
- [18] S. Blanes, F. Casas, J.A. Oteo, and J. Ros. The magnus expansion and some of its applications. *Physics Reports*, 470(5), 2009. (cit. on page. 8).
- [19] IU. L. Daletskii and M. G. Krein. *Stability of solutions of differential equations in Banach space / Ju. L. Daleckii, M.G. Krein*. American Mathematical Society Providence, R.I. ; Great Britain, 2003. (cit. on page. 12).
- [20] Andrew D. Ludlow, Martin M. Boyd, Jun Ye, E. Peik, and P. O. Schmidt. Optical atomic clocks. *Rev. Mod. Phys.*, 87, 2015. (cit. on pages 19, 28, and 53).
- [21] S. M. Brewer, J.-S. Chen, A. M. Hankin, E. R. Clements, C. W. Chou, D. J. Wineland, D. B. Hume, and D. R. Leibbrandt.  $^{27}\text{Al}^+$  quantum-logic clock with a systematic uncertainty below  $10^{-18}$ . *Phys. Rev. Lett.*, 123, 2019. (cit. on pages 19 and 53).

- [22] Hans G. Dehmelt. Monoion oscillator as potential ultimate laser frequency standard. *IEEE Transactions on Instrumentation and Measurement*, IM-31(2), 1982. (cit. on page. 19).
- [23] Fritz Riehle, Patrick Gill, Felicitas Arias, and Lennart Robertsson. The CIPM list of recommended frequency standard values: guidelines and procedures. *Metrologia*, 55(2), 2018. (cit. on page. 19).
- [24] C. Lisdat, G. Grosche, N. Quintin, C. Shi, S. M. F. Raupach, C. Grebing, D. Nicolodi, F. Stefani, A. Al-Masoudi, S. Dörscher, S. Häfner, J.-L. Robyr, N. Chiodo, S. Bilicki, E. Bookjans, A. Koczwara, S. Koke, A. Kuhl, F. Wiotte, F. Meynadier, E. Camisard, M. Abgrall, M. Lours, T. Legero, H. Schnatz, U. Sterr, H. Denker, C. Chardonnet, Y. Le Coq, G. Santarelli, A. Amy-Klein, R. Le Targat, J. Lodewyck, O. Lopez, and P.-E. Pottie. A clock network for geodesy and fundamental science. *Nature Communications*, 7, 2016. (cit. on pages 19 and 53).
- [25] Jacopo Grotti, Silvio Koller, Stefan Vogt, Sebastian Häfner, Uwe Sterr, Christian Lisdat, Heiner Denker, Christian Voigt, Ludger Timmen, Antoine Rolland, Fred N. Baynes, Helen S. Margolis, Michel Zampaolo, Pierre Thoumany, Marco Pizzocaro, Benjamin Rauf, Filippo Bregolin, Anna Tampellini, Piero Barbieri, Massimo Zucco, Giovanni A. Costanzo, Cecilia Clivati, Filippo Levi, and Davide Calonico. Geodesy and metrology with a transportable optical clock. *Nature Physics*, 14, 2018. (cit. on pages 19 and 53).
- [26] W. F. McGrew, X. Zhang, R. J. Fasano, S. A. Schäffer, K. Beloy, D. Nicolodi, R. C. Brown, N. Hinkley, G. Milani, M. Schioppo, T. H. Yoon, and A. D. Ludlow. Towards an international height reference frame using clock networks. *Nature*, 564(7734), 2018. (cit. on pages 19 and 53).
- [27] Heiner Denker, Ludger Timmen, Christian Voigt, Stefan Weyers, Ekkehard Peik, Helen S. Margolis, Pacôme Delva, Peter Wolf, and Gérard Petit. Geodetic methods to determine the relativistic redshift at the level of  $10^{-18}$  in the context of international timescales: A review and practical results. *Journal of Geodesy*, 92(5), 2018. (cit. on pages 19 and 53).
- [28] Tanja E. Mehlstäubler, Gesine Grosche, Christian Lisdat, Piet O. Schmidt, and Heiner Denker. Atomic clocks for geodesy. *Reports on Progress in Physics*, 81(6), 2018. (cit. on pages 19 and 53).

- [29] Hu Wu and Jürgen Müller. *Towards an International Height Reference Frame Using Clock Networks*. Springer Berlin Heidelberg, Berlin, Heidelberg, 2019. (cit. on pages 19 and 53).
- [30] Jürgen Müller and Hu Wu. Using quantum optical sensors for determining the Earth’s gravity field from space. *Journal of Geodesy*, 94(8), 2020. (cit. on pages 19 and 53).
- [31] Masao Takamoto, Ichiro Ushijima, Noriaki Ohmae, Toshihiro Yahagi, Kensuke Kokado, Hisaaki Shinkai, and Hidetoshi Katori. Test of general relativity by a pair of transportable optical lattice clocks. *Nature Photonics*, 14, 2020. (cit. on pages 19 and 53).
- [32] P. Delva, N. Puchades, E. Schönemann, F. Dilssner, C. Courde, S. Bertone, F. Gonzalez, A. Hees, Ch. Le Poncin-Lafitte, F. Meynadier, R. Prieto-Cerdeira, B. Sohet, J. Ventura-Traveset, and P. Wolf. Gravitational Redshift Test Using Eccentric Galileo Satellites. *Physical Review Letters*, 121(23), 2018. (cit. on pages 19 and 53).
- [33] Sven Herrmann, Felix Finke, Martin Lülff, Olga Kichakova, Dirk Puetzfeld, Daniela Knickmann, Meike List, Benny Rievers, Gabriele Giorgi, Christoph Günther, Hansjörg Dittus, Roberto Prieto-Cerdeira, Florian Dilssner, Francisco Gonzalez, Erik Schönemann, Javier Ventura-Traveset, and Claus Lämmerzahl. Test of the Gravitational Redshift with Galileo Satellites in an Eccentric Orbit. *Physical Review Letters*, 121(23), 2018. (cit. on pages 19 and 53).
- [34] M. S. Safronova, D. Budker, D. DeMille, Derek F. Jackson Kimball, A. Derevianko, and Charles W. Clark. Search for new physics with atoms and molecules. *Rev. Mod. Phys.*, 90, 2018. (cit. on pages 19 and 53).
- [35] D. J. Berkeland, J. D. Miller, J. C. Bergquist, W. M. Itano, and D. J. Wineland. Minimization of ion micromotion in a paul trap. *Journal of Applied Physics*, 83(10), 1998. (cit. on pages 19, 20, 21, 38, 40, 41, and 102).
- [36] S. Weyers, V. Gerginov, M. Kazda, J. Rahm, B. Lipphardt, G. Dobrev, and K. Gibble. Advances in the accuracy, stability, and reliability of the PTB primary fountain clocks. *Metrologia*, 55(6), 2018. (cit. on page 19).
- [37] C. W. Chou, D. B. Hume, J. C. J. Koelemeij, D. J. Wineland, and T. Rosenband. Frequency comparison of two high-accuracy  $\text{Al}^+$  optical clocks. *Phys. Rev. Lett.*, 104, 2010. (cit. on page 19).

- [38] N. Huntemann, M. Okhapkin, B. Lipphardt, S. Weyers, Chr. Tamm, and E. Peik. High-accuracy optical clock based on the octupole transition in  $^{171}\text{Yb}^+$ . *Phys. Rev. Lett.*, 108, 2012. (cit. on page. 19).
- [39] J. Keller, H. L. Partner, T. Burgermeister, and T. E. Mehlstäubler. Precise determination of micromotion for trapped-ion optical clocks. *Journal of Applied Physics*, 118(10), 2015. (cit. on pages 19, 20, and 21).
- [40] C. W. Chou, D. B. Hume, T. Rosenband, and D. J. Wineland. Optical clocks and relativity. *Science*, 329(5999), 2010. (cit. on page. 19).
- [41] Tobias Bothwell, Colin J. Kennedy, Alexander Aeppli, Dhruv Kedar, John M. Robinson, Eric Oelker, Alexander Staron, and Jun Ye. Resolving the gravitational redshift across a millimetre-scale atomic sample. *Nature*, 602(7897), 2022. (cit. on page. 19).
- [42] Magdalena Zych and Āaslav Brukner. Quantum formulation of the einstein equivalence principle. *Nature Physics*, 14(10), 2018. (cit. on pages 19 and 23).
- [43] B. D. Josephson. Temperature-dependent shift of  $\gamma$  rays emitted by a solid. *Phys. Rev. Lett.*, 4, 1960. (cit. on page. 20).
- [44] J.T. Dehn. On the equivalence of the second-order doppler shift and the mass-change shift in the mössbauer effect. *Physics Letters A*, 32(4), 1970. (cit. on page. 20).
- [45] J. Keller, T. Burgermeister, D. Kalincev, A. Didier, A. P. Kulosa, T. Nordmann, J. Kiethe, and T. E. Mehlstäubler. Controlling systematic frequency uncertainties at the  $10^{-19}$  level in linear coulomb crystals. *Phys. Rev. A*, 99, 2019. (cit. on pages 20 and 28).
- [46] Valeriy Yudin and Alexey Taichenachev. Mass defect effects in atomic clocks. *Laser Physics Letters*, 15(3), 2018. (cit. on pages 20, 28, 45, and 46).
- [47] Rebecca Haustein, Gerard J. Milburn, and Magdalena Zych. Mass-energy equivalence in harmonically trapped particles. *arXiv:1906.03980*, 2019. (cit. on pages 20, 28, 41, 42, and 43).
- [48] Supurna Sinha and Joseph Samuel. Quantum limit on time measurement in a gravitational field. *Classical and Quantum Gravity*, 32(1), 2014. (cit. on pages 20 and 43).

- 
- [49] Matthias Sonnleitner and Stephen M. Barnett. Mass-energy and anomalous friction in quantum optics. *Phys. Rev. A*, 98, 2018. (cit. on pages [20](#), [21](#), [22](#), [23](#), [25](#), [81](#), [84](#), [85](#), [90](#), [91](#), and [92](#)).
- [50] Philip K. Schwartz and Domenico Giulini. Post-Newtonian Hamiltonian description of an atom in a weak gravitational field. *Phys. Rev. A*, 100, 2019. (cit. on pages [20](#), [21](#), [22](#), [23](#), [24](#), [28](#), [93](#), [94](#), [95](#), and [97](#)).
- [51] K. Bely. Prospects of a  $\text{Pb}^{2+}$  ion clock. *Physical Review Letters*, 127(1), 2021. (cit. on pages [21](#) and [47](#)).
- [52] Charis Anastopoulos and Bei-Lok Hu. Relativistic particle motion and quantum optics in a weak gravitational field. *arXiv:2106.12514*, 2021. (cit. on page. [23](#)).
- [53] Shishir Khandelwal, Maximilian P.E. Lock, and Mischa P. Woods. Universal quantum modifications to general relativistic time dilation in delocalised clocks. *Quantum*, 4, 2020. (cit. on page. [23](#)).
- [54] Alexander R. H. Smith and Mehdi Ahmadi. Quantum clocks observe classical and quantum time dilation. *Nature Communications*, 11(1), 2020. (cit. on page. [23](#)).
- [55] Krzysztof Pachucki. Long-wavelength quantum electrodynamics. *Physical Review A*, 69(5), 2004. (cit. on pages [23](#) and [52](#)).
- [56] Krzysztof Pachucki. Electrodynamics of a compound system with relativistic corrections. *Physical Review A*, 76(2), 2007. (cit. on pages [23](#) and [52](#)).
- [57] Francis E. Close and Hugh Osborn. Relativistic center-of-mass motion and the electromagnetic interaction of systems of charged particles. *Phys. Rev. D*, 2, 1970. (cit. on pages [25](#), [81](#), and [91](#)).
- [58] Edwin Albert Power and T. Thirunamachandran. The multipolar hamiltonian in radiation theory. *Proceedings of the Royal Society of London. A. Mathematical and Physical Sciences*, 372(1749), 1980. (cit. on pages [26](#) and [87](#)).
- [59] Magdalena Zych, Lukasz Rudnicki, and Igor Pikovski. Gravitational mass of composite systems. *Physical Review D*, 99, 2019. (cit. on page. [27](#)).
- [60] D. J. Wineland, J. J. Bollinger, W. M. Itano, and D. J. Heinzen. Squeezed atomic states and projection noise in spectroscopy. *Phys. Rev. A*, 50, 1994. (cit. on pages [30](#) and [32](#)).



- [61] H Landa, M Drewsen, B Reznik, and A Retzker. Classical and quantum modes of coupled Mathieu equations. *Journal of Physics A: Mathematical and Theoretical*, 45(45), 2012. (cit. on pages 46, 99, 100, 102, and 103).
- [62] Lowell S. Brown and Gerald Gabrielse. Geonium theory: Physics of a single electron or ion in a penning trap. *Rev. Mod. Phys.*, 58, 1986. (cit. on pages 47 and 48).
- [63] F. Crimin, B. M. Garraway, and J. Verdú. The quantum theory of the Penning trap. *Journal of Modern Optics*, 65(4), 2018. (cit. on page. 47).
- [64] Kyle Arnold, Elnur Hajiyev, Eduardo Paez, Chern Hui Lee, M. D. Barrett, and John Bollinger. Prospects for atomic clocks based on large ion crystals. *Phys. Rev. A*, 92, 2015. (cit. on page. 52).
- [65] Tobias Bothwell, Dhruv Kedar, Eric Oelker, John M Robinson, Sarah L Bromley, Weston L Tew, Jun Ye, and Colin J Kennedy. JILA SrI optical lattice clock with uncertainty of  $2.0 \times 10^{-18}$ . *Metrologia*, 56(6), 2019. (cit. on pages 52 and 53).
- [66] Alexander Aeppli, Anjun Chu, Tobias Bothwell, Colin J. Kennedy, Dhruv Kedar, Peiru He, Ana Maria Rey, and Jun Ye. Hamiltonian engineering of spin-orbit coupled fermions in a wannier-stark optical lattice clock. *arXiv.2201.05909*, 2022. (cit. on page. 52).
- [67] R. X. Schüssler, H. Bekker, M. Braß, H. Cakir, J. R. Crespo López-Urrutia, M. Door, P. Filianin, Z. Harman, M. W. Haverkort, W. J. Huang, P. Indelicato, C. H. Keitel, C. M. König, K. Kromer, M. Müller, Y. N. Novikov, A. Rischka, C. Schweiger, S. Sturm, S. Ulmer, S. Eliseev, and K. Blaum. Detection of metastable electronic states by penning trap mass spectrometry. *Nature*, 581(7806), 2020. (cit. on page. 52).
- [68] T.L. Nicholson, S.L. Campbell, R.B. Hutson, G.E. Marti, B.J. Bloom, R.L. McNally, W. Zhang, M.D. Barrett, M.S. Safronova, G.F. Strouse, W.L. Tew, and J. Ye. Systematic evaluation of an atomic clock at  $2 \times 10^{-18}$  total uncertainty. *Nature Communications*, 6(1), 2015. (cit. on page. 53).
- [69] N. Huntemann, C. Sanner, B. Lipphardt, Chr. Tamm, and E. Peik. Single-ion atomic clock with  $3 \times 10^{-18}$  systematic uncertainty. *Phys. Rev. Lett.*, 116, 2016. (cit. on page. 53).

- [70] N. Poli, C. W. Oates, P. Gill, and G. M. Tino. Optical atomic clocks. *La Rivista del Nuovo Cimento*, 36(12), 2013. (cit. on page. 53).
- [71] Ekkehard Peik, Tobias Schneider, and Christian Tamm. Laser frequency stabilization to a single ion. *Journal of Physics B: Atomic, Molecular and Optical Physics*, 39(1), 2005. (cit. on page. 53).
- [72] Ian D Leroux, Nils Scharnhorst, Stephan Hannig, Johannes Kramer, Lennart Pelzer, Mariia Stepanova, and Piet O Schmidt. On-line estimation of local oscillator noise and optimisation of servo parameters in atomic clocks. *Metrologia*, 54(3), 2017. (cit. on page. 53).
- [73] J. Keller, D. Kalincev, T. Burgermeister, A. P. Kulosa, A. Didier, T. Nordmann, J. Kiethe, and T.E. Mehlstäubler. Probing time dilation in coulomb crystals in a high-precision ion trap. *Phys. Rev. Applied*, 11, 2019. (cit. on page. 53).
- [74] Kyle Arnold, Elnur Hajiyev, Eduardo Paez, Chern Hui Lee, M. D. Barrett, and John Bollinger. Prospects for atomic clocks based on large ion crystals. *Phys. Rev. A*, 92, 2015. (cit. on page. 53).
- [75] N. Herschbach, K. Pyka, J. Keller, and T. E. Mehlstäubler. Linear paul trap design for an optical clock with coulomb crystals. *Applied Physics B*, 107(4), 2011. (cit. on page. 53).
- [76] C. Champenois, M. Marciante, J. Pedregosa-Gutierrez, M. Houssin, M. Knoop, and M. Kajita. Ion ring in a linear multipole trap for optical frequency metrology. *Phys. Rev. A*, 81, 2010. (cit. on page. 53).
- [77] W.M. Itano. External-field shifts of the  $^{199}\text{Hg}^+$  optical frequency standard. *Journal of Research of the National Institute of Standards and Technology*, 105(6), 2000. (cit. on page. 53).
- [78] T. Schneider, E. Peik, and Chr. Tamm. Sub-hertz optical frequency comparisons between two trapped  $^{171}\text{Yb}^+$  ions. *Physical Review Letters*, 94(23), 2005. (cit. on page. 53).
- [79] R. Lange, N. Huntemann, C. Sanner, H. Shao, B. Lipphardt, Chr. Tamm, and E. Peik. Coherent Suppression of Tensor Frequency Shifts through Magnetic Field Rotation. *Physical Review Letters*, 125(14), 2020. (cit. on page. 54).
- [80] E. R. Andrew, A. Bradbury, and R. G. Eades. Nuclear Magnetic Resonance Spectra from a Crystal rotated at High Speed. *Nature*, 182(4650), 1958. (cit. on page. 54).

- 
- [81] Lorenza Viola and Seth Lloyd. Dynamical suppression of decoherence in two-state quantum systems. *Phys. Rev. A*, 58, 1998. (cit. on page. 54).
- [82] Lorenza Viola, Emanuel Knill, and Seth Lloyd. Dynamical decoupling of open quantum systems. *Phys. Rev. Lett.*, 82, 1999. (cit. on page. 54).
- [83] Paolo Zanardi. Symmetrizing evolutions. *Physics Letters A*, 258(2), 1999. (cit. on page. 54).
- [84] Mark S. Byrd and Daniel A. Lidar. *Quantum Information Processing*, 1(1/2), 2002. (cit. on page. 54).
- [85] P. Facchi, S. Tasaki, S. Pascazio, H. Nakazato, A. Tokuse, and D. A. Lidar. Control of decoherence: Analysis and comparison of three different strategies. *Physical Review A*, 71(2), 2005. (cit. on page. 54).
- [86] Kaveh Khodjasteh and Daniel A. Lidar. Rigorous bounds on the performance of a hybrid dynamical-decoupling quantum-computing scheme. *Physical Review A*, 78(1), 2008. (cit. on page. 54).
- [87] Kaveh Khodjasteh and Lorenza Viola. Dynamically error-corrected gates for universal quantum computation. *Physical Review Letters*, 102(8), 2009. (cit. on page. 54).
- [88] Kaveh Khodjasteh and Lorenza Viola. Dynamical quantum error correction of unitary operations with bounded controls. *Physical Review A*, 80(3), 2009. (cit. on page. 54).
- [89] Kaveh Khodjasteh, Daniel A. Lidar, and Lorenza Viola. Arbitrarily accurate dynamical control in open quantum systems. *Physical Review Letters*, 104(9), 2010. (cit. on page. 54).
- [90] Lidar D.A. Review of decoherence free subspaces, noiseless subsystems, and dynamical decoupling. *Adv. Chem. Phys.* 154, 295, 2012. (cit. on page. 54).
- [91] İ. Yalçinkaya, B. Çakmak, G. Karpat, and F. F. Fanchini. Continuous dynamical decoupling and decoherence-free subspaces for qubits with tunable interaction. *Quantum Information Processing*, 18(5), 2019. (cit. on page. 54).
- [92] Nati Aharon, Nicolas Spethmann, Ian D. Leroux, Piet O. Schmidt, and Alex Retzker. Robust optical clock transitions in trapped ions using dynamical decoupling. *New Journal of Physics*, 21(8), 2019. (cit. on pages 54, 55, 58, and 60).

- 
- [93] Michael J. Biercuk, Hermann Uys, Aaron P. VanDevender, Nobuyasu Shiga, Wayne M. Itano, and John J. Bollinger. Optimized dynamical decoupling in a model quantum memory. *Nature*, 458(7241), 2009. (cit. on page. 54).
- [94] Jiangfeng Du, Xing Rong, Nan Zhao, Ya Wang, Jiahui Yang, and R. B. Liu. Preserving electron spin coherence in solids by optimal dynamical decoupling. *Nature*, 461(7268), 2009. (cit. on page. 54).
- [95] S. Damodarakurup, M. Lucamarini, G. Di Giuseppe, D. Vitali, and P. Tombesi. Experimental inhibition of decoherence on flying qubits via “bang-bang” control. *Physical Review Letters*, 103(4), 2009. (cit. on page. 54).
- [96] G. de Lange, Z. H. Wang, D. Ristè, V. V. Dobrovitski, and R. Hanson. Universal dynamical decoupling of a single solid-state spin from a spin bath. *Science*, 330(6000), 2010. (cit. on page. 54).
- [97] Alexandre M. Souza, Gonzalo A. Álvarez, and Dieter Suter. Robust dynamical decoupling for quantum computing and quantum memory. *Physical Review Letters*, 106(24), 2011. (cit. on page. 54).
- [98] Boris Naydenov, Florian Dolde, Liam T. Hall, Chang Shin, Helmut Fedder, Lloyd C. L. Hollenberg, Fedor Jelezko, and Jörg Wrachtrup. Dynamical decoupling of a single-electron spin at room temperature. *Physical Review B*, 83(8), 2011. (cit. on page. 54).
- [99] T. van der Sar, Z. H. Wang, M. S. Blok, H. Bernien, T. H. Taminiau, D. M. Toyli, D. A. Lidar, D. D. Awschalom, R. Hanson, and V. V. Dobrovitski. Decoherence-protected quantum gates for a hybrid solid-state spin register. *Nature*, 484(7392), 2012. (cit. on page. 54).
- [100] Ravid Shaniy, Nitzan Akerman, Tom Manovitz, Yotam Shapira, and Roei Ozeri. Quadrupole shift cancellation using dynamic decoupling. *Phys. Rev. Lett.*, 122, 2019. (cit. on pages 54, 55, and 60).
- [101] Karen M. Fonseca-Romero, Sigmund Kohler, and Peter Hänggi. Coherence stabilization of a two-qubit gate by ac fields. *Phys. Rev. Lett.*, 95, 2005. (cit. on page. 54).
- [102] Pochung Chen. Geometric continuous dynamical decoupling with bounded controls. *Phys. Rev. A*, 73, 2006. (cit. on page. 54).

- [103] Jens Clausen, Guy Bensky, and Gershon Kurizki. Bath-optimized minimal-energy protection of quantum operations from decoherence. *Phys. Rev. Lett.*, 104, 2010. (cit. on page. 54).
- [104] Xiangkun Xu, Zixiang Wang, Changkui Duan, Pu Huang, Pengfei Wang, Ya Wang, Nanyang Xu, Xi Kong, Fazhan Shi, Xing Rong, and Jiangfeng Du. Coherence-protected quantum gate by continuous dynamical decoupling in diamond. *Phys. Rev. Lett.*, 109, 2012. (cit. on page. 54).
- [105] F. F. Fanchini, J. E. M. Hornos, and R. d. J. Napolitano. Continuously decoupling single-qubit operations from a perturbing thermal bath of scalar bosons. *Phys. Rev. A*, 75, 2007. (cit. on page. 54).
- [106] F. F. Fanchini and R. d. J. Napolitano. Continuous dynamical protection of two-qubit entanglement from uncorrelated dephasing, bit flipping, and dissipation. *Phys. Rev. A*, 76, 2007. (cit. on page. 54).
- [107] F. F. Fanchini, R. d. J. Napolitano, B. Çakmak, and A. O. Caldeira. Protecting the  $\sqrt{\text{swap}}$  operation from general and residual errors by continuous dynamical decoupling. *Phys. Rev. A*, 91, 2015. (cit. on page. 54).
- [108] P. Rabl, P. Cappellaro, M. V. Gurudev Dutt, L. Jiang, J. R. Maze, and M. D. Lukin. Strong magnetic coupling between an electronic spin qubit and a mechanical resonator. *Phys. Rev. B*, 79, 2009. (cit. on page. 54).
- [109] Adam Zaman Chaudhry and Jiangbin Gong. Decoherence control: Universal protection of two-qubit states and two-qubit gates using continuous driving fields. *Phys. Rev. A*, 85, 2012. (cit. on page. 54).
- [110] J-M Cai, B Naydenov, R Pfeiffer, L P McGuinness, K D Jahnke, F Jelezko, M B Plenio, and A Retzker. Robust dynamical decoupling with concatenated continuous driving. *New Journal of Physics*, 14(11), 2012. (cit. on pages 54, 55, and 58).
- [111] Abdelghani Laraoui and Carlos A. Meriles. Rotating frame spin dynamics of a nitrogen-vacancy center in a diamond nanocrystal. *Phys. Rev. B*, 84, 2011. (cit. on page. 54).
- [112] A. Bermudez, F. Jelezko, M. B. Plenio, and A. Retzker. Electron-mediated nuclear-spin interactions between distant nitrogen-vacancy centers. *Phys. Rev. Lett.*, 107, 2011. (cit. on page. 54).

- [113] A. Bermudez, P. O. Schmidt, M. B. Plenio, and A. Retzker. Robust trapped-ion quantum logic gates by continuous dynamical decoupling. *Phys. Rev. A*, 85, 2012. (cit. on page. 54).
- [114] N. Timoney, I. Baumgart, M. Johanning, A. F. Varón, M. B. Plenio, A. Retzker, and Ch. Wunderlich. Quantum gates and memory using microwave-dressed states. *Nature*, 476(7359), 2011. (cit. on page. 54).
- [115] Marcus W. Doherty, Neil B. Manson, Paul Delaney, Fedor Jelezko, Jörg Wrachtrup, and Lloyd C.L. Hollenberg. The nitrogen-vacancy colour centre in diamond. *Physics Reports*, 528(1), 2013. (cit. on page. 54).
- [116] A Albrecht, G Koplovitz, A Retzker, F Jelezko, S Yochelis, D Porath, Y Nevo, O Shoseyov, Y Paltiel, and M B Plenio. Self-assembling hybrid diamond–biological quantum devices. *New Journal of Physics*, 16(9), 2014. (cit. on page. 54).
- [117] D. Andrew Golter, Thomas K. Baldwin, and Hailin Wang. Protecting a solid-state spin from decoherence using dressed spin states. *Phys. Rev. Lett.*, 113, 2014. (cit. on page. 54).
- [118] V. J. Martínez-Lahuerta, L. Pelzer, K. Dietze, L. Krinner, P. O. Schmidt, and K. Hammerer. Quadrupole transitions and quantum gates protected by continuous dynamic decoupling, 2023. (cit. on pages 55 and 69).
- [119] D.F.V. James. Quantum dynamics of cold trapped ions with application to quantum computation. *Applied Physics B: Lasers and Optics*, 66(2), 1998. (cit. on page. 62).
- [120] Alberto Galindo and Pedro Pascual. *Quantum Mechanics I*. 2012. (cit. on page. 63).
- [121] G. Tommaseo, T. Pfeil, G. Revalde, G. Werth, P. Indelicato, and J. P. Desclaux. The  $g_j$ -factor in the ground state of  $\text{Ca}^+$ . *The European Physical Journal D - Atomic, Molecular, Optical and Plasma Physics*, 25(2), 2003. (cit. on pages 67 and 107).
- [122] M. Chwalla, J. Benhelm, K. Kim, G. Kirchmair, T. Monz, M. Riebe, P. Schindler, A. Villar, W. Hänsel, C. Roos, R. Blatt, M. Abgrall, G. Santarelli, G. Rovera, and Ph. Laurent. Absolute frequency measurement of the  $^{40}\text{Ca}^+ 4s^2S_{1/2} - 3d^2D_{5/2}$  clock transition. *Physical Review Letters*, 102(2), 2009. (cit. on pages 67 and 107).

- 
- [123] J.R. Johansson, P.D. Nation, and Franco Nori. Qutip 2: A python framework for the dynamics of open quantum systems. *Computer Physics Communications*, 184(4), 2013. (cit. on page. 70).
- [124] John David Jackson. *Classical Electrodynamics, 2nd Edition*. Wiley, 1975. (cit. on pages 81 and 84).
- [125] L D Landau. *The Classical Theory of Fields: Volume 2 (Course of Theoretical Physics Series)*. Butterworth-Heinemann, 1980. (cit. on page. 81).
- [126] Claude Cohen-Tannoudji, Jacques Dupont-Roc, and Gilbert Grynberg. *Photons and Atoms*. Wiley, 1997. (cit. on pages 81, 83, and 86).
- [127] V. E. Lembessis, M. Babiker, C. Baxter, and R. Loudon. Theory of radiation forces and momenta for mobile atoms in light fields. *Phys. Rev. A*, 48, 1993. (cit. on pages 81 and 91).
- [128] S. Eilers. *Massendefekt elektronischer Übergänge in Atomen und Ionen*. Bachelor's thesis, Leibniz University Hannover, 2018. (cit. on page. 81).
- [129] C.G. Darwin M.A. Li. the dynamical motions of charged particles. *The London, Edinburgh, and Dublin Philosophical Magazine and Journal of Science*, 39(233), 1920. (cit. on page. 84).
- [130] E. A. Power and S. Zienau. Coulomb gauge in non-relativistic quantum electro-dynamics and the shape of spectral lines. *Philosophical Transactions of the Royal Society of London. Series A, Mathematical and Physical Sciences*, 251(999), 1959. (cit. on page. 86).
- [131] R. G. Woolley. Molecular quantum electrodynamics. *Proceedings of the Royal Society of London. A. Mathematical and Physical Sciences*, 321(1547), 1971. (cit. on page. 86).
- [132] M. Babiker and R. Loudon. Derivation of the power-zienau-woolley hamiltonian in quantum electrodynamics by gauge transformation. *Proceedings of the Royal Society of London. A. Mathematical and Physical Sciences*, 385(1789), 1983. (cit. on page. 86).
- [133] Cecilia Cormick, Tobias Schaetz, and Giovanna Morigi. Trapping ions with lasers. *New Journal of Physics*, 13(4), 2011. (cit. on page. 91).
- [134] S. Eilers. *Relativistic Corrections to the Master Equation for Dipole Interacting Atoms*. Master's thesis, Leibniz University Hannover, 2022. (cit. on page. 93).

# ACADEMIC CURRICULUM VITAE

## Personal Data

NAME: Víctor José Martínez Lahuerta  
BORN: 16 April 1994 in Girona, Spain  
ADDRESS: Arnold-Böcklin-Straße 16, 28209 Bremen

## Education

07/2018–present	Doktor der Naturwissenschaften, Dr. rer. nat. Leibniz Universität Hannover Thesis: <i>Relativistic corrections and precision measurements in optical atomic clocks and trapped ions</i> , Supervisor: Prof. Dr. K. Hammerer
9/2012–01/2018	BACHELOR'S DEGREE OF MATHEMATICS University of Barcelona
9/2012–01/2018	BACHELOR'S DEGREE OF PHYSICS University of Barcelona
2010–2012	INTERNATIONAL BACCALAUREATE Bell-lloc del Pla Girona
1998–2012	SCHOOL Bell-lloc del Pla Girona